Fixed-Filter Multimicrophone Hearing Aids with Binaural Output

by

Joseph Gilles Desloge

Submitted to the Department of Electrical Engineering
and Computer Science
in partial fulfillment of the requirements for the degree of

Master of Science in Electrical Engineering

at the

MASSACHUSETTS INSTITUTE OF TECHNOLOGY

September 1994

Author 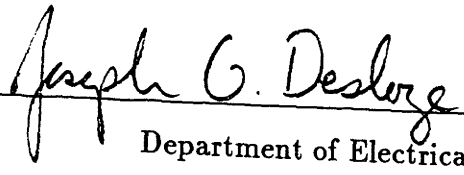

Department of Electrical Engineering and Computer Science
August 30, 1994

Certified by 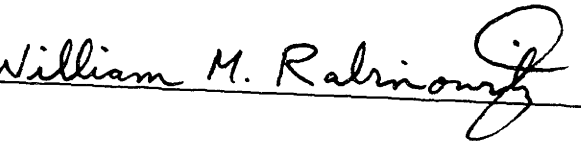

William M. Rabinowitz
Principal Research Scientist
Thesis Supervisor

Certified by 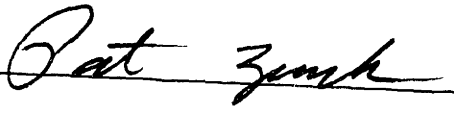

Patrick M. Zurek
Principal Research Scientist
Thesis Supervisor

Accepted by 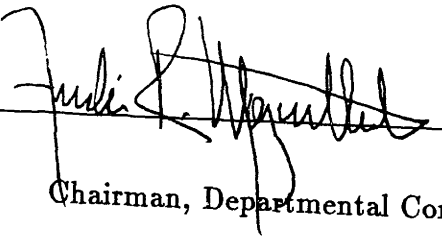

F. R. Morgenthaler
Chairman, Departmental Committee on Graduate Students

Fixed-Filter Multimicrophone Hearing Aids with Binaural Output

by

Joseph Gilles Desloge

Submitted to the Department of Electrical Engineering and Computer Science on August 30, 1994, in partial fulfillment of the requirements for the degree of Master of Science in Electrical Engineering.

Abstract

This thesis develops and evaluates several designs for a binaural output, multimicrophone hearing aid that exhibits a directional sensitivity in a desired 'target' direction (directly in front of the wearer) while also providing a realistic sense of space. Two primary classes of system structure are considered – dual-array, which uses two independent microphone arrays to produce the output signals, and single-array, which uses one array to produce both output signals. Furthermore, within each class, several system designs are explored, including complex systems which optimize system performance according to particular criteria and much simpler systems which only approach optimal performance. In all cases, the systems are designed for free-field operation. The system evaluation consists of two sections, physical and behavioral, and compares several test systems to the Naked Ear and Dual-Cardioid binaural hearing aid reference systems. The physical evaluation compares theoretical with actual free-field performance and explores the degrading effects of head-mounting upon the free-field designed test systems. These results indicate that all systems behave as expected in the free-field and that head-mounting causes little performance degradation. The behavioral evaluation assesses system performance along two dimensions – speech intelligibility and sound localization – that are directly affected by the directionality and binaural cue fidelity of the test systems. Results with normal-hearing indicate that all test systems exhibit comparable speech-intelligibility enhancements (roughly 3 dB of gain) relative to the Naked Ear and Dual-Cardioid reference systems, and that the binaural systems allow for reasonably accurate sound localization. Finally, the evaluations show that simplified, sub-optimal systems achieve performance levels equivalent to that of more complex, optimal systems.

Thesis Supervisor: William M. Rabinowitz
Title: Principal Research Scientist

Thesis Supervisor: Patrick M. Zurek
Title: Principal Research Scientist

Acknowledgements

This work was supported by grant DC00270-08 from the National Institute for Deafness and Other Communicative Disorders and a fellowship from the National Science Foundation.

This work is largely the result of a combined effort by several people. My advisors, Bill Rabinowitz and Pat Zurek, have helped me out tremendously by providing valuable theoretical insights and helping me to understand the sometime perplexing results of this project. I thank them for their patience and assistance. I would also like to thank the other members of the 'multi-mic' team – Julie Greenberg, Mike O'Connell, and Dan Welker – for the technical support and friendship that they have given me over the course of my research. They provided me with many of the tools that I needed to make this hearing aid a viable, working unit.

I must also thank all of the members of the Sensory Communications Group – they have made the recent (rather hectic) months both endurable and enjoyable. In particular, I admire Joe Frisbie (the 'head graduate student') for his ability to make the lab welcoming and to draw the lab together as a social unit. I also value the friendship of Doug Brungart and Paul Staelin – they provided me with some much needed (and some not-so-much needed) breaks from my work and engaged me in a friendly competition that encouraged me to finish this research.

Finally, I would like to thank my family, which has supported me in everything that I am and everything that I have decided to do. My life without their love and trust would be unimaginably empty.

Contents

Chapter 1

Introduction

Typical listening environments are often complex, with different sound sources arriving simultaneously from different locations. In such an environment, shown in Figure 1-1, a typical hearing-impaired, or even normal-hearing, listener might have difficulty focusing in on a 'target' sound source while tuning out 'jammer' sources.

Multimicrophone hearing aids provide one means of creating a directional hearing aid, i.e. a hearing aid that is more sensitive to sounds arriving from a certain target direction, usually assumed to be directly ahead of the wearer [6]. Such aids use a head mounted array of microphones to form the system output signal, as shown in Figure 1-1. Note that the signal processing in these systems can be either time-invariant (fixed) [21],[22],[23] or adaptive (indicated by the dashed line) [20],[9]. While adaptive systems have proven much better at jammer cancellation under ideal conditions, they have problems in reverberant environments and in situations where the target signal is misaligned from its assumed direction, [9]. Fixed systems, while they do not achieve the jammer cancellation of adaptive systems, can still realize considerable directional gains with processing that is relatively simple and robust.

As indicated in Figure 1-1, current multimicrophone designs typically produce a *monaural* system output. This results in the loss of binaural sound localization cues and, hence, the loss of a sense of space. The goal of this thesis is to develop fixed

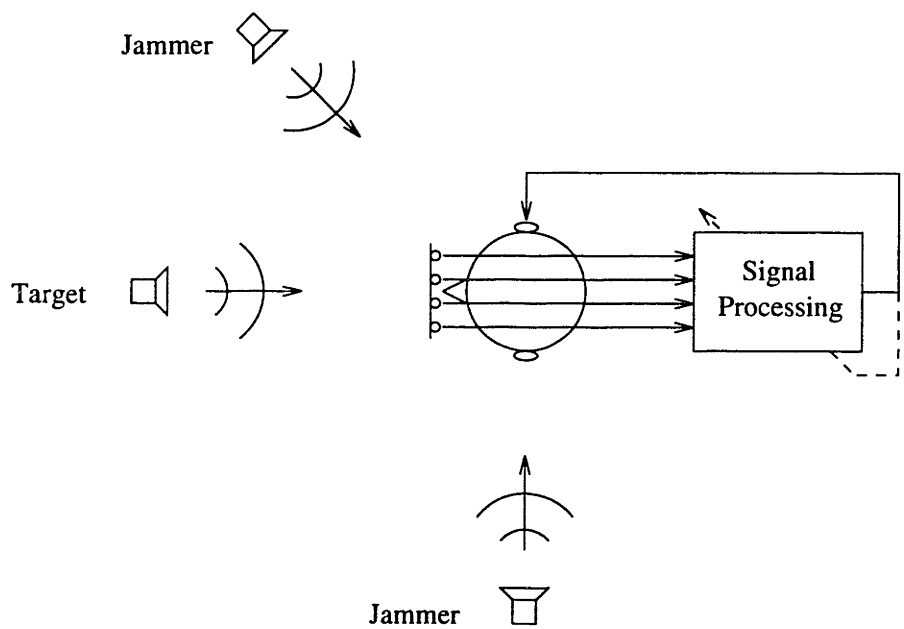

Figure 1-1: Typical, complex listening environment showing a monaural multimicrophone hearing aid structure, with dashed lines indicating possibly adaptive processing.

multimicrophone systems that produce a binaural output. Such hearing aids would retain the directional benefits of the monaural output multimicrophone system while giving the wearer a realistic sense of space. A binaural output would also allow the wearer to use some of their own natural binaural abilities to distinguish between the target and jammer signals, which would further improve the wearer's ability to understand a target speech signal in a noisy environment [3],[4],[27].

Hence, the goal of this thesis is to produce a fixed-filter[1] multimicrophone hearing aid with a binaural output such that:

- Each output signal possesses a directional characteristic that is most sensitive in a desired 'target' direction, assumed to be directly ahead of the wearer.

- The inter-output signal differences match, or at least reflect, the naturally occuring binaural differences between the ears.

One approach to a directional hearing aid with binaural output is simply a conventional binaural hearing aid implemented with two directional (e.g. cardioid) microphones. A microphone is located near each ear and its output is sent directly to the corresponding ear. This 'Dual-Cardioid' binaural aid achieves limited levels of directionality, and, because it can be implemented with current hearing aid configurations, it will serve as the reference against which all other binaural systems will be compared.

The Dual-Cardioid aid is a special case of one general class of binaural-output multimicrophone hearing aids that uses two independent microphone arrays to produce the binaural output, with the arrays placed so as to guarantee realistic binaural cues. Soede has briefly explored this possibility [22], and his results indicate that such a system does, in fact, increase the wearer's speech intelligibility in noise to a greater degree than a single, monaural multimicrophone hearing aid. This thesis will explore

[1] Welker [25] has studied one method of producing an adaptive multimicrophone hearing aid that produces a binaural output.

this class of system in more depth and will also introduce binaural output systems that use only one array to generate both system outputs.

The structure of this thesis is as follows:

- Chapter 2: Background Theory contains two parts. (1) A brief review of monaural output array theory – which presents the tools used to discuss and analyze microphone arrays and summarizes the performance realized by such systems. (2) An introduction to binaural listening theory, which presents the primary binaural cues that this system should maintain and also discusses the relative importance of these cues for sound localization.

- Chapter 3: System Design presents several methods for designing a multimicrophone hearing aid with binaural output that meets the two goals above or, when these goals conflict, achieves a suitable compromise between them.

- Chapter 4: Physical Evaluation presents the performance of several example systems designed using the methods of Chapter 3. These measurements allow a comparison among the various systems as well as an exploration of the effects of head-mounting upon arrays that were designed for the free-field.

- Chapter 5: Behavioral Evaluation presents the results of a behavioral evaluation conducted on several test systems, in which normal-hearing listeners used the systems for both speech intelligibility in noise and sound localization tests.

- Chapter 6: Conclusion draws the results of Chapters 4 and 5 together as a final comparison of the various multimicrophone systems with binaural output.

- Appendices A and B present some useful derivations of expressions used in this thesis.

- Appendix C presents some additional physical measurements to support the discussion in Chapter 4.

- Appendices D, E, and F present measurements and subject data to support the results of Chapter 5.

It should be noted here that two forms of multimicrophone hearing aid with binaural output have been developed and patented by Gorike [8] and Zwicker and Beckenbauer [28], respectively. These aids are relatively simple, and they form a subset of the aids considered in this thesis.

Chapter 2

Background Theory

Multimicrophone hearing aids with binaural output result from the combination of two distinct concepts: single output, directional array theory (applied to hearing aids), which involves generating a hearing aid with spatial selectivity, and binaural listening theory, which involves preserving the natural binaural cues. This chapter presents the aspects of these two theories that Chapter 3 will combine when discussing design methods for binaural, multimicrophone hearing aids.

2.1 Monaural Array Theory

Fixed filter multimicrophone hearing aids have been thoroughly studied [21],[22],[23] and their design, performance and performance limitations are all well understood. This section presents a brief review of monaural array theory, especially those aspects of it that will be used in the generation of a binaural output array system.

2.1.1 Coordinate System

Figure 2-1 shows the standard polar coordinate system used to describe all arrays discussed in this thesis. In this system, a source arriving from the (θ, ϕ) direction makes an angle of θ with the z-axis and the projection of the source arrival direction

into the x-y plane makes an angle of ϕ with the x-axis. For this thesis, the target source is always assumed to arrive from the $(\theta, \phi) = (0, 0)$ direction.

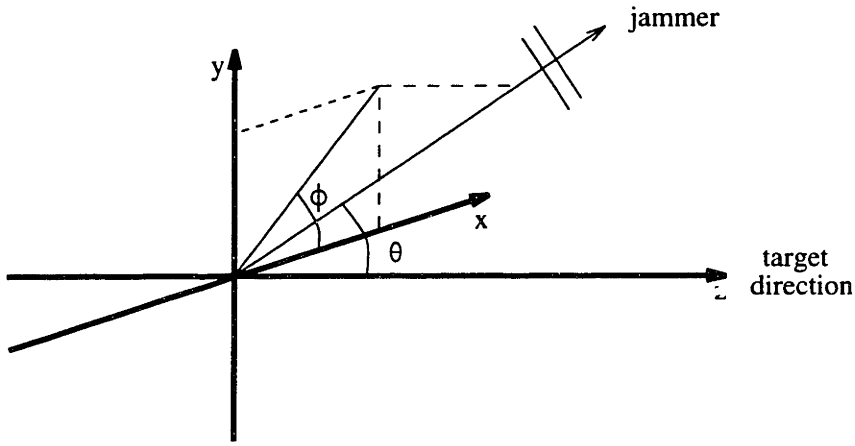

Figure 2-1: Coordinate system used to describe microphone arrays.

2.1.2 Basic Array Structure

For ease of analysis, this thesis considers only *linear* microphone arrays consisting of equally spaced elements. These arrays fall into two main categories, broadside and endfire, shown in Figure 2-2. For broadside arrays, the array axis lies perpendicular to the target signal arrival direction. For endfire arrays, the array axis lies along the target signal arrival direction. In both of these cases, the inter-element spacing is assumed to be d and the total span of an n element array is $(n-1)d$. Note that, when implemented with omnidirectional elements, both of these arrays exhibit cylindrically-symmetric behavior about the array axis. This is not necessarily true for arrays implemented with directional elements, however, because the directional response of the microphone may possess a different symmetry than the array. This thesis considers only 'mini-endfire' directional elements, which exhibit cylindrical symmetry about the z axis of Figure 2-1; therefore, broadside arrays implemented with these

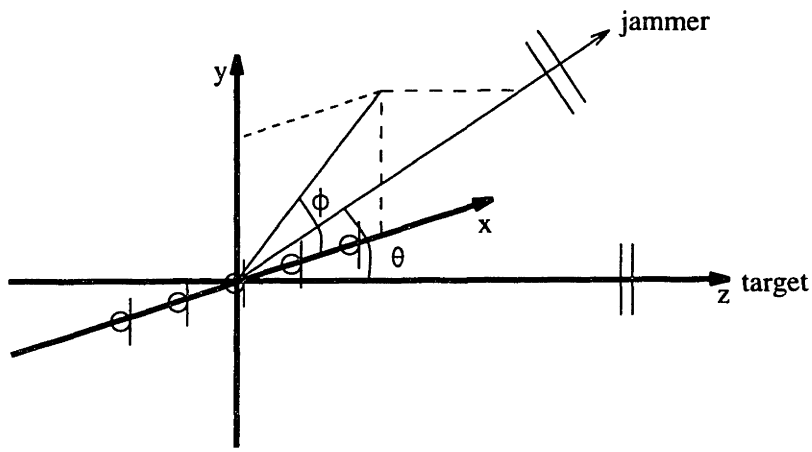

(a) Broadside array orientation.

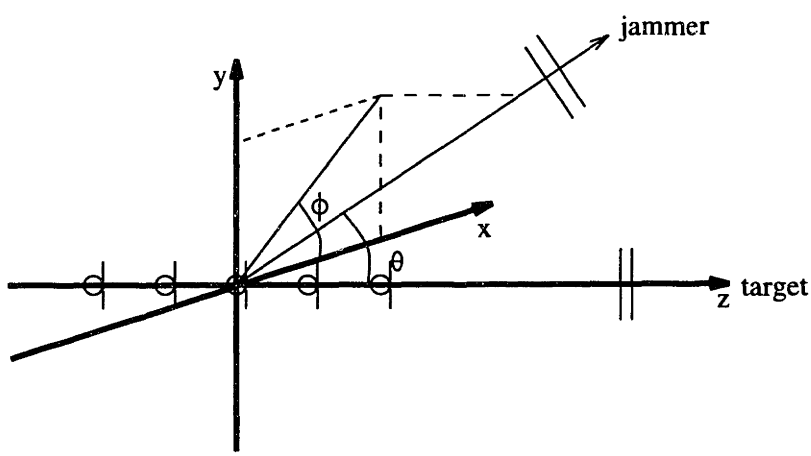

(b) Endfire array orientation.

Figure 2-2: Linear array structures.

elements lose their cylindrical symmetry while endfire arrays retain it [23].

Figure 2-3 shows the internal structure of a sample, n element array system[1]. The system output signal is formed by applying a frequency-dependent weight, $W_i(\omega)$, to each input signal, $X_i(\omega)$ = the electrical signal produced by the microphones, and summing the resulting signals. Hence, the output signal, $Y(\omega)$, is given by:

$$Y(\omega) = \sum_{i=0}^{n-1} X_i(\omega) W_i(\omega).$$

For simplicity of notation, $Y(\omega)$ can be expressed as a vector product:

$$Y(\omega) = \underline{W}^T(\omega)\underline{X}(\omega), \tag{2.1}$$

where $\underline{W}(\omega)$ and $\underline{X}(\omega)$ are the vectors of the array weights and array inputs, given by:

$$\underline{W}(\omega) = \begin{pmatrix} W_0(\omega) \\ W_1(\omega) \\ \vdots \\ W_{n-1}(\omega) \end{pmatrix} \quad \text{and} \quad \underline{X}(\omega) = \begin{pmatrix} X_0(\omega) \\ X_1(\omega) \\ \vdots \\ X_{n-1}(\omega) \end{pmatrix}$$

Before exploring the detailed properties of these arrays, first consider the methods for mounting them upon human wearers. Broadside arrays could lie along the front of a pair of eyeglasses or along a headband. Endfire arrays, on the other hand, could lie along an eyeglass temple. All arrays considered in this project are designed for the free-field, i.e. in free space, although a head-worn system is clearly *not* in the free-field. The motivation behind free-field design is that it is extremely simple, and, provided that the resulting performance loss from head mounting is not too great, these designs can lead to practical, wearable hearing aids. Based on Soede [21] and

[1]The diagram shows the array in the broadside orientation. The endfire array is *identical* in all aspects but orientation.

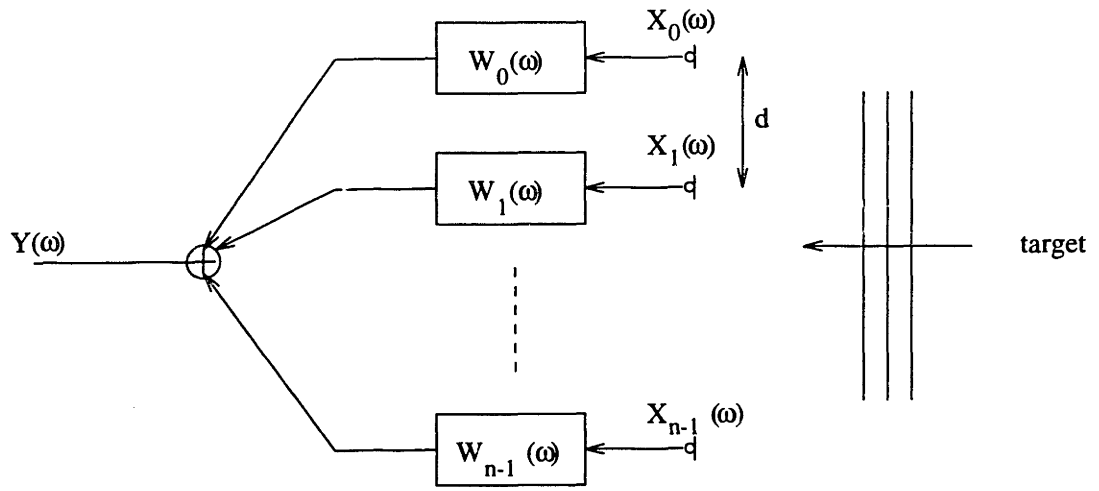

Figure 2-3: Internal structure of n element array system, showing formation of the output signal, $Y(\omega)$, as a sum of the system inputs, $X_i(\omega)$, multiplied by their respective weights, $W_i(\omega)$. In this system, d is the inter-element spacing and the total array span is $(n-1)d$.

Stadler [24], relatively little performance may be lost by using free-field designed systems on the head. The effects of head mounting on the systems designed in this thesis will be presented in Chapter 4.

2.1.3 Array Parameters

This section presents several useful parameters which assist in the description and evaluation of microphone array performance. These expressions are derived for the system structure given in Figure 2-3.

Microphone directional response, $P(\omega, \theta, \phi)$

The use of directional microphones significantly improves the directionality of the overall system. In this case, the directional response of the i^{th} microphone, i.e. the gain of the microphone for a source arriving from the (θ, ϕ) direction $P_i(\omega, \theta, \phi)$, is

needed for system design and evaluation. This thesis considers only arrays of *identical* elements, which results in:

$$P_i(\omega, \theta, \phi) = P(\omega, \theta, \phi), \quad i = 0, 1, \ldots, n-1.$$

For a more thorough description of directional microphones, consult Stadler [24].

Source-to-array transfer functions, $H_i(\omega, \theta, \phi)$

The set of transfer functions from a source located in the (θ, ϕ) direction to array element i, $H_i(\omega, \theta, \phi)$, together with $P(\omega, \theta, \phi)$, provide the means for expressing the array inputs, $X_i(\omega)$, in terms of a source signal, $S(\omega)$, arriving from the (θ, ϕ) direction: $X_i(\omega, \theta, \phi) = H_i(\omega, \theta, \phi)P(\omega, \theta, \phi)S(\omega)$. Hence, the $H_i(\omega, \theta, \phi)$ are necessary for discussing system behavior.

The actual transfer function from a given source to any array varies with source arrival direction *and* source distance from the array. To make these transfer functions independent of source distance, the arrival direction information is extracted by regarding the electrical input from element 0, $X_0(\omega, \theta, \phi)$, as a reference against which all remaining input signals are determined. In this case, $X_0(\omega, \theta, \phi) = S(\omega)$ and $H_0(\omega, \theta, \phi) = 1$. Relative to element 0, The remaining elements, $X_1, X_2, \ldots, X_{n-1}$, receive *time-shifted* versions[2] of $S(\omega)$: $X_i(\omega, \theta, \phi) = e^{-j\alpha_i(\omega,\theta,\phi)}S(\omega)$, where α_i is the additional phase experienced by $S(\omega)$ between microphones 0 and i. Provided that a source is located sufficiently far from the array that it can be regarded as arriving in plane waves, free-field arrays of equally-spaced elements result in an identical incremental phase, $\alpha(\omega, \theta, \phi)$, between each adjacent pair of microphones. Consequently, the additional phase between microphones 0 and i is equal to i of these incremental phases. Hence,

$$\alpha_i(\omega, \theta, \phi) = i\alpha(\omega, \theta, \phi).$$

[2]For these arrays, the amplitude differences between array elements are relatively small and are ignored in the design process – only inter-element delays are used.

This leads to an expression of $H_i(\omega,\theta,\phi)$ in terms of $\alpha(\omega,\theta,\phi)$:

$$H_i(\omega,\theta,\phi) = e^{-ji\alpha(\omega,\theta,\phi)},$$

or:

$$\underline{H}(\omega,\theta,\phi) = \begin{pmatrix} H_0(\omega,\theta,\phi) \\ H_1(\omega,\theta,\phi) \\ \vdots \\ H_{n-1}(\omega,\theta,\phi) \end{pmatrix} = \begin{pmatrix} 1 \\ e^{-j\alpha(\omega,\theta,\phi)} \\ \vdots \\ e^{-j(n-1)\alpha(\omega,\theta,\phi)} \end{pmatrix}. \tag{2.2}$$

Appendix A shows that, in the free-field, $\alpha_{broadside}(\omega,\theta,\phi) = \frac{\omega d}{c} sin\theta cos\phi$ and $\alpha_{endfire}(\omega,\theta,\phi) = \frac{\omega d}{c} cos\theta$, where d = the inter-element spacing and c = the speed of sound.

As mentioned above, the source-to-array transfer functions together with the microphone directional response provide the means for expressing the array inputs in terms of a source, $S(\omega)$ arriving from the (θ,ϕ) direction: directional response, $P(\omega,\theta,\phi)$:

$$X_i(\omega,\theta,\phi) = H_i(\omega,\theta,\phi)P(\omega,\theta,\phi)S(\omega).$$

In vector, this leads to:

$$\underline{X}(\omega,\theta,\phi) = \begin{pmatrix} X_0(\omega,\theta,\phi) \\ X_1(\omega,\theta,\phi) \\ \vdots \\ X_{n-1}(\omega,\theta,\phi) \end{pmatrix} = \underbrace{\underline{H}(\omega,\theta,\phi)P(\omega,\theta,\phi)}_{\underline{H}_d(\omega,\theta,\phi)} S(\omega). \tag{2.3}$$

Thus, th e directionality of the microphones can be absorbed into the source-to-array transfer function by defining a directional vector of transfer functions: $\underline{H}_d(\omega,\theta,\phi) = \underline{H}(\omega,\theta,\phi)P(\omega,\theta,\phi)$. $\underline{H}_d(\omega,\theta,\phi)$ is the vector of transfer functions from the source to the array input *after* being received by the directional element.

Directional Array Gain, $G(\omega, \theta, \phi)$

The directional array gain, $G(\omega, \theta, \phi)$, describes the directional behavior of the microphone array:

$$G(\omega, \theta, \phi) = \frac{\text{Output signal produced for } S(\omega) \text{ from } (\theta, \phi)}{S(\omega)} = \frac{Y(\omega, \theta, \phi)}{S(\omega)}.$$

The expression for the output signal formed by general input signals, $X_0(\omega), \ldots, X_{n-1}(\omega)$ (Equation 2.1) together with the expression for the array inputs that arise for $S(\omega)$ from the (θ, ϕ) direction (Equation 2.3) leads to an expression for the numerator above:

$$Y(\omega, \theta, \phi) = \underline{W}^T(\omega)\underline{X}(\omega, \theta, \phi) = \underline{W}^T(\omega)\underline{H}_d(\omega, \theta, \phi)S(\omega),$$

and so,

$$\begin{aligned} G(\omega, \theta, \phi) &= \frac{Y(\omega, \theta, \phi)}{S(\omega)} = \frac{\underline{W}^T(\omega)\underline{H}_d(\omega, \theta, \phi)S(\omega)}{S(\omega)}, \\ &= \underline{W}^T(\omega)\underline{H}_d(\omega, \theta, \phi) = \sum_{i=0}^{n-1} W_i(\omega)e^{-ji\alpha(\omega,\theta,\phi)}P(\omega, \theta, \phi), \end{aligned} \tag{2.4}$$

where the last equality comes from the fact that the i^{th} term of $\underline{H}_d(\omega, \theta, \phi)$ is the product of the i^{th} source-to-array transfer function, $e^{-ji\alpha(\omega,\theta,\phi)}$, and the microphone directional response, $P(\omega, \theta, \phi)$.

Directivity, $D(\omega)$

Directivity, $D(\omega)$, serves as a frequency-dependent measure of a microphone array's average directionality. Essentially, it reflects the system's sensitivity to a source from the target direction relative to its sensitivity to an isotropic source. By definition:

$$\begin{aligned} D(\omega) &= \frac{\text{Output power from target direction}}{\text{Average output power from all directions}} \\ &= \frac{|G(\omega, 0, 0)|^2}{\frac{1}{4\pi}\int_{\phi=0}^{2\pi}\int_{\theta=0}^{\pi} |G(\omega, \theta, \phi)|^2 \sin\theta \, d\theta d\phi} \end{aligned}$$

$$= \frac{\underline{W}^T(\omega)\underline{H}_d(\omega,0,0)\underline{H}_d^H(\omega,0,0)\underline{W}^*(\omega)}{\underline{W}^T(\omega)S_{zz}(\omega)\underline{W}^*(\omega)}, \tag{2.5}$$

where ^{T} = transpose, * = complex conjugate, ^{H} = hermitian (complex conjugate transpose), and $S_{zz}(\omega)$ is the *cross spectral density matrix* for isotropic noise, given by:

$$S_{zz}(\omega) = \frac{1}{4\pi}\int_{\phi=0}^{2\pi}\int_{\theta=0}^{\pi} H_d(\omega,\theta,\phi)H_d^H(\omega,\theta,\phi)\,sin\theta\,d\theta d\phi. \tag{2.6}$$

As discussed in Section 2.1.4 which follows, maximally directional multimicrophone hearing aids are designed to maximize the directivity at each frequency.

Noise sensitivity, $\Psi(\omega)$

Noise sensitivity, $\Psi(\omega)$, serves as a frequency-dependent measure of the sensitivity of the array to *uncorrelated* noise at the array inputs, [5],[20]:

$$\begin{aligned}\Psi(\omega) &= \frac{\sum_{i=0}^{n-1} W_i^2(\omega)}{|G(\omega,0,0)|^2}, \\ &= \frac{\underline{W}^T(\omega)\underline{W}^*(\omega)}{\underline{W}^T(\omega)\underline{H}_d(\omega,0,0)\underline{H}_d^H(\omega,0,0)\underline{W}(\omega)}.\end{aligned} \tag{2.7}$$

Typically, maximum directivity systems possess large microphone weights (particularly at low frequencies), and, consequently, the noise sensitivity is very high. For this reason, practical multimicrophone hearing aids are designed to maximize directivity *subject to* maintaining $\Psi(\omega)$ at a reasonable level.

Broadband Directivity, D_{IW}, and Noise Sensitivity, Ψ_{IW}

Directivity and noise sensitivity, as discussed above, are functions of frequency. It is often convenient to have a single number, rather than a function, to describe system behavior, which leads to the concept of a *broadband* directivity, D_{IW}, and noise sensitivity, Ψ_{IW} (which are similarly defined by Stadler and Rabinowitz, [23]). These broadband performance metrics are formed by taking the intelligibility-weighted sum

of $D(\omega)$ and $\Psi(\omega)$, in dB, at the 14 center frequencies of the third-octave bands from 200 to 4000 Hz:

$$\mathrm{D}_{IW} = \sum_{i=1}^{14} \gamma_i \, 10log(D(\omega_i)), \tag{2.8}$$

$$\Psi_{IW} = \sum_{i=1}^{14} \gamma_i \, 10log(\Psi(\omega_i)), \tag{2.9}$$

where the ω_i are the center frequencies, γ_i are intelligibility weights (as derived from French and Steinberg [7], Kryter [12],[13], and ANSI [1] and as used by Peterson [20]) applied to each band[3].

2.1.4 Maximum Directivity, Monaural Output Multimicrophone Hearing Aids

Maximum Directivity Systems

The array directivity, $D(\omega)$, given in Equation 2.5, measures the degree to which the system reduces isotropic noise relative to the target direction. In other words, this reflects the *average* directional behavior of the array, and, consequently, optimal fixed-filter microphone arrays are designed to maximize the directivity at each frequency. As shown in Stadler and Rabinowitz [23], the vector of system filters, $\underline{W}(\omega)$, which maximizes directivity is:

$$\underline{W}^T(\omega) = (\underline{H}_d^H(\omega,0,0)S_{zz}^{-1}(\omega)\underline{H}_d(\omega,0,0))^{-1}\underline{H}_d^H(\omega,0,0)S_{zz}^{-1}(\omega), \tag{2.10}$$

where $\underline{H}_d(\omega,0,0)$ is the target-to-array directional transfer function and $S_{zz}(\omega)$ is the cross spectral density matrix defined in Equation 2.6.

[3]The weights γ_i are 0.0128, 0.0320, 0.0320, 0.0447, 0.0447, 0.0639, 0.0639, 0.0767, 0.0959, 0.1182, 0.1214, 0.1086, 0.1086, and 0.0767.

Maximum Directivity Systems with Constrained Noise Sensitivity

Noise sensitivity, $\Psi(\omega)$, as presented in Section 2.1.3, measures the overall system sensitivity to uncorrelated noise at the microphones. Typically, maximum directivity systems exhibit unreasonably large levels of noise sensitivity, which causes severe degradation of system performance and renders these systems impractical to implement. As discussed in Stadler and Rabinowitz [23], it is possible to design systems that maximize directivity while constraining the noise sensitivity to be below a given level. For such a system, the optimum weight vector comes from the equation:

$$\underline{W}^T(\omega) = (\underline{H}_d^H(\omega,0,0)(S_{zz}(\omega) + \beta I^{-1}(\omega)\underline{H}_d(\omega,0,0))^{-1}\underline{H}_d^H(\omega,0,0)(S_{zz}(\omega) + \beta I)^{-1}. \tag{2.11}$$

This closely resembles Equation 2.10, except that uncorrelated noise of power β has been introduced at each of the microphones. By varying β, the noise sensitivity can be adjusted until it reaches the desired level – larger β leads to lower noise sensitivity and vice versa. For any given β, the filters $W_0(\omega),\ldots,W_{n-1}(\omega)$ that result from Equation 2.11 produce maximum directivity for the resulting noise sensitivity.

Equation 2.11 provides the means for designing a practical, realizable fixed-filter multimicrophone hearing aid that maximizes average directional behavior.

An Example Monaural Output System

In order to understand the potential performance of monaural output, fixed-filter multimicrophone hearing aids, consider the following example. This sample system has the following properties:

- Four cardioid microphones, equally spaced with 14 cm total span ($d = 4.67$ cm).
- Individual directional response for the cardioid microphone:

$$|P(\omega,\theta,\phi)| = 2|sin(\frac{\omega p}{2c}(cos\theta + 1))|$$

where p = microphone port spacing = 8.5 mm and c = the speed of sound = 345 m/s.

- Designed and evaluated for the free field case.
- Designed so that, at any given frequency, $\Psi(\omega)$ is *less* than the single microphone noise sensitivity[4] plus 5 dB.

This example system results in $D_{IW} = 8.03$ dB and $\Psi_{IW} = 7.50$ dB. The azimuth plane directional characteristic is demonstrated by a polar plot of the directional response magnitude with $\phi = 0$, i.e. $20log(|G(\omega, \theta, \phi)|)$, plotted as a function of θ for a specific frequency. Results for four frequencies are given in Figure 2-4. Note that these plots place the 0 dB curve as the outermost circle and the radial grid has 10 dB decrements. At each frequency, the system is most sensitive in the target direction ($\theta = 0$), with the sensitivity becoming more focused as frequency increases. As an overall directional characteristic, Figure 2-5 shows the intelligibility-weighted polar plot $|G_{IW}(\theta, \phi = 0)|$, where

$$|G_{IW}(\theta, \phi = 0)| = \sum_{i=1}^{14} \gamma_i 20log(|G(\omega_i, \theta, \phi = 0)|).$$

This definition is similar to that of the broadband directivity D_{IW} and noise sensitivity Ψ_{IW}.

2.2 Binaural Listening Theory

Human listeners maintain an auditory sense of the space about them through a variety of cues. The cues that are most dominant and useful for sound localization are binaural cues, which involve differences in the sounds arriving at the two ears [18]. This section presents the two primary binaural localization cues and discusses the relative importance of each one in the actual task of binaural listening.

[4]The noise sensitivity of a single microphone with directional response $P(\omega, \theta, \phi)$ is simply $\frac{1}{|P(\omega,0,0)|^2}$.

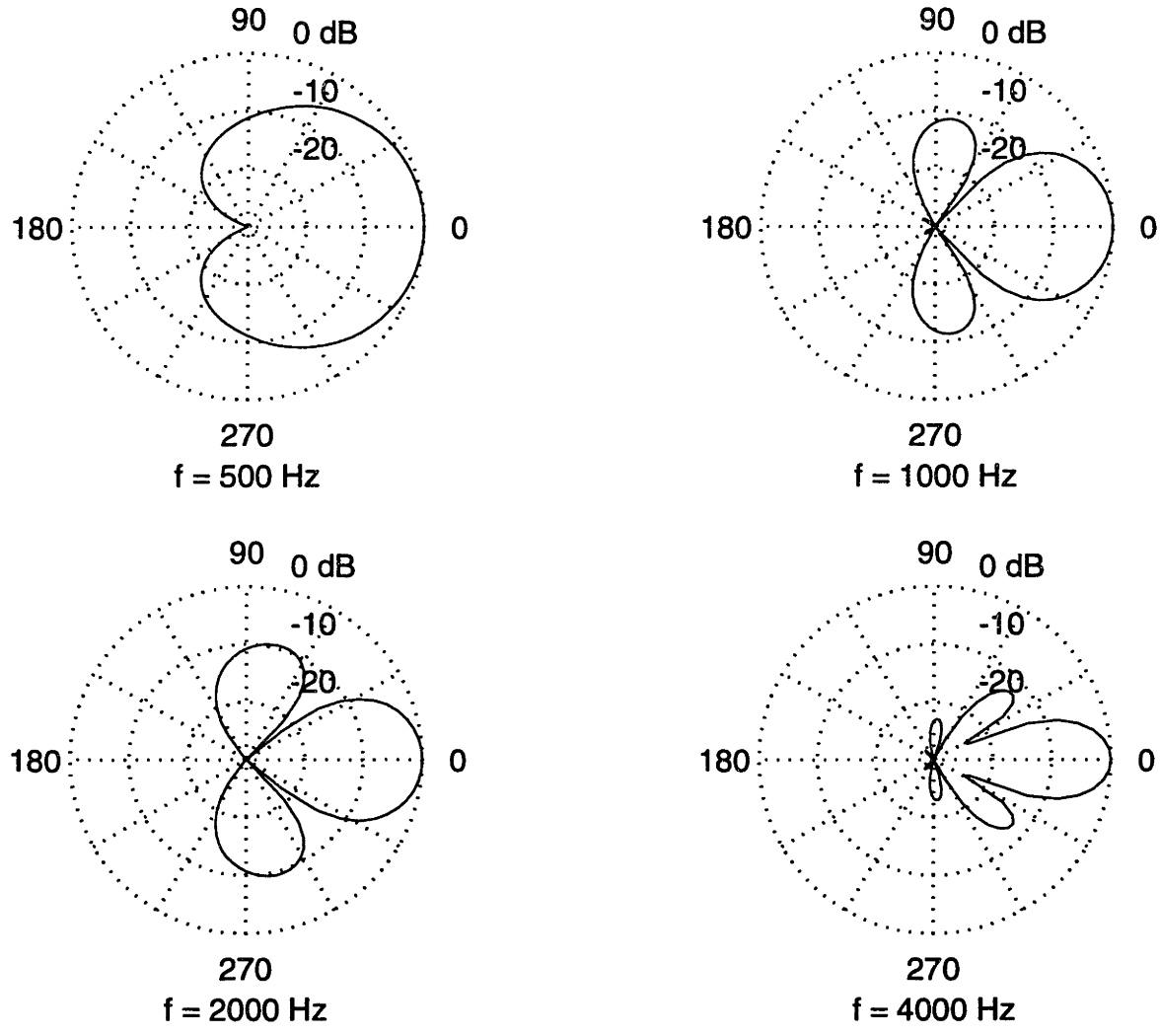

Figure 2-4: Polar plots showing the directional characteristic, in the azimuth plane, of the example broadside system at four frequencies.

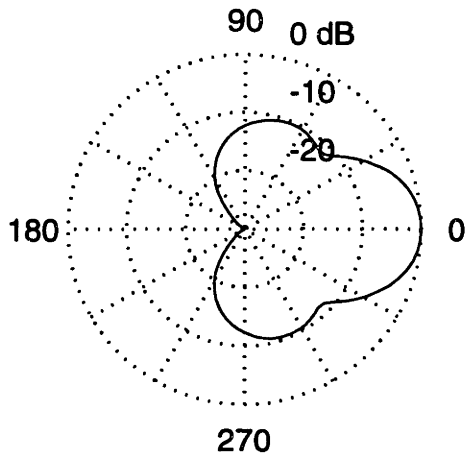

Figure 2-5: Polar plot showing the intelligibility weighted directional characteristic, in the azimuth plane, of the example broadside system.

2.2.1 Binaural Localization Cues - ITDs and ILDs

The two most important binaural cues for sound localization [18] are:

1. Interaural Time Differences (ITDs): These cues arise from the fact that a sound arriving from a certain angle will arrive at one ear earlier than at the other.

2. Interaural Level Differences (ILDs): These cues arise from the fact that a sound source will be more intense (i.e. louder) at one ear than at the other.

Listeners are quite sensitive to these time/phase and magnitude differences between the ears, and can exploit these cues as an aid to localize sound sources.

Studies have shown that ITDs are the prominent sound localization cue at low frequencies while ILDs are the prominent cue at high frequencies [18]. This makes intuitive sense, as the high-frequency signals tend to alias between the ears and the usefulness of ITDs in localization diminishes. While high-frequency *envelope* ITDs can potentially contribute to sound localization [11],[15], a study by Middlebrooks and Green [16] indicates that these cues are quite weak and are overridden by ILD

cues. A study by Wightman and Kistler [26] demonstrates that the low-frequency ITDs are, in fact, the *dominant* sound localization cue. For this reason, our efforts toward binaural cue preservation will focus on ITD maintenance.

In addition to providing a realistic sense of space, binaural cues also increase the wearer's comprehension of speech in noisy environments [27],[3],[4]. Binaural systems exploit the listener's natural abilities to use binaural cues as a means of 'focusing' on a given target source. This thesis will explore how the addition of binaural cues to the directionality of multimicrophone hearing aids affects a wearer's ability to understand speech in noisy backgrounds.

Chapter 3

System Design

Our goal is to produce a multimicrophone hearing aid that possesses both a directional characteristic *and* a binaural output. The previous chapter discussed each of these two concepts separately, and now methods of 'marrying' them together must be investigated.

3.1 System Structures

There are two basic classes of system structure that can be used to meet the above requirements:

1. Dual-Array Systems: This class of systems is the simplest extension of monaural output microphone array theory to binaural output systems. It uses two independent monaural arrays to produce the output signals (one array per output), where each array is designed to maximize directionality and the physical spacing between the two arrays yields the desired binaural cues.

   Figure 3-1(a) portrays this system as consisting of two endfire arrays. Endfire arrays suit dual-array systems, because they can be easily placed along eyeglass temples to reflect the signals arriving at a single ear, thus ensuring that the inter-array output differences reflect the natural binaural differences. Although

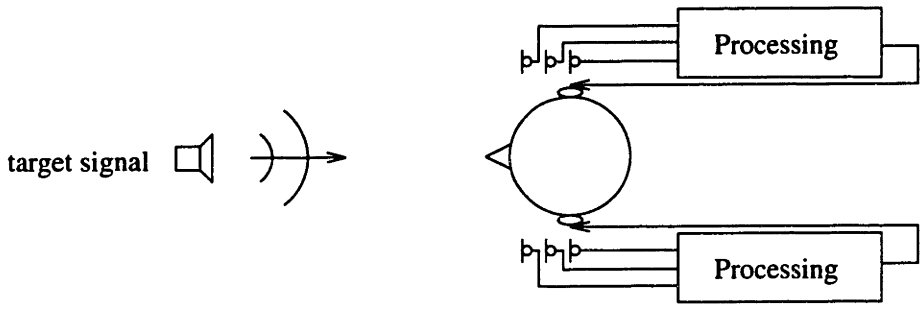

(a) Dual-Array System

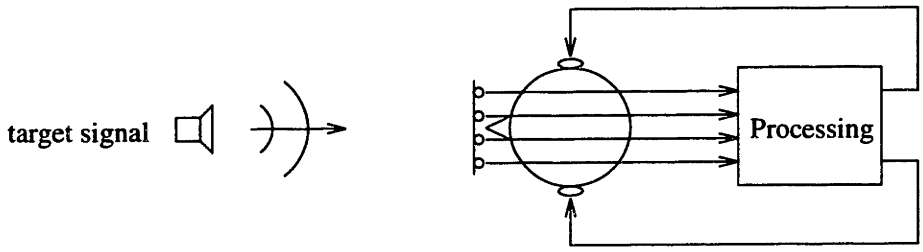

(b) Single-Array System

Figure 3-1: Two classes of system structure for a multimicrophone hearing aid with binaural output.

broadside arrays can also be used to construct dual-array systems, the physical span requirements of two sufficiently directional broadside arrays, placed to reflect the inter-ear spacing, would reduce the head-mountability of such a system.

Soede [22] conducted a behavioral evaluation using a system implemented with dual endfire arrays, on both normal and hearing-impaired listeners. His results indicated that speech intelligibility was improved over that obtained with a single, monaural output array.

2. Single-Array Systems: This class of systems uses one array to produce both system outputs, and, consequently, the system filters must be designed to *both* increase directionality and maintain binaural cues. (Note that with dual-array systems the filters maximize directionality only. Unfortunately, as discussed below, there is a trade-off between these two goals – directivity must be sacrificed so that binaural cues can be maintained.

Figure 3-1(b) depicts this system implemented with a broadside array. Broadside arrays are the only reasonable choice for single-array systems, because the span of the array reflects the natural inter-ear spacing. Endfire arrays, on the other hand, can not be used for these systems. To see why this is so, recall from Section 2.1.2 that free-field endfire arrays possess a cylindrical symmetry about the array. This symmetry means that a source, $S(\omega)$, arriving at an angle of either $+\eta$ or $-\eta$ in the azimuth plane would produce the *same* input signals, $X_i(\omega)$, at the array, and, hence, both arrival directions would yield the same output signals. However, the natural binaural cues presented by these two arrival directions should be *opposite*, and so the free-field endfire array cannot produce a realistic binaural output.

3.2 Dual-Array Systems

Figure 3-2 shows the detailed structure of a dual-array implementation of a multi-microphone hearing aid with binaural output: two independent arrays generate the two output signals $Y_0(\omega)$ and $Y_1(\omega)$. The two arrays are *identical*, so that the same weight vector, $W(\omega)$, serves to convert the array inputs into the output signals:

$$Y_0(\omega) = \underline{W}^T(\omega)\underline{X}_0(\omega) \tag{3.1}$$

$$Y_1(\omega) = \underline{W}^T(\omega)\underline{X}_1(\omega), \tag{3.2}$$

where $\underline{X}_0(\omega)$ and $\underline{X}_1(\omega)$ are the vectors of inputs to arrays 0 and 1 respectively. This equality of the two arrays results in symmetrical system behavior about the mid-sagittal plane.

3.2.1 Design Criteria

In dual-array systems, each array is designed to maximize directionality only. The output binaural cues arise from the physical separation of the two arrays and are *not* an issue in the design of the array filters. Section 3.3 will discuss, however, that single-array systems must directly account for binaural cue fidelity in the design process. As discussed in Chapter 2, directivity, $D(\omega)$, serves as the standard measure of fixed array directionality:

$$D(\omega) = \frac{\underline{W}^T(\omega)\underline{H}_d(\omega,0,0)\underline{H}_d^H(\omega,0,0)\underline{W}^*(\omega)}{\underline{W}^T(\omega)S_{zz}(\omega)W^*(\omega)}, \tag{3.3}$$

where, as defined in Chapter 2, $\underline{W}(\omega)$ = vector of filters, $\underline{H}_d(\omega,0,0)$ = vector of target-source-to-array transfer functions, and $S_{zz}(\omega)$ = the cross spectral density matrix.

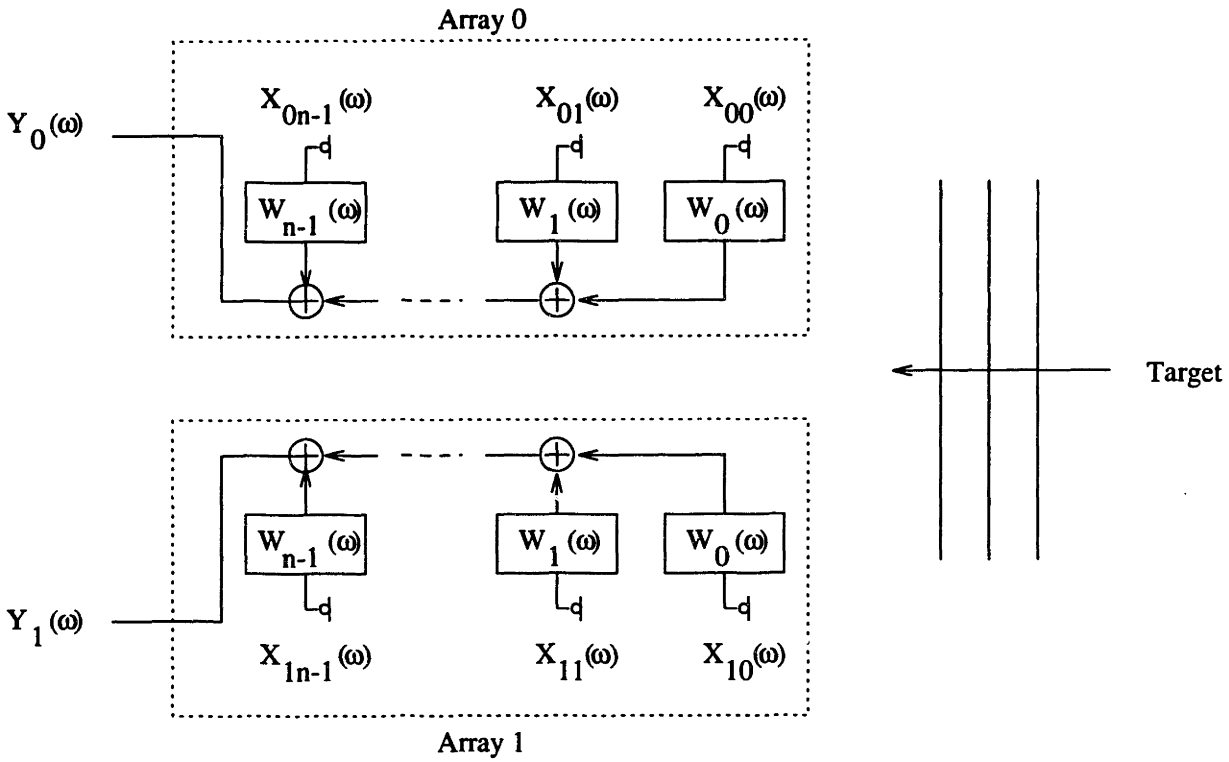

Figure 3-2: General structure of a Dual Endfire System.

3.2.2 System Design - Dual Endfire System

For dual-array systems, each (endfire) array maximizes $D(\omega)$, and the system filters arise directly from Equation 2.11, as presented in Chapter 2: These optimum directivity arrays require reasonably complex filters to implement, and, therefore, it is useful to consider some simplified endfire systems whose performance approaches that of the optimal system but requires very simple processing. Two such sub-optimal endfire systems are:

- Delay/Sum: Appropriate delays are applied to front microphone inputs so that all inputs from the target direction add *in phase* at the system output (see Figure 3-3(a)).

- +/- Gradient: This system consists of two elements and forms its output by subtracting the rear input from the front input (see Figure 3-3(b)). Clearly this array cancels sources coming directly from the side of the array, because the same signal is then incident on both array inputs. With directional elements, front/back discrimination is also achieved.

These sub-optimal systems are very simple to implement and since they result in only small losses in overall system directionality, they will be considered in the system evaluations of Chapters 4 and 5.

3.3 Single-Array Systems

Figure 3-4 shows the detailed structure of a single-array system with a binaural output, in which each array element is coupled through an independent weighting to each output signal. Essentially, this system consists of two processors, one to generate $Y_0(\omega)$ and one to generate $Y_1(\omega)$, both sharing the same physical set of elements:

$$Y_0(\omega) = \underline{W}^T(\omega)\underline{X}(\omega) \tag{3.4}$$

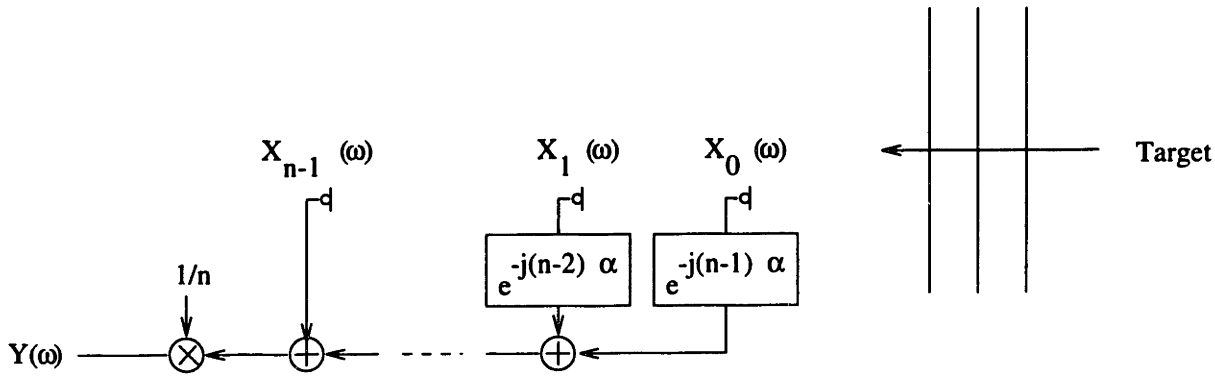

(a)Structure of Delay/Sum endfire array, where $\alpha = \alpha_{endfire}(\omega, 0, 0)$ is the inter-element delay experienced by the target signal. (See Section 2.1.3)

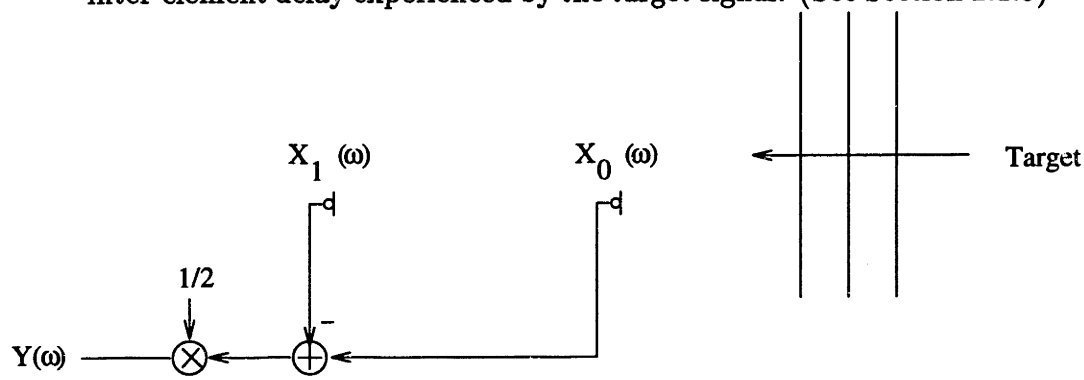

(b) Structure of the +/- Gradient array.

Figure 3-3: Structures of sub-optimal endfire arrays

and

$$Y_1(\omega) = \underline{W}_{rev}^T(\omega)\underline{X}(\omega), \tag{3.5}$$

where $\underline{X}(\omega)$ is the vector of array inputs, $\underline{W}(\omega)$ is the vector of system filters used to produce $Y_0(\omega)$ and $\underline{W}_{rev}(\omega)$ is the 'reversed' version of $\underline{W}(\omega)$:

$$\underline{W}_{rev}(\omega) = \begin{pmatrix} W_0(\omega) \\ W_1(\omega) \\ \vdots \\ W_{n-1}(\omega) \end{pmatrix} \quad \text{and} \quad \underline{W}_{rev}(\omega) = \begin{pmatrix} W_{n-1}(\omega) \\ W_{n-2}(\omega) \\ \vdots \\ W_0(\omega) \end{pmatrix}.$$

The reverse symmetry between the filters used to generate $Y_0(\omega)$ and $Y_1(\omega)$ guarantees symmetical system behavior about the mid-sagittal plane.

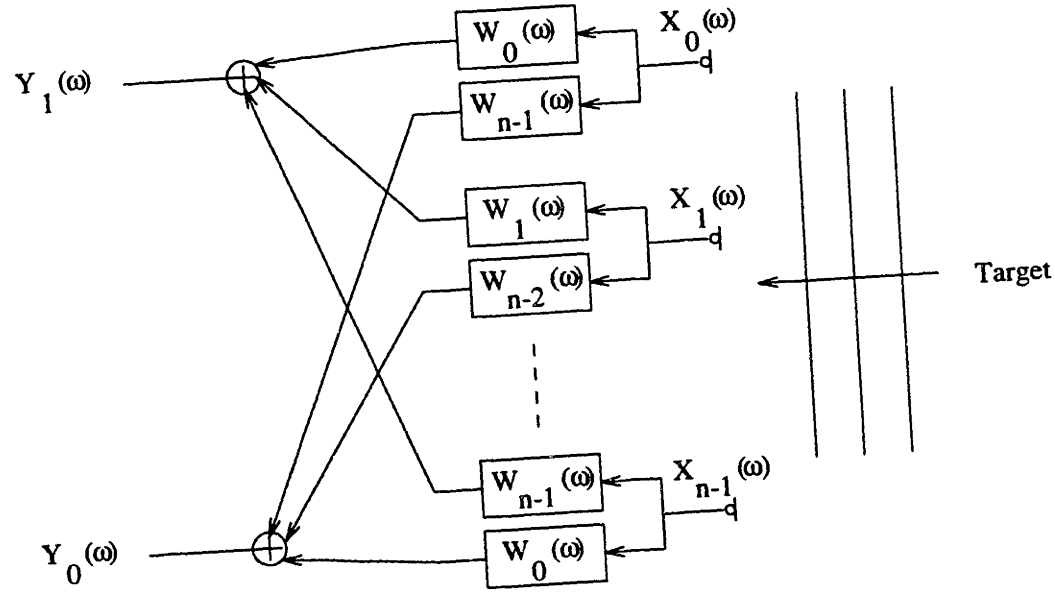

Figure 3-4: General system structure of single-array system.

3.3.1 Design Criteria

The n system filters, $W_i(\omega)$, must be selected to meet the two goals of producing a binaural output such that:

- Each output exhibits a directional characteristic that is most sensitive to sources arriving from straight ahead.

- The output inter-signal differences reflect the natural binaural differences.

The following two design criteria are used to measure the degree to which a system achieves these two goals – one criterion is for directionality and the other is for binaural cue maintenance. (The relationship between these two criteria, as well as the method for combining them to produce a practical hearing aid, is discussed in Section 3.3.2.)

Directivity, $D(\omega)$

As discussed with dual-array systems, directivity, $D(\omega)$, serves as the standard measure of the array's directional performance. In principle, each output signal, $Y_0(\omega)$ and $Y_1(\omega)$, could possess a unique directivity. However, the enforced symmetry among the system filters, as shown in Equations 3.4 and 3.5, ensures that both system outputs possess the *same* directivity.

Appendix B demonstrates how the expression for the directivity can be expressed in terms of $n-1$ system weight ratios, $R_1(\omega) = \frac{W_1(\omega)}{W_0(\omega)}, \ldots, R_{n-1}(\omega) = \frac{W_{n-1}(\omega)}{W_0(\omega)}$, and

$$D(\omega) = \frac{\underline{R}^T(\omega)P(\omega,0,0)\underline{H}(\omega,0,0)\underline{H}^H(\omega,0,0)P^*(\omega,0,0)\underline{R}^*(\omega)}{\underline{R}^T(\omega)S_{zz}(\omega)\underline{R}^*(\omega)}, \qquad (3.6)$$

where $\underline{R}(\omega)$ is defined as:

$$\underline{R}(\omega) = \begin{pmatrix} 1 \\ R_1(\omega) \\ R_2(\omega) \\ \vdots \\ R_{n-1}(\omega) \end{pmatrix}.$$

These ratios, together with the constraint of unit gain in the target direction, completely specify the system filters and, moreover, they allow for the simplification of the system design process by reducing the number of variables by one. This variable reduction is helpful in the combined system approach to single-array systems presented in Section 3.3.2, because this approach involves intensive numerical optimization in order to determine $\underline{W}(\omega)$.

ITD Error, $E(\omega)$

No standard measure, such as $D(\omega)$ for directionality, exists to measure binaural cue fidelity, and, therefore, one had to be determined for specifying system design. Chapter 2 presented the two primary binaural cues for sound localization in the azimuth plane: interaural time differences (ITDs) and interaural level differences (ILDs). Since low-frequency ITDs are the *dominant* sound localization cue [26] [2], a design criterion based on ITD maintenance was selected. Specifically, we form $E(\omega)$, defined as the RMS ITD error at ω, averaged over three-space:

$$E(\omega) = \sqrt{\frac{1}{4\pi}\int_0^{2\pi}\int_0^{\pi}(\mathrm{ITD}_{desired}(\omega,\theta,\phi) - \mathrm{ITD}_{output}(\omega,\theta,\phi))^2 sin\theta \; d\theta d\phi} \qquad (3.7)$$

where $\mathrm{ITD}_{desired}$ is the ITD that the system is trying to preserve and ITD_{output} is the ITD actually generated by the system.

For the system in Figure 3-4, $\mathrm{ITD}_{desired}$ is assumed to be the inter-signal difference experienced by the two outermost array elements, $X_0(\omega)$ and $X_{n-1}(\omega)$, which are

nominally separated by a headwidth. This ITD reflects the true ITDs at the wearer's ears (assuming that the outermost elements are near the ears), and it is specified simply from the array structure. For the purposes of this thesis, $\text{ITD}_{desired}$ is defined as the *phase delay* between $X_0(\omega)$ and $X_{n-1}(\omega)$, which, as shown in Appendix B, is simply:

$$\text{ITD}_{desired}(\omega,\theta,\phi) = \frac{(n-1)d}{c} sin\theta cos\phi. \tag{3.8}$$

The source-to-array transfer functions, $\underline{H}(\omega)$, together with the system filters, $W_i(\omega)$, determine ITD_{output}, which, as shown in Appendix B, can be expressed in terms of the ratios, $R_i(\omega)$, that were defined above:

$$\begin{aligned}\text{ITD}_{output}(\omega,\theta,\phi) &= (n-1)\alpha(\omega,\theta,\phi) \\ &\quad + tan^{-1}\left(\frac{\sum_{i=1}^{n-1}|R_i(\omega)|sin[\angle R_i(\omega)-(i-1)\alpha(\omega,\theta,\phi)]}{1+\sum_{i=1}^{n-1}|R_i(\omega)|cos[\angle R_i(\omega)-(i-1)\alpha(\omega,\theta,\phi)]}\right) \\ &\quad - tan^{-1}\left(\frac{\sum_{i=1}^{n-1}|R_i(\omega)|sin[\angle R_i(\omega)+(i-1)\alpha(\omega,\theta,\phi)]}{1+\sum_{i=1}^{n-1}|R_i(\omega)|cos[\angle R_i(\omega)+(i-1)\alpha(\omega,\theta,\phi)]}\right).\end{aligned} \tag{3.9}$$

It should be noted that each of the systems designed in this thesis had the property that the phases of terms within the weight vector, $\underline{W}(\omega)$, were equal, and so $\angle R_i(\omega) = 0,\ \forall\ i$. In this case, Appendix B shows that the expression for ITD_{output} can be simplified to:

$$\begin{aligned}\text{ITD}_{output}(\omega,\theta,\phi) &= (n-1)\alpha(\omega,\theta,\phi) \\ &\quad - 2tan^{-1}\left(\frac{\sum_{i=1}^{n-1}R_i(\omega)sin[i\alpha(\omega,\theta,\phi)]}{1+\sum_{i=1}^{n-1}R_i(\omega)cos[i\alpha(\omega,\theta,\phi)]}\right).\end{aligned} \tag{3.10}$$

Provided that single-array systems will always possess equal phase weight vectors, this simplifies the optimization for system design further by reducing the optimization $n-1$ complex variables to $n-1$ real variables.

It can be argued that $\angle R_i(\omega)$ will always equal zero for optimal single-array systems. To see why this is so, consider maximally directive, monaural broadside systems

first. Inspection of the target-to-array transfer functions, $\underline{H}_d(\omega, \theta, \phi)$, and the cross spectral density matrix, $S_{zz}(\omega)$, reveals that the equation for the optimal system weights (Equation 2.11) always results in *real* system filters[1], which means that the maximally directive system always delays the target signal so that it adds *in phase* (except for shifts of π) when forming the system output. Extending this argument to binaural output single-array systems: although they do not actually form the maximally directive signal, they realize the maximum achievable directivity subject to constraints on $E(\omega)$ by ensuring that the target signal always adds in phase at the system outputs. Hence, these single-array systems also possess the property that all weight vectors have identical phase responses[2] and, consequently, $\angle R_i(\omega) = 0$.

Substituting Equations 3.8 and 3.10 into Equation 3.7 leads to a frequency-dependent measure of ITD error, $E(\omega)$, which depends only upon the system structure and the system ratios.

$D(\omega)$ and $E(\omega)$ serve as measures of the two system goals – larger $D(\omega)$ results in more directionality and smaller $E(\omega)$ results in better binaural-cue fidelity. Hence, the goal of single-array systems is to maximize $D(\omega)$ and to maintain $E(\omega) = 0$.

3.3.2 $D(\omega)$ vs $E(\omega)$ Trade-off and Possible System Designs

The goals of maximizing $D(\omega)$ and minimizing $E(\omega)$ are at odds with one another and cannot be simultaneously satisfied:

- Recall from Chapter 2 that, for any given array, there is a unique set of filters that maximizes the directivity for a given output, given by Equation 2.11. If the system were designed so that each output signal possessed maximum directivity, then the two outputs would be generated using exactly the same filters and,

[1] Obviously, the system cannot actually be real (i.e. non-causal), but a linear delay can be added to each filter to ensure causality.

[2] This argument does *not* apply to systems implemented with non-broadside arrays. It can be shown that for maximum directivity endfire arrays, the target signal does not always add in phase at the system output, a phenomenon known as oversteering [21]

consequently, the two output signals would be identical – the output would be *diotic.*

- As stated above, the desired ITD is assumed to be the ITD experienced by the two outermost array elements. In this case, a system would maintain $E(\omega) = 0$ by simply passing the outermost microphone inputs to their respective ears with no other coupling between the array inputs and the outputs: $W_0(\omega) = 1$ and $W_i(\omega) = 0$, $i = 1, 2, \ldots, n-1$. The system forms each output using a single microphone and, consequently, it does not take advantage of the array structure to increase overall system directionality.

Notwithstanding these extremes a continuous trade-off between $D(\omega)$ and $E(\omega)$ is possible at any given frequency, and two facts can be exploited that allow this trade-off to be used to combine the system goals:

1. Low-frequency ITDs are the dominant sound localization cue [26],[2].

2. Only minimal directivities can be realized by broadside arrays at low frequencies [21],[23].

This suggests the design of a system which focuses on ITD preservation at low frequencies and directivity maximization at high frequencies. Two main types of systems emerge: (1) a Combined system, which uses the $D(\omega)$-$E(\omega)$ trade-off to achieve some combination of the two goals at each frequency, with the relative importance of each goal governed by the two facts above, and (2) a Lowpass/Highpass system, that maintains $E(\omega) = 0$ at low frequencies and maximizes $D(\omega)$ at high frequencies.

Combined System

Figure 3-5 shows the $D(\omega)$ vs $E(\omega)$ trade-off at 1000 Hz for a four-element broadside array of cardioid elements with a total span of 14 cm. These results were obtained by maximizing $D(\omega)$ as a function of the *maximum* allowable $E(\omega)$. It shows that

directivity gains that exceed those of a single microphone (indicated by an 'x' at 0 ITD error on the plot) can be achieved by allowing some ITD error.

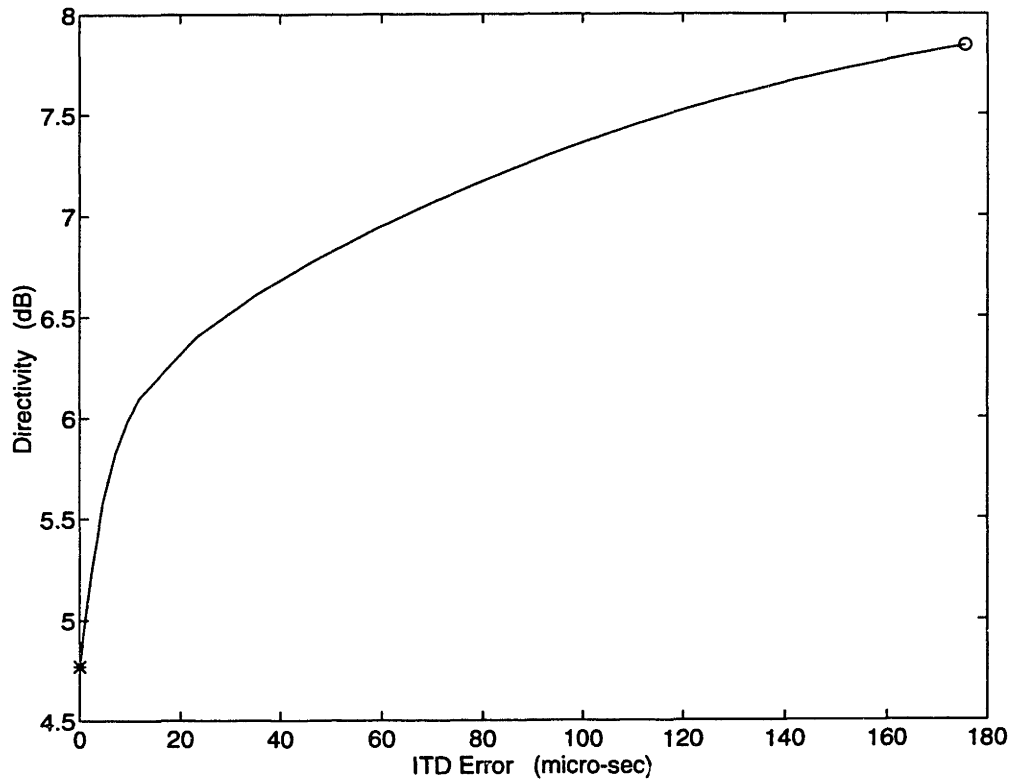

Figure 3-5: $D(\omega)$ vs $E(\omega)$ trade off at f=1000 Hz.

The Combined system incorporates this trade-off and the system ratios, $R_i(\omega)$, are then determined by maximizing $D(\omega)$ while maintaining $E(\omega)$ below a given, frequency dependent threshold:

$$\begin{aligned} &\max_{R_i} D(\omega) \\ &\text{constrained so that : } \quad E(\omega) < \tau(\omega) = \text{threshold ITD error.} \end{aligned} \tag{3.11}$$

For this design process, the error threshold, $\tau(\omega)$, reflects the ITD sound localization importance as a function of frequency. At each frequency, the resulting system op-

erates at some point along a trade-off curve, such as that of Figure 3-5, governed by $\tau(\omega)$.

Recall from Chapter 2 that systems which maximize $D(\omega)$ possess unreasonably large levels of noise sensitivity. This is also the case for the Combined system when designed using the optimization above. Unfortunately, no 'clean' method, analogous to that of Equation 2.11, exists for incorporating noise sensitivity into this design process, and $\Psi(\omega)$ is controlled by adding it as a second constraint in the numerical optimization that the $R_i(\omega)$ must satisfy:

$$\begin{aligned} &\max_{R_i} D(\omega) \\ \text{constrained so that :} \quad &E(\omega) < \tau(\omega) \\ \text{and :} \quad &\Psi(\omega) < \Psi_{max}(\omega). \end{aligned} \tag{3.12}$$

In this way, $\Psi(\omega)$ can be maintained at an acceptable level.

Lowpass/Highpass System

The Lowpass/Highpass system divides the frequency spectrum into two bands, separated by a cut-off frequency, f_c, and focuses on ITD preservation ($E(\omega) = 0$) below f_c and directivity maximization above f_c[3]. In terms of Figure 3-5, the system operates at the $E(\omega) = 0$ point, marked by an 'x', for $f < f_c$ and at the maximum $D(\omega)$ point, marked by an 'o', for $f > f_c$. The Lowpass/Highpass system is actually a special case of the Combined System, with the system ratios selected to:

$$\begin{aligned} &\max_{R_i} D(\omega) \\ \text{constrained so that :} \quad &E(\omega) < \tau(\omega) \begin{cases} 0 & \omega \leq 2\pi f_c \\ \infty & \omega > 2\pi f_c \end{cases} \\ \text{and :} \quad &\Psi(\omega) < \Psi_{\max} \end{aligned} \tag{3.13}$$

[3]This lowpass/highpass approach was used by Welker [25] to develop an adaptive binaural multimicrophone aid, in which the common high-frequency component of the outputs was generated using the Griffiths-Jim adaptive beamformer [9]

Although the system filters can be designed via the numerical optimization above and implemented with the structure of Figure 3-4, there is a simpler implementation which leads to a simpler design method. Figure 3-6 shows this implementation: the outermost array input signals, $X_0(\omega)$ and $X_{n-1}(\omega)$, are lowpass filtered and sent directly to their respective ears while a common high-frequency component is formed using the optimal directivity weights (obtained from Equation 2.11 for the desired level of $\Psi(\omega)$).

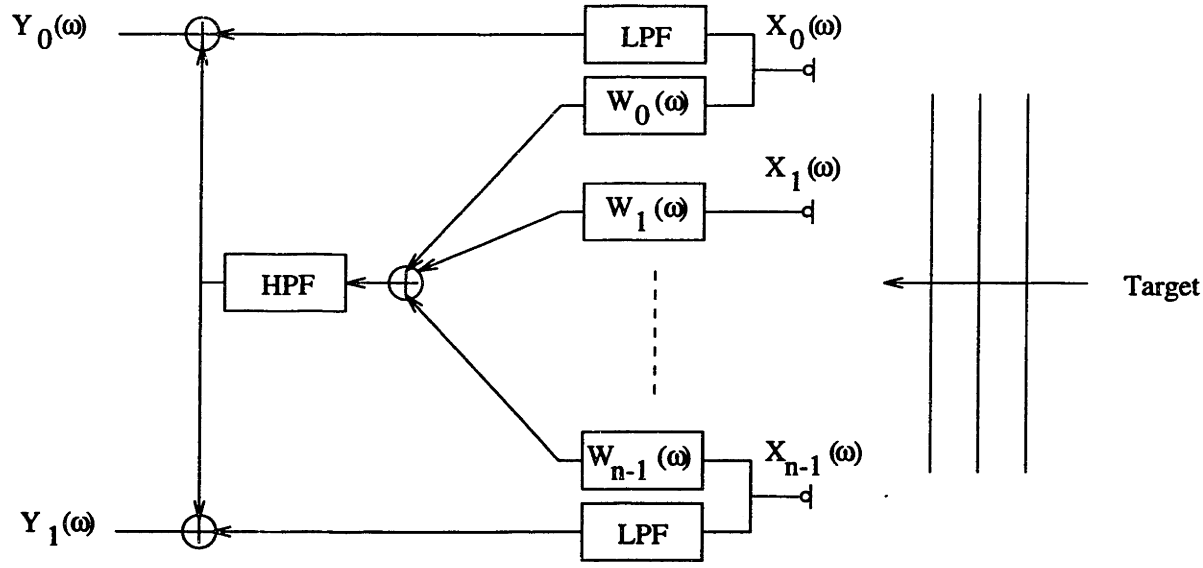

Figure 3-6: Simplified Lowpass/Highpass system structure.

The design of this system is much simpler than that of the Combined system, because the optimum directivity filters have a closed form solution, and they require no numerical optimization. More importantly, this system is easier to implement: given an n-element array, it requires only $n + 3$ filtering operations versus the $2n$ required for the general single-array structures and, hence, the Combined system.

Sub-optimal Lowpass/Highpass Systems One property of broadside arrays is that arrays implemented with optimum directivity weights achieve only small gains

in $D(\omega)$ over arrays implemented with uniform weights (where the array inputs are simply averaged to form the output) [21],[23]. Moreover, most of the loss in $D(\omega)$ occurs at the *low* frequencies, which suggests that uniform weights could be used to generate the common high frequency component of the output signals of the Lowpass/Highpass system without causing a substantial decrease in performance. The main advantage to such a system is its simple structure, shown in Figure 3-7, and ease of implementation. It could be easily implemented using analog circuitry. In Chapters 4 and 5, it will be evaluated and compared with the optimal single array systems as well as optimal and sub-optimal dual-array systems.

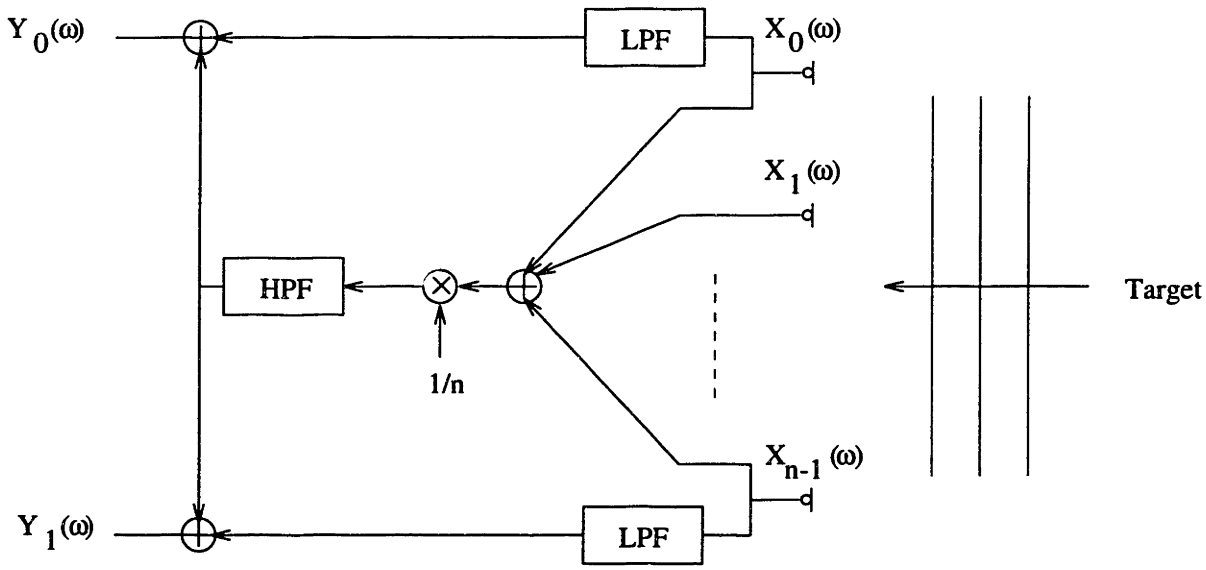

Figure 3-7: Sub-optimal Lowpass/Highpass System with the high-frequency output component formed using uniform weights on the array.

This chapter has presented the two main classes of binaural-output multimicrophone systems (dual-array and single-array) as well as several design methods (both

optimal and sub-optimal) for these classes. Since these systems are based on different design criteria (maximizing directionality vs. maximizing both directionality and binaural cue fidelity) and implemented with different array structures (endfire vs. broadside), they should perform differently. The following chapters will explore system performance and will compare these two classes as well as the design methods within each class.

Chapter 4

Physical Evaluation

This chapter presents the results of a physical evaluation made on several test systems. It begins by examining the free-field and head-mounted performance of an 'optimal' conventional binaural hearing aid, the Dual-Cardioid aid, that consists of two cardioid microphones located near the ears with the outputs sent directly to the respective ears. This system serves as a reference against which to compare the performance of the binaural output microphone array hearing aids. The chapter continues by presenting the results for several example dual- and single-array systems, designed as discussed in Chapter 3, which were tested in both free-field and head-mounted situations.

The evaluation involved two types of measurements: (1) the azimuth-plane directional characteristic, $|G(\omega, \theta, \phi = 0)|$, and (2) the azimuth-plane output ITDs.

4.1 Testing Procedure

All measurements were performed in an anechoic chamber, with the test system mounted on either a stand (for the free-field case) or on a KEMAR manikin (for the head-mounted case). The stand (or KEMAR) was mounted upon a turntable, which could be programmably turned to any position in the azimuth plane, with an

Optimus Pro-7 loudspeaker placed 1 m away from the turntable. This combination of turntable and loudspeaker allowed convenient measurement of array performance for sound sources arriving from any azimuth angle (see Figure 4-1).

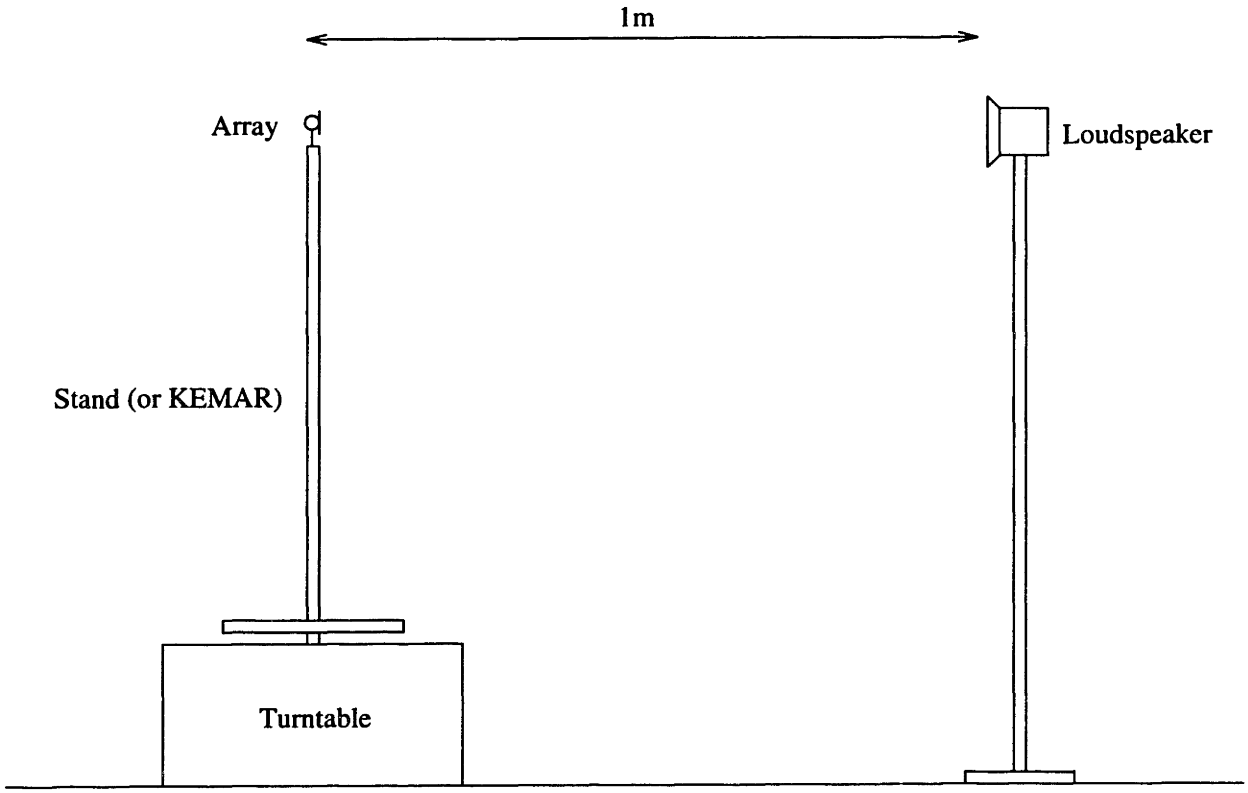

Figure 4-1: Basic testing environment, with the array located on a turntable and the speaker 1 m away. The array is mounted on either a stand (for free-field measurements) or on KEMAR (for head mounted measurements). All measurements were made in an anechoic chamber.

4.1.1 Directional Characteristic Measurements

Measurements of the test systems' azimuth-plane directional characteristics were taken at 10° intervals from 0° to 350°. These measurements were made by first

turning the array so that the source was located at the desired angle, θ_0, presenting a periodic chirp (produced by an HP35660A spectrum analyzer) to the system, and measuring the resulting value of $|G(\omega, \theta_0, \phi = 0)|$ (using the spectrum analyzer). This $|G(\omega, \theta_0, \phi = 0)|$ was then summed over frequency to determine the total power in each of the fourteen third octave bands, with center frequencies from 200 to 4000 Hz. These fourteen powers, rather than the actual measured $|G(\omega, \theta, \phi = 0)|^2$, were then interpreted as the measured values of $|G(\omega, \theta_0, \phi = 0)|^2$ at these center frequencies.

A revised directivity measure allows for an easy comparison of the measured directional characteristics with the theoretically predicted one. Since the measurements were made only in the azimuth plane $|G(\omega, \theta, \phi = 0)|$, it was useful to form a two-dimensional (azimuthal) version of directivity, defined as:

$$D_{az}(\omega) = \frac{|G(\omega, 0, 0)|^2}{\frac{1}{2\pi}\int_0^{2\pi} |G(\omega, \theta, 0)|^2 d\theta}. \tag{4.1}$$

This differs from the standard directivity definition, given in Equation 2.5, in that the denominator contains the average system output power from the azimuth plane only and not from all of three-space[1]. As with conventional directivity, an intelligibility-weighted version of azimuth directivity, $D_{IW,az}$, can be formed. Although $D_{IW,az}$ does not equal D_{IW}, it preserves the correct relative ordering, within each class, for all systems tested in this study. Consequently, this two-dimensional measure will serve as the primary means of comparing directional performance in the following sections.

4.1.2 ITD Measurements

In a manner similar to that above, azimuth-plane ITD measurements were taken at 30° increments from 0° to 330°. These measurements were taken by turning the array to the desired θ_0, presenting a periodic chirp to the speaker, and measuring the

[1]The denominator integral here was approximated by a finite sum for all measured results, as the values of $|G(\omega, \theta, \phi = 0)|$ were taken at only 36 values of θ.

resulting inter-output phase differences. These phase differences were then smoothed with a 7-point moving average filter and converted into output ITDs via:

$$\mathrm{ITD}_{output}(\omega, \theta_0, \phi = 0) = \frac{\text{inter-output phase difference}(\omega, \theta_0, \phi = 0)}{\omega}. \quad (4.2)$$

Rather than considering the RMS ITD error, as defined in Chapter 3 and which is a design criterion only for single-array systems, this chapter will present ITD results in the form of the actual output ITDs produced by the system for a source arriving from 0°, 30°, 60°, and 90°. By comparing the actual output ITDs with the theoretically predicted output ITDs, the degree of ITD fidelity can be observed.

4.2 Conventional, Dual-Cardioid Binaural Hearing Aid

This system consisted of two cardioid microphones, separated by 14 cm for free-field measurements and located near the ears for head-mounted measurements. For either mounting, the output of each microphone was sent directly to the corresponding ear. Each microphone (Knowles EL-3085) had a (theoretical) directional response of:

$$|P(\omega, \theta, \phi)| = 2|sin(\frac{\omega p}{2c}(cos\theta + 1))|,$$

where p = microphone port spacing = 14 mm and c = the speed of sound = 345 m/s. Furthermore, the responses of the two microphones were (roughly) equalized through the application of a scale factor to one microphone. This system was implemented in real time using two Ariel DSP-96 boards, each of which contained a Motorola DSP96002 signal processing chip and dual channel I/O. (Although one board would have easily sufficed for this system, the remaining systems required four channels of A/D input, and so two boards were necessary.) This implementation included filtering each output with a single-pole (p=0.897), single-zero (z=0.572) IIR filter

to compensate for the linear ω dependence evident in the microphone directional response, $|P(\omega, \theta, \phi)|$, for low frequencies.

4.2.1 Directionality Measurements

Table 4.1 shows the theoretically predicted free-field values of D_{IW} and $D_{IW,az}$ as well as the free-field and head-mounted values of $D_{IW,az}$ for this system, with the measured values given for the right (R) and the left (L) outputs. These results indicate that head mounting causes only a small (less than 1 dB) degradation in the system directionality.

Table 4.1: Directionality (in dB) of conventional Dual-Cardioid binaural hearing aid in the free-field and head-mounted near the ears.

Theoretical D_{IW} (dB) Free-Field	Theoretical $D_{IW,az}$ (dB) Free-Field	Measured $D_{IW,az}$ (dB)	
		Free-Field	Head-Mounted
4.59	4.03	4.20(R) 4.15(L)	3.34(R) 3.34(L)

To further illustrate the effects of head-mounting upon this system, Figures 4-2 and 4-3 show the intelligibility-weighted azimuth-plane polar plots, $|G_{IW}(\theta, \phi = 0)|$ for the right and left ears, respectively. The measured free-field curves follow theory very well, while the head-mounted curves, as expected, display head-shadow effects. Figure 4-2 (c) shows that the cardioid microphone mounted on the right side of the head is more sensitive to sound arriving from the right and less sensitive to sound arriving from the left, which is a direct result of head-shadowing upon sources from the left. The opposite behavior is evident for the left microphone (Figure 4-3 (c)). Nevertheless, in the head-mounted case, the directional patterns of the two outputs

still possess an increased sensitivity in the target direction – head mounting degrades directionality only slightly. In fact, the quantitative loss in directivity is due primarily to the gain (above 0 dB) evident between roughly 0° and 45° toward the ear with the microphone.

4.2.2 Output ITD Measurements

For the free-field mounting, the expected output ITDs of this system are simply the ITDs experienced by two microphones located 14 cm apart. This result is the same as the value for $\text{ITD}_{desired}$, given in Equation 3.8, for the case of a single-array system with a total array span of $(n-1)d = 14$ cm. Substituting this value into Equation 3.8 leads to theoretical free-field output ITDs of:

$$\text{ITD}_{output}(\omega, \theta, \phi) = \frac{0.14}{c} sin\theta \, cos\phi.$$

Figure 4-4 shows the measured free-field and head-mounted output ITDs for sources arriving from angles of 0°, 30°, 60°, and 90°, with the theoretical curves (generated using the equation above) indicated by dotted lines in each plot. As expected, the free-field results agree with the theoretical predictions quite well. The head-mounted system, on the other hand, produces consistently larger output ITDs than the theoretical predictions. This arises because the actual distance between the two cardioid microphones at the ears is *greater* than the 14 cm free-field separation and because of sound diffraction about the head [14].

4.3 Dual-Array Systems

The dual-array systems were designed for the free-field and possessed the following structure:

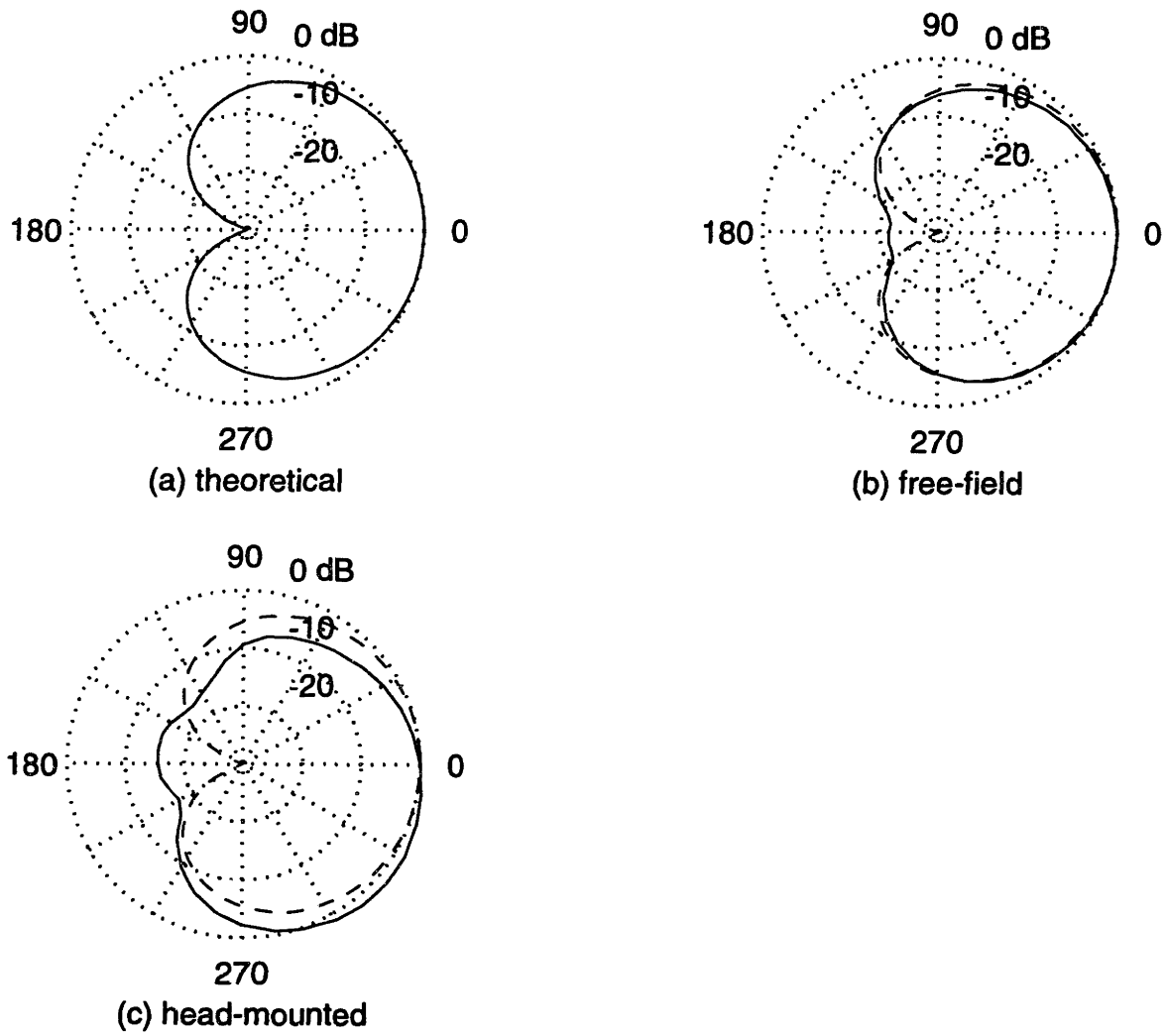

Figure 4-2: Intelligibility-weighted polar plot of the dual cardioid directional response – right ear (270°): (a) theoretical pattern, (b) measured free-field pattern, and (c) measured head -mounted pattern. In both measured plots, the theoretical curve is indicated by a dashed line.

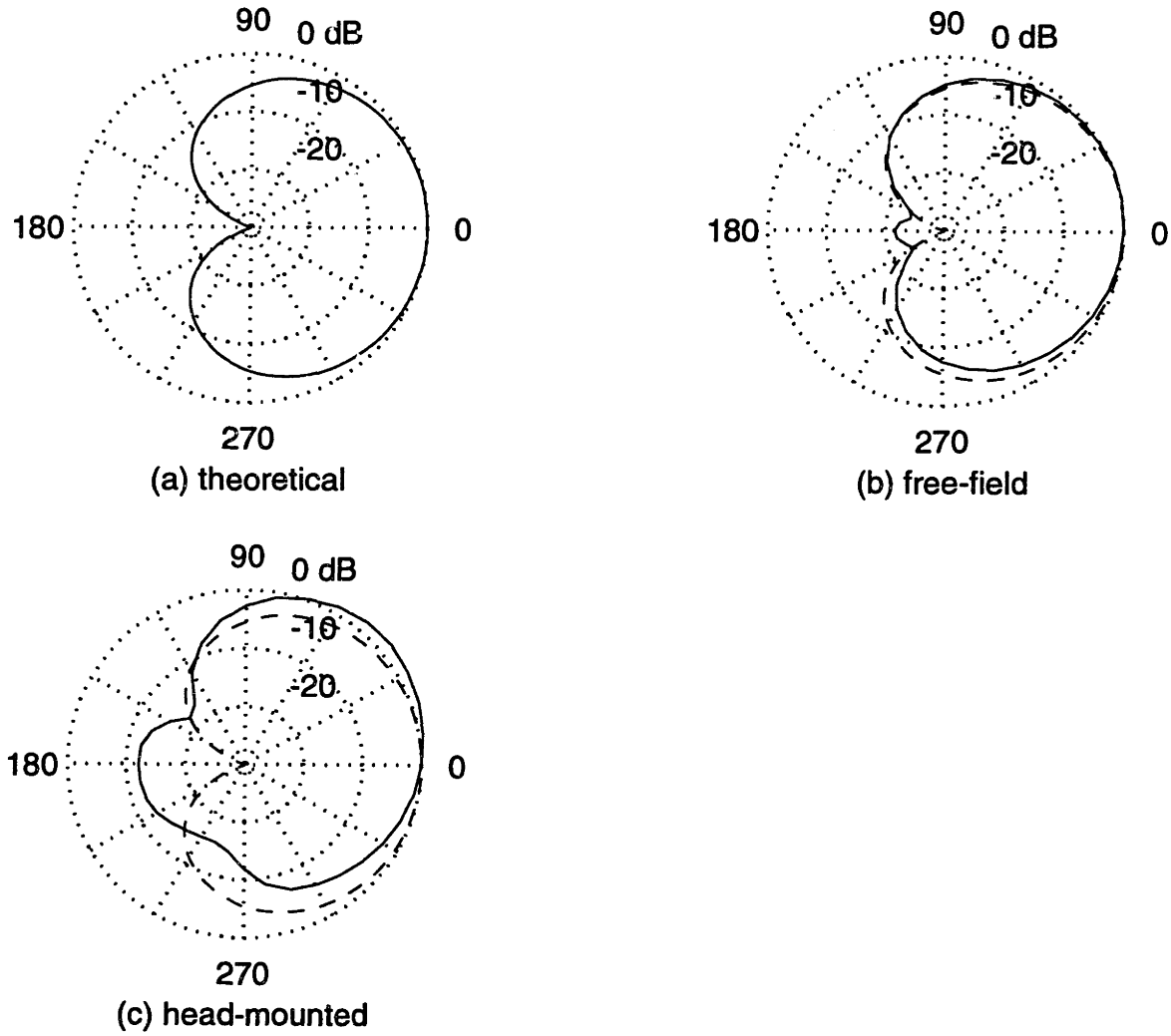

Figure 4-3: Intelligibility-weighted polar plot of the dual cardioid directional response – left ear (90°): (a) theoretical pattern, (b) measured free-field pattern, and (c) measured head-mounted pattern. In both measured plots, the theoretical curve is indicated by a dashed line.

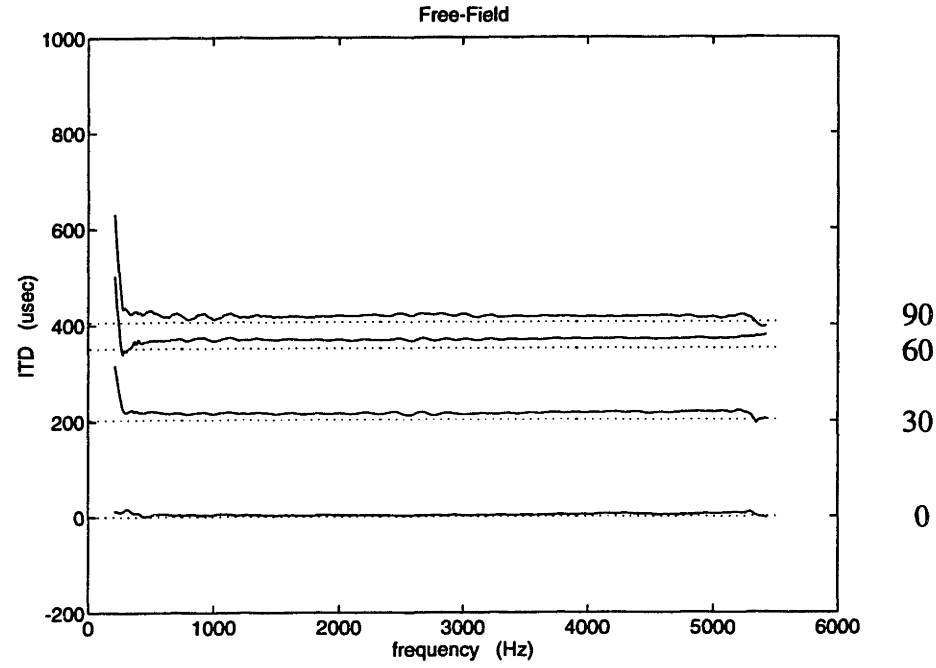

(a)

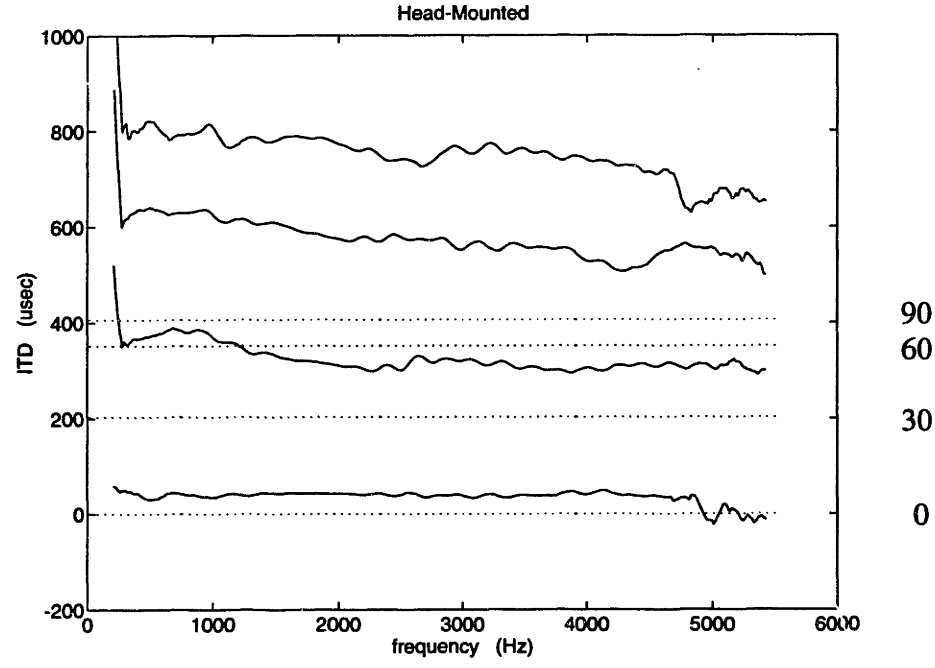

(b)

Figure 4-4: Measured output ITDs for the conventional, dual cardioid, binaural hearing aids for (a) free-field and (b) head-mounted near the ears. Dotted lines indicate theoretical free-field results.

- Dual, two-cardioid-element endfire arrays, with a center-to-center microphone spacing of 9.2 cm (2.6 cm for the special case of the Dual +/- Gradient arrays)[2]

- Individual cardioid microphone (Knowles EL-3085) response:

$$|P(\omega,\theta,\phi)| = 2|sin(\frac{\omega p}{2c}(cos\theta + 1))|,$$

  where p = the microphone port spacing = 14 mm. Note: these microphones are the same type as the ones used for the conventional, Dual-Cardioid, binaural hearing aid of Section 4.2, and the individual responses were roughly equalized by applying scale factors to three of the four microphones.

These systems were implemented in real time using two Ariel DSP-96 boards – one board per array. As with the Dual-Cardioid system, the outputs of these systems were processed by a single-pole (p=0.897), single-zero (z=0.571) IIR filter to compensate for the linear ω dependence of the microphones at low frequencies[3].

4.3.1 Test Systems

Three sample dual-array systems, based on the designs of Section 3.2 were tested, all of which produced a binaural output. One system is the optimal dual-array system, while the remaining two systems make use of the sub-optimal, but simplified, endfire array structures. Figures 4-5 through 4-7 display the three different structures used to implement these systems. Note that the Optimal Directivity system was designed so that $\Psi(\omega) \leq \Psi_{single}(\omega) + 5\ dB$, where $\Psi_{single}(\omega)$ is the noise sensitivity of a single

[2]These distances are the distances between the centers of the two microphone elements. As discussed below, each microphone had a port spacing of 14 mm. For this reason, the *total* array span was the center-to-center span *plus* 2*(one half of the port spacing). Hence, the total array span was 10.6 cm (or 4.0 cm for the Dual +/- Gradient arrays).

[3]The subtraction of the two cardioid microphones in the Dual +/- Gradient system, which will be presented in Section 4.3.1, resulted in a low-frequency ω^2 dependence in the overall system response, and so the outputs of this system were processed by two identical single-pole (p=0.897), single-zero (z=0.571) IIR filters in cascade.

microphone, $\frac{1}{|P(\omega,0,0)|^2}$. The test systems were:

1. Dual-Optimal Endfire: Each of the two arrays was designed to maximize the directivity of the corresponding output signal. This system is an optimal dual-array system, and serves as an upper bound on free-field performance for the given array structure.

   Structure: General Dual-Array, Figure 4-5, with filters $W_0(\omega)$ and $W_1(\omega)$ determined according to Equation 2.11.

2. Dual-Delay/Sum: The input from the front microphone was delayed so that the target source would add *in phase* with the input from the second microphone.

   Structure: Dual-Delay/Sum Array, Figure 4-6, with the first input delayed by three samples (which is the delay for the 9.2 cm microphone separation with a sampling frequency of 11.25 kHz).

3. Dual +/- Gradient: For each array, the output was formed by subtracting the rear input from the front input. Note: in this case, the microphones were separated by only 2.6 cm.

   Structure: Dual +/- Gradient Array, Figure 4-7.

For the Dual-Optimal Endfire system, the filters $W_i(\omega)$ were implemented using 127-tap FIR equiripple approximations.

4.3.2 Array Mountings

The Dual-Optimal Endfire and Dual-Delay/Sum systems were tested for two different mounting conditions: (1) free-field, with the arrays located 14 cm apart, and (2) head-mounted with the arrays along the temples of a pair of eyeglasses (see Figure 4-8). The Dual +/- Gradient system was tested for three different mounting conditions: (1) free-field, (2) eyeglass temple mounted near the front of the eyeglasses, and (3) eyeglass temple mounted near the ears (see Figure 4-9).

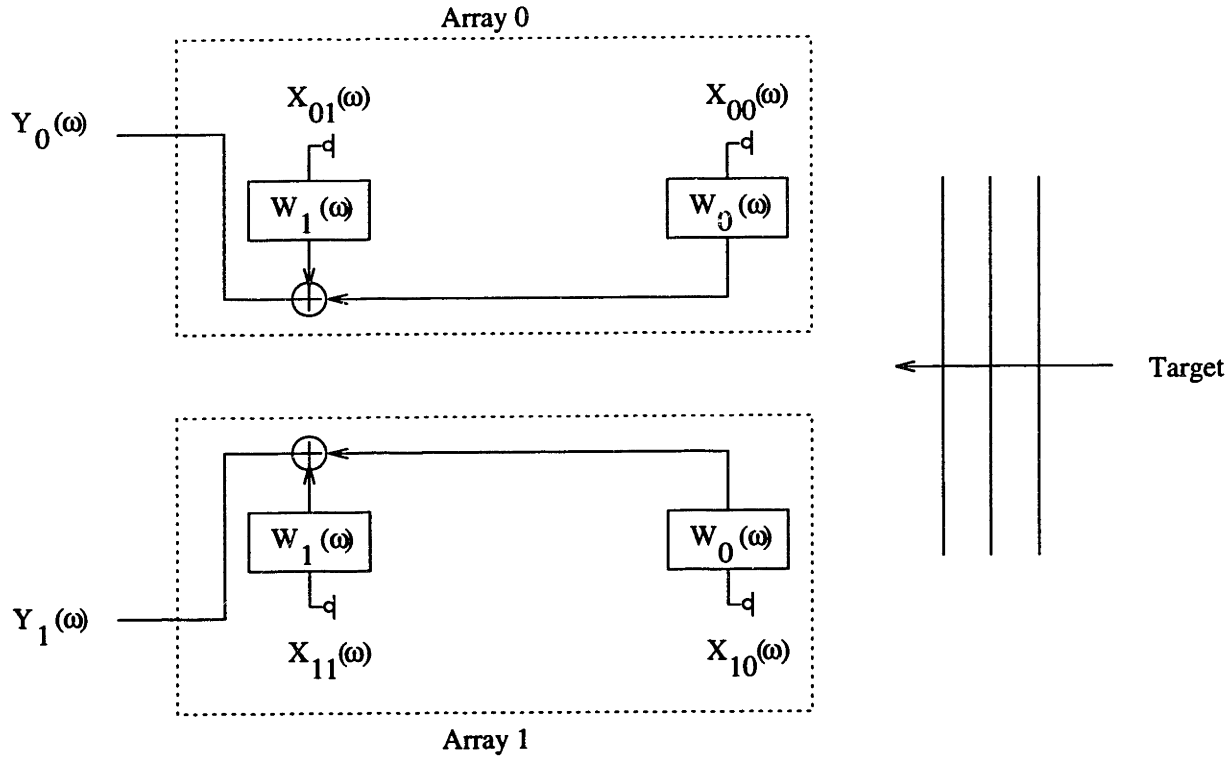

Figure 4-5: General Dual-Array Structure, used for Dual Optimal Endfire system.

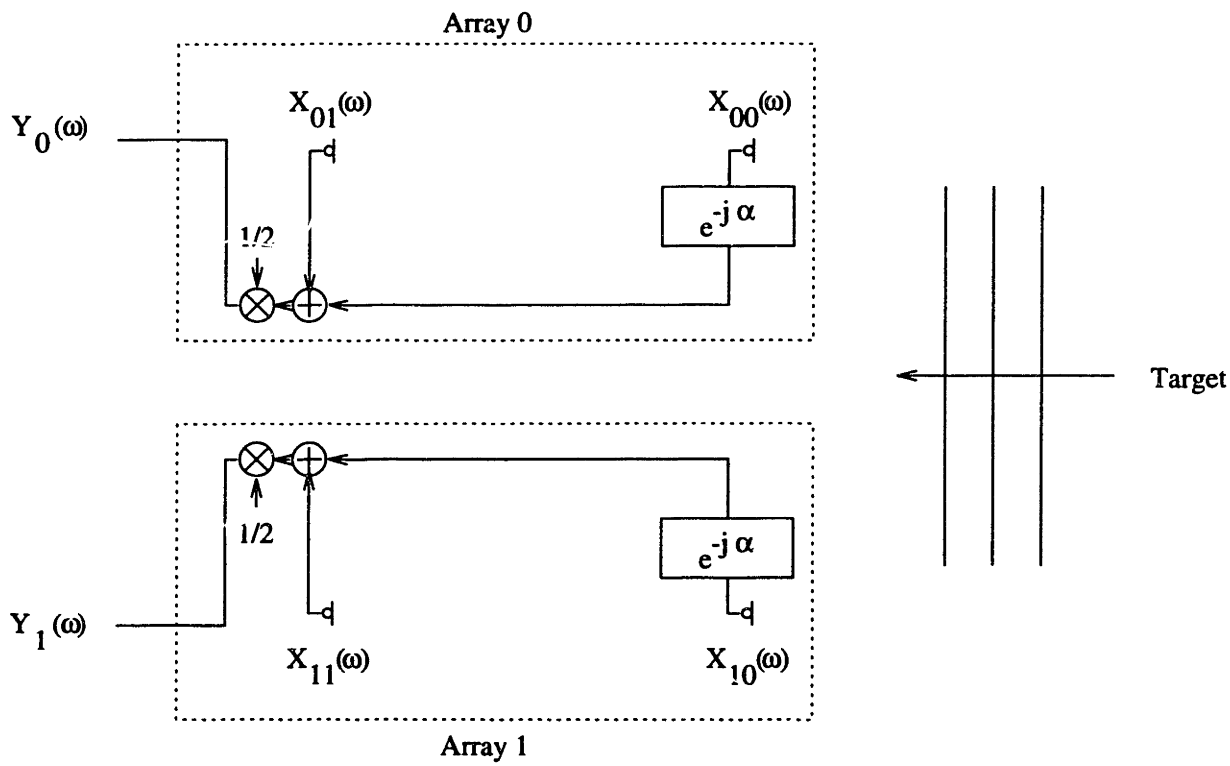

Figure 4-6: Dual-Delay/Sum Array Structure, where $\alpha = \alpha_{endfire}(\omega, \theta, \phi)$ (the inter-microphone incremental phase difference), as defined in Chapter 2, for a 9.2 cm microphone spacing.

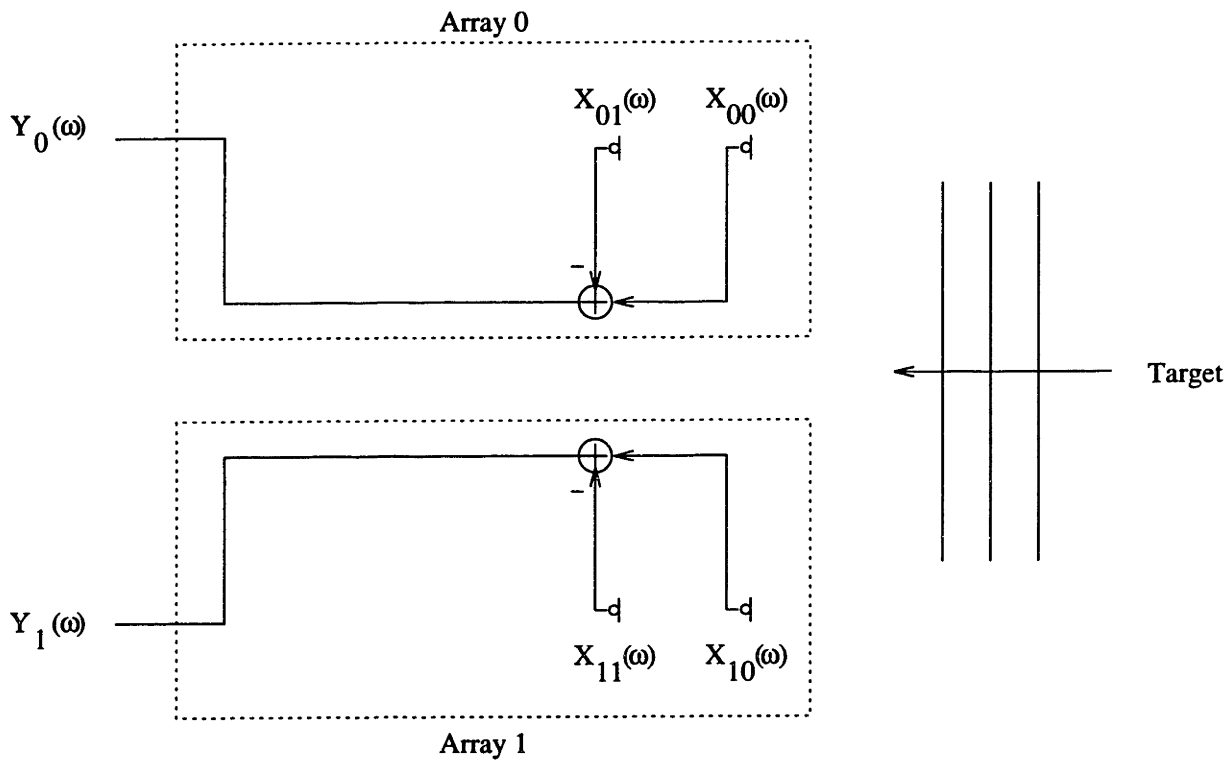

Figure 4-7: Dual +/- Gradient Array Structure.

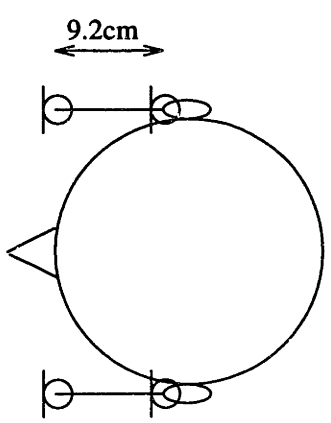

Figure 4-8: Eyeglass temple mounting for Dual-Optimal Endfire and Dual-Delay/Sum dual-array systems.

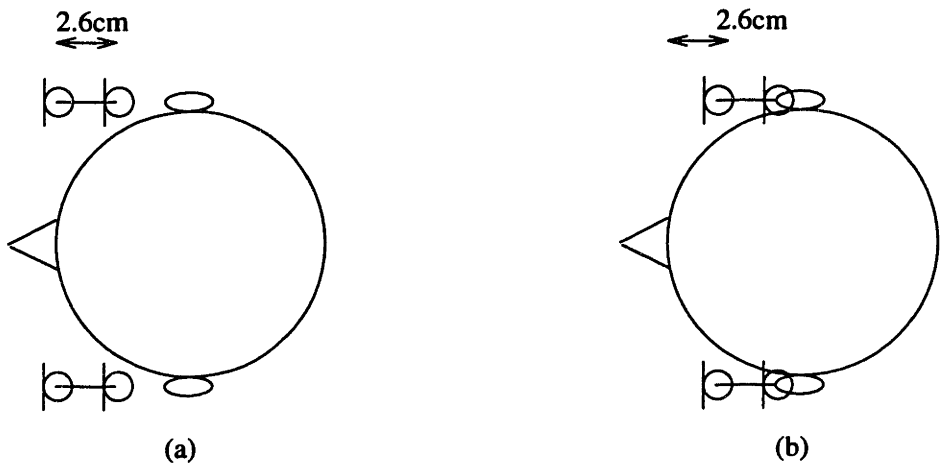

Figure 4-9: Eyeglass temple mounting for the Dual +/- Gradient dual-array system (a) at the front of the glasses and (b) at the ears.

4.3.3 Directionality Measurements

Table 4.2 shows the theoretically predicted free-field values of D_{IW}, $D_{IW,az}$, and Ψ_{IW} for the three test systems. Interesting properties to note are:

1. The Dual-Delay/Sum system realizes lower directivity than the Dual-Optimal Endfire system.

2. The Dual +/- Gradient system achieves high directivity with very simple processing, a gain which is offset by its high noise sensitivity.

3. The measure $D_{IW,az}$ yields much *lower* values than the conventional D_{IW}, a fact that arises due to the 'narrowness' of endfire directional patterns both horizontally *and* vertically. Since the azimuth directivity does not reflect the vertical 'narrowness', it results in considerably lower values than the conventional, three-dimensional directivity.

Table 4.3 repeats the theoretical free field values of D_{IW} and $D_{IW,az}$ together with the measured values of $D_{IW,az}$ for the different mounting cases. Since all of the test

Table 4.2: Theoretical free-field values of D_{IW}, $D_{IW,az}$ and Ψ_{IW} for the three dual-array test systems.

Dual-Array Syst.	D_{IW} (dB)	$D_{IW,az}$ (dB)	Ψ_{IW} (dB)
Dual-Optimal Endfire	8.12	6.22	3.69
Dual-Delay/Sum	6.31	5.15	0.42
Dual +/- Gradient	8.53	6.46	10.89

systems produced a binaural output, directivities were measured for both the right (R) and left (L) outputs.

Considering Table 4.3 *within each column* reveals that head mounting does not greatly alter the relative ordering of the systems' directivities. The one noticeable change in ordering is that while the Dual +/- Gradient system theoretically possesses the highest directivities, the Dual-Optimal Endfire system exhibits the highest measured directivities. The Dual +/- Gradient systems suffers a significant performance loss, relative to theoretical levels, which arises from the high noise sensitivity levels – this system is more susceptible to non-identical microphones, etc. In general, however, head mounting does not affect any one system any more or less than it affects the other two.

Considering Table 4.3 *within each row* reveals that head-mounting does result in performance degradation relative to the free-field mounting. The Dual-Optimal Endfire and Dual-Delay/Sum systems both demonstrate similar levels of degradation, while the Dual +/- Gradient system behaves slightly differently. When mounted towards the front of the eyeglasses, it behaves almost the same as it does in the free-field, but, when mounted near the ears, the performance levels decrease. Considering the results for all three systems, head mounting causes the greatest directivity loss

Table 4.3: Theoretical free-field D_{IW} and $D_{IW,az}$ and measured $D_{IW,az}$ for the three dual-array test systems. The measured values are given for the right (R) and left (L) outputs.

Dual-Array System	Theoretical D_{IW} (dB) Free-Field	Theoretical $D_{IW,az}$ (dB) Free-Field	Measured $D_{IW,az}$ (dB) Free-Field	Measured $D_{IW,az}$ (dB) Eyeglass
Dual-Optimal Endfire $D(\omega)$	8.12	6.22	6.39 (R) 6.42 (L)	5.44 (R) 5.48 (L)
Dual-Delay/Sum	6.31	5.15	5.48 (R) 5.63 (L)	4.73 (R) 4.99 (L)
Dual +/- Gradient (front of glasses)	8.53	6.46	5.75 (R) 5.80 (L)	5.77 (R) 5.43 (L)
Dual +/- Gradient (near the ears)				5.10 (R) 4.86 (L)

when the microphones are closer to the head, i.e. when the head shadow effects are largest. The Dual +/- Gradient system is the best example of this – when mounted near the ears, all four microphones are located *directly* next to the head, and this system exhibits the greatest directivity loss re free-field. In contrast, when it is mounted at the front of the eyeglasses, none of the microphones is directly next to the head, and little performance is lost re free-field. The remaining systems fall between these extremes, with two microphones next to the ears and two microphones at the front of the glasses. This behavior makes sense – the mounting environment is least like the free-field (i.e. sound diffraction is greatest) when the array is very close to the head.

To further appreciate the effect of head-mounting upon the directional performance of these test systems, Figures 4-10 and 4-11 show the intelligibility-weighted polar plots, $|G_{IW}(\theta, \phi = 0)|$, for the right outputs of the Dual-Optimal Endfire and Dual +/- Gradient systems, respectively[4].

Figure 4-10 shows that the Dual-Optimal Endfire system free-field measurements correspond very closely with the expected values and that head mounting degrades the performance only slightly. As expected for the head-mounted case, the side of the array that experiences little head shadowing (towards 270° for the right array) still exhibits a portion of the theoretical null characteristics, while the other side, which experiences a significant amount of diffraction effects due to head shadowing, does not. Overall, the eyeglass-mounted array still possesses an enhanced directionality in the desired target direction and retains roughly the free-field directionality gains.

Figure 4-11 shows that the Dual +/- Gradient system free-field measurements also correspond with the theoretical predictions. Performance is only slightly degraded when the arrays are mounted on eyeglass temples *near the front* of the eyeglasses, and, as shown for the Dual-Optimal Endfire system, sources that experience little head

[4]The Dual-Delay/Sum system exhibits a similar relationship between the theory and actual measurements as shown for the Dual-Optimal Endfire system, and, for all three systems, the left outputs behave almost identically to the right outputs, except for an obvious left-right flip.

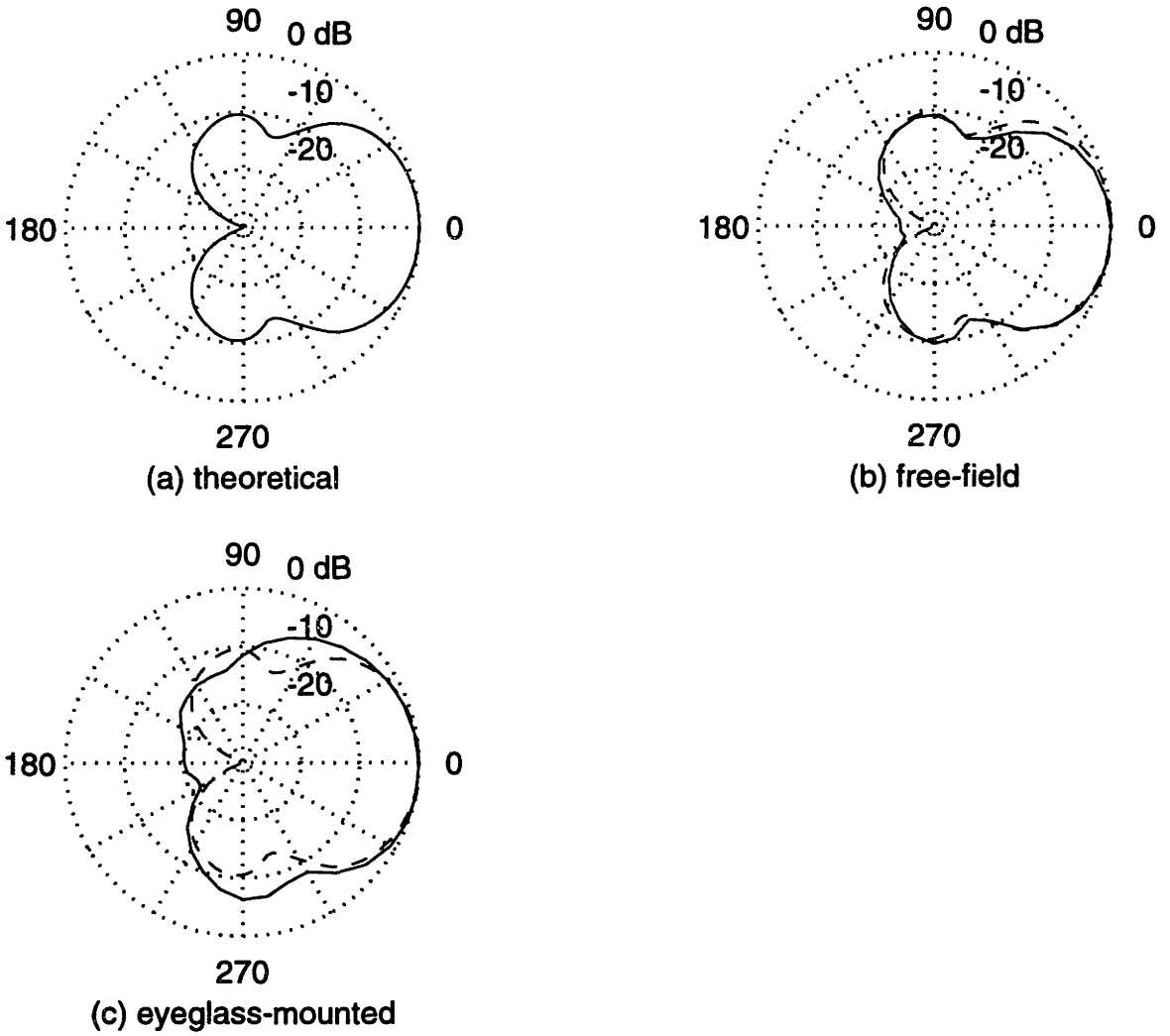

Figure 4-10: Intelligibility-weighted polar plot of $|G_{IW}(\theta, \phi = 0)|$ for the right output of the Dual-Optimal Endfire test system for (a) the theoretical free-field, (b) the measured free-field and (c) the measured eyeglass-mounted case.

shadow experience a directional pattern similar to that of the free-field while sources shadowed by the head experience different behavior. When the arrays are mounted near the ears, however, the system loses more of its directional performance, with neither side behaving like the free-field case. This second eyeglass mounting places both microphones very close to the head (much closer than the first Dual +/- Gradient eyeglass mounting), which strongly affects the overall system directionality. Overall, however, this system does still demonstrate some improvement in directionality over the conventional dual cardioid binaural hearing aid, Figures 4-2 and 4-3.

The intelligibility-weighted polar plots of the left outputs of these systems behave in a similar manner to the right outputs (with the obvious 'flip' in behavior due to switching from one side of the head to the other) and the Dual-Delay/Sum system exhibits behavior similar to that of the Dual-Optimal Endfire System.

4.3.4 Output ITD Measurements

Theoretically, free-field dual-array systems with the arrays located 14 cm apart should produce the same output ITDs as two microphones spaced 14 cm apart. (This assumes *identical* microphones in each array so that the two arrays would process signals from any given source direction identically.) Hence, the theoretical output ITDs are the same as the $\mathrm{ITD}_{desired}$ for the single-array systems with the total array span, $(n-1)d$, replaced by 14 cm and, from Equation 3.8:

$$\mathrm{ITD}_{output}(\omega, \theta, \phi) = \frac{14\ cm}{c} sin\theta\ cos\phi.$$

Figures 4-12 through 4-14 show the measured free-field and eyeglass-mounted output ITDs for the three test systems with sources arriving from 0°, 30°, 60°, and 90°.

Figures 4-12 and 4-13 indicate that the Optimal Endfire and Dual-Delay/Sum systems both operate as predicted in the free-field, with the small 'jumps' evident in these ITD measurements arising due to nulls in the directional pattern, with associ-

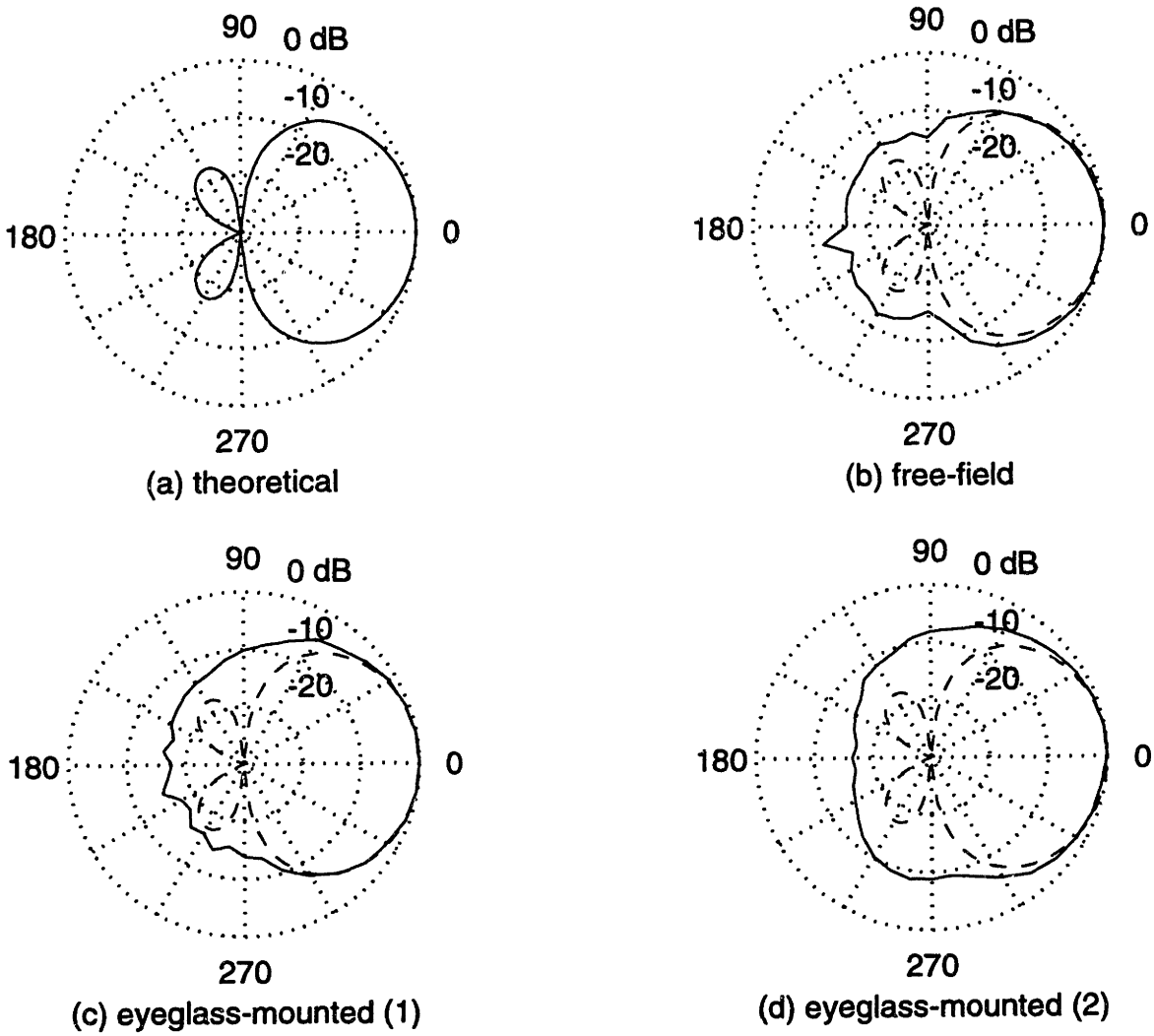

Figure 4-11: intelligibility-weighted polar plot of $|G_{IW}(\theta, \phi = 0)|$ for the right output of the Dual +/- Gradient test system for (a) the theoretical free-field, (b) the measured free-field and the measured eyeglass mounted cases (c) near the front of the glasses and (d) near the ears.

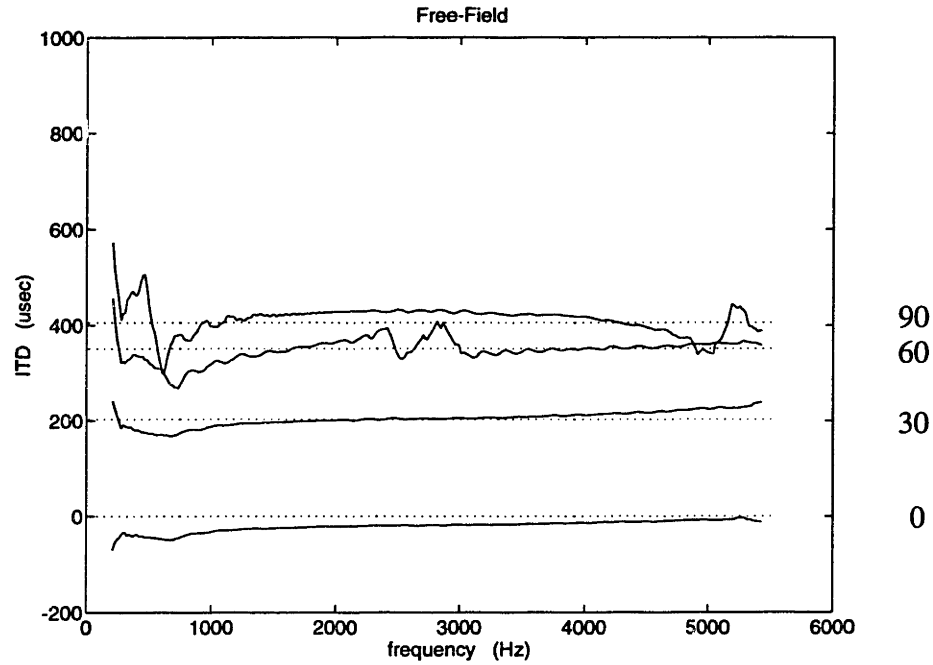

(a)

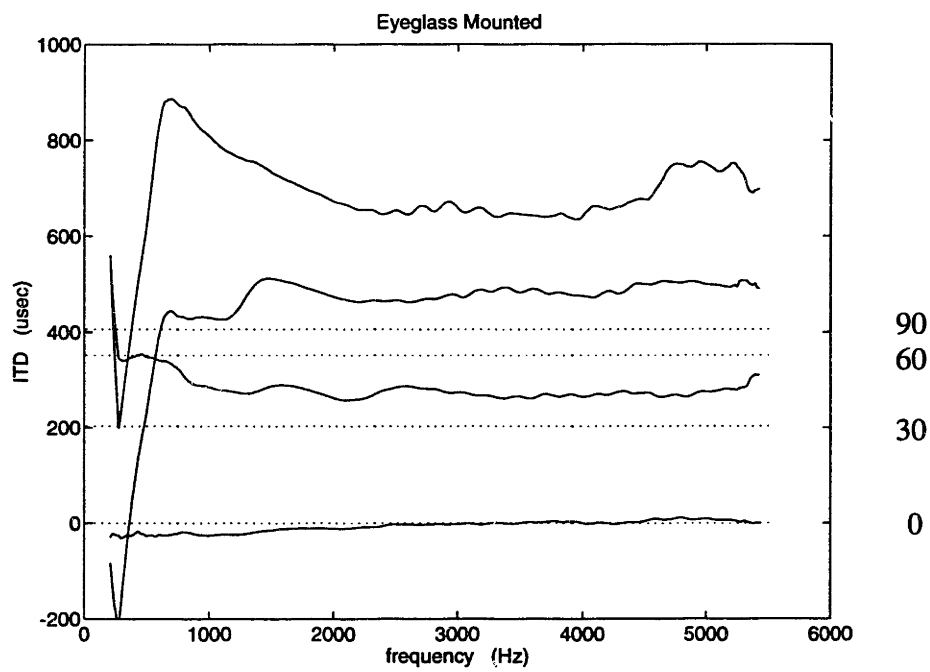

(b)

Figure 4-12: Dual-Optimal Endfire system output ITDs for (a) free-field and (b) eyeglass-mounted. Dotted lines indicate theoretical free-field behavior.

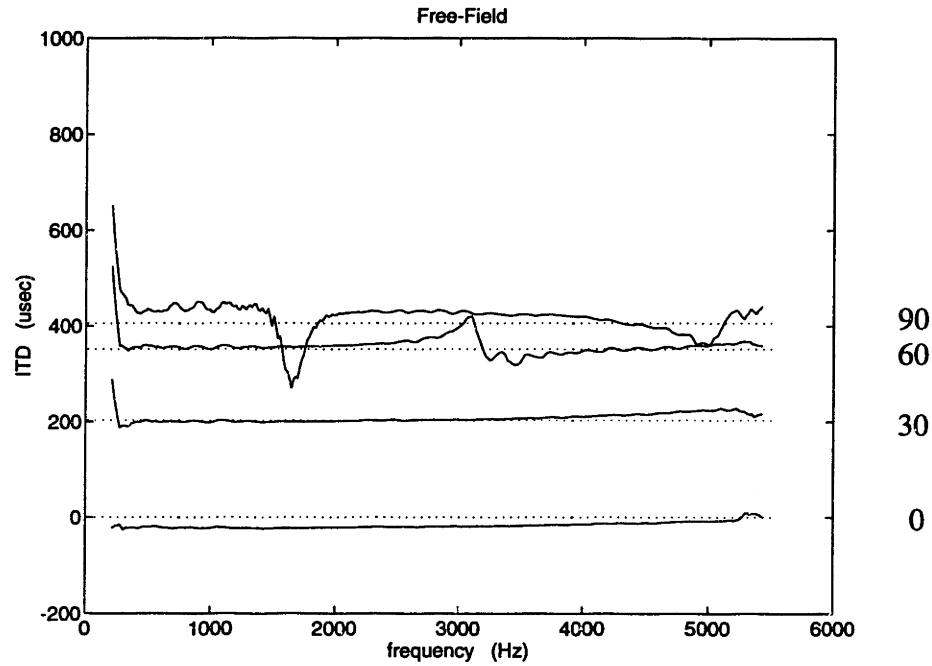

(a)

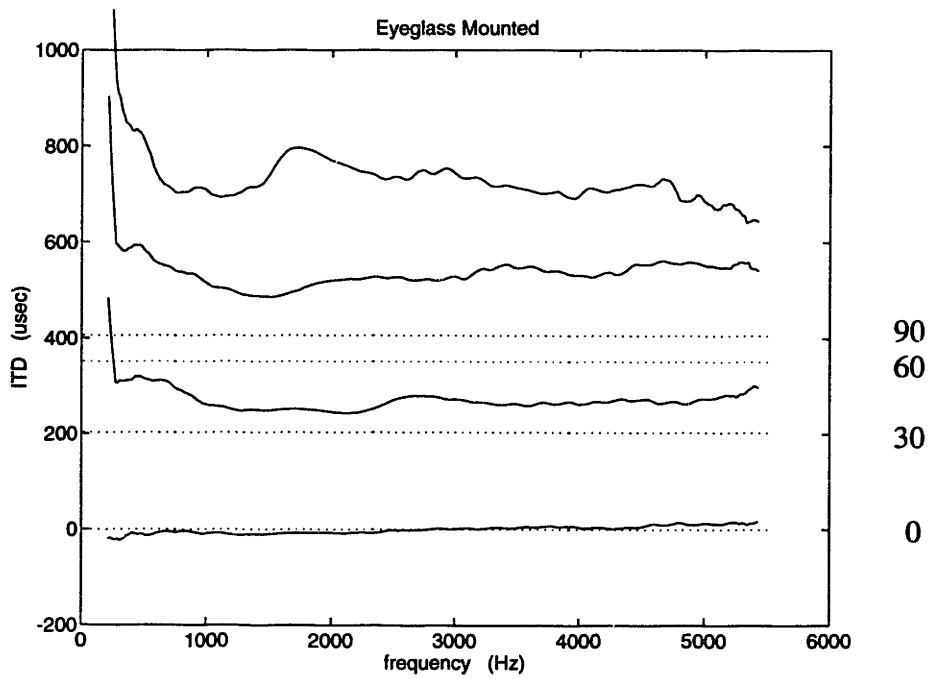

(b)

Figure 4-13: Dual-Delay/Sum system output ITDs for (a) free-field and (b) eyeglass-mounted. Dotted lines indicate theoretical free-field behavior.

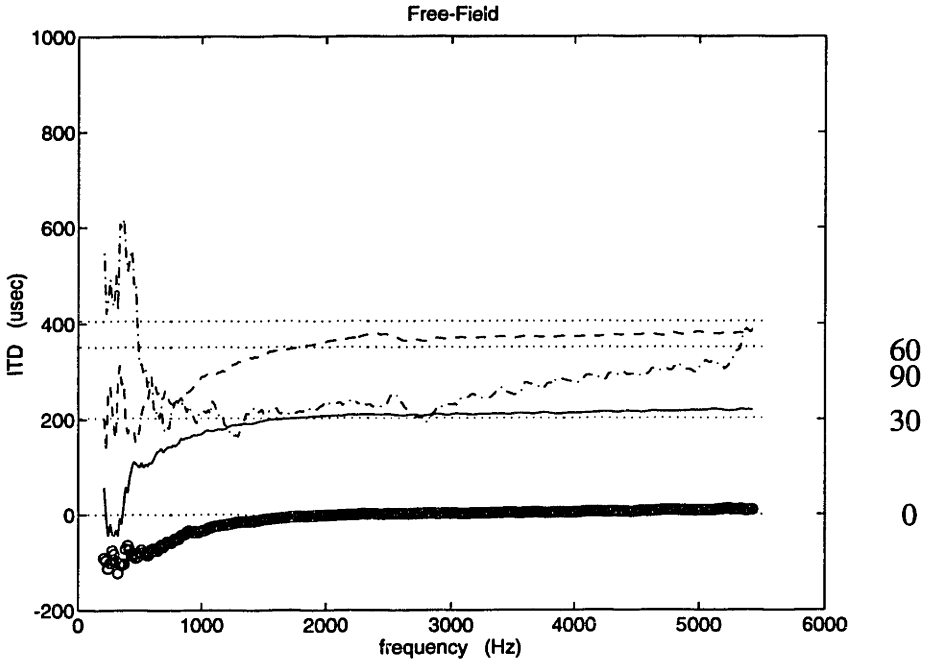

(a)

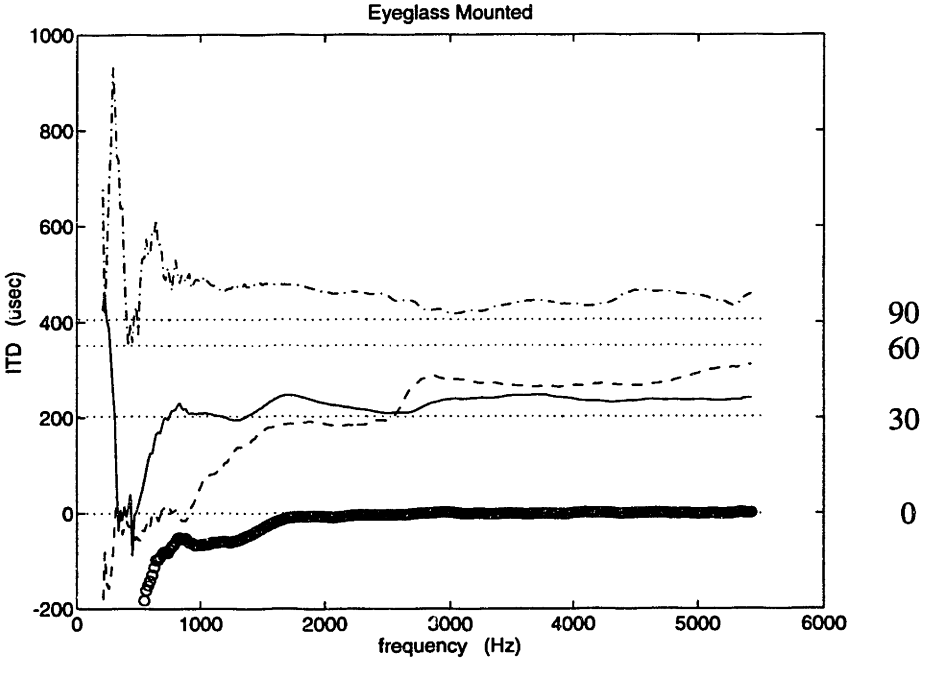

(b)

Figure 4-14: Dual +/- Gradient system output ITDs for (a) free-field, (b) eyeglass-mounted near the front of the eyeglasses, and (c) eyeglass-mounted at the ears: 0° = 'o', 30° = '-', 60° = '–', and 90° = '-.'. Dotted lines indicate theoretical free-field behavior.

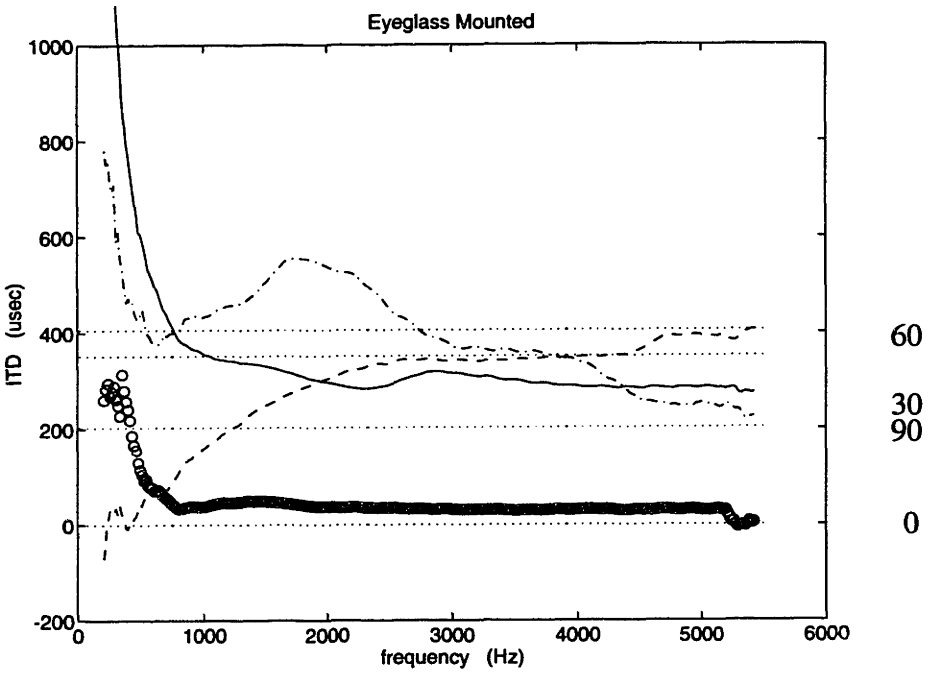

(c)

Figure 4-14 (continued)

ated large phase shifts, that are unequal at the ears. Head mounting increases the ITDs similarly in both cases, so that they resemble the 'true' ITDs at the ears, shown in Figure 4-4 (b). The large deviations evident in these ITD curves at low frequencies arise due to the low-frequency linear ω dependence in the cardioid microphone responses. The low-frequency signals out of the microphones are very small, and, consequently, the array is more susceptible to slight magnitude and phase differences between the microphones, which results in poorly preserved ITDs.

Figure 4-14 shows that the Dual +/- Gradient system does *not* behave as expected for either the free-field or the head-mounted cases. To understand these plots, first note that they are plotted in a slightly different manner than the other ITD plots in this thesis – due to the erratic nature of these ITDs, each of the four curves was plotted in a different line type. The theoretical ITDs are also plotted using the standard dotted lines. For the free-field case, the ITDs for sources arriving from 0°, 30°, and 60° behave as expected – they follow the theoretical free-field curves reasonably well. The source arriving from 90°, however, produces output ITDs that are substantially different from the theoretical predictions – they are smaller than expected. This arises largely from the fact that the Dual +/- Gradient system has a magnitude *null* at 90° for all frequencies (see Figure 4-11), which results in output signals with poorly defined phase (as explained below) for sources arriving from 90°. Hence, the resulting ITDs are of questionable meaning in this case. For the two head-mounted cases, the 0° and 30° curves again behave as expected – they are slightly larger than the theoretically predicted values, which results from head shadowing. The 60° and 90° curves, on the other hand, behave erratically. While the null at 90° (as discussed above) partially explains this behavior, the main cause for this is uncertain. One possible cause is that, since there are two partial cancellations at low frequencies, slight differences in the magnitude and phase responses of the individual cardioid microphones and errors in their placement can result in wide deviations in output ITDs. Since the microphone differences would be most obvious for sources

that are close to nulls, the ITDs behave most erratically for sources arriving from 60° and 90°. As with the Dual-Optimal Endfire and Dual-Delay/Sum systems, the low-frequency ω^2 dependence[5] also causes low-frequency ITD deviations.

4.4 Single-Array Systems

The single-array systems were designed for the free-field case and possessed the following structure:

- Four-element broadside array (span = 14 cm) consisting of equally-spaced cardioid elements.

- Individual cardioid microphone (Knowles EB-1979) response:

$$|P(\omega,\theta,\phi)| = 2|sin(\frac{\omega p}{2c}(cos\theta + 1))|,$$

  where p = microphone port spacing = 8.5 mm. The four responses were roughly equalized by the application of a scale factor to three of the microphones. Note that these microphones are slightly different than those used in the Dual-Cardioid and Dual-Array systems of Sections 4.2 and 4.3 in that they have a smaller port spacing (8.5 mm versus 14 mm).

These systems were implemented in real time using two Ariel DSP-96 boards, each equipped with a Motorola DSP96002 signal processing chip and a dual channel I/O. The need for two boards arose due only to the I/O requirements (four A/D channels were needed for the four microphones) and not to processing requirements. All output signals were processed with a single-pole (p=0.897), single-zero (z=0.571) IIR filter to compensate for the linear ω dependence of the microphones at low frequencies.

[5]Recall that, for this array, the low-frequency dependence is ω^2 rather than linear ω, which was the dependence for the previous two systems.

4.4.1 Test Systems

Five sample systems – two monaural and three binaural – were evaluated. Three of the systems served as 'boundary' systems, marking the theoretical limits of directional (maximum directivity) and binaural cue (zero RMS ITD error) performance, while the remaining two systems are a Combined system and a Lowpass/Highpass system, which, as presented in Chapter 3, operate between these boundaries. The listing below describes each test system and tells which of the three possible structures, defined in Chapter 3 and repeated in Figures 4-15 through 4-17, was used in the actual implementation. Note, all systems with noise sensitivity considerations were designed so that $\Psi(\omega) \leq \Psi_{single}(\omega) + 5$ dB at all frequencies, where $\Psi_{single}(\omega) = \frac{1}{|P(\omega,0,0)|^2}$ is the single-microphone noise sensitivity.

1. Pass Through: The inputs to the outermost microphones, $X_0(\omega)$ and $X_3(\omega)$, were sent directly to their respective ears, which resulted in the 'perfect'[6] maintenance of ITDs ($E(\omega) = 0$), but achieved only single microphone directivity – it served as a lower bound on both directivity and RMS ITD error.

   Structure: Sub-optimal Lowpass/Highpass (Figure 4-17) with the lowpass and highpass filters having an infinite cutoff frequency[7].

2. Optimal Directivity: The filters were designed to maximize directivity at all frequencies, which resulted in maximum directionality while producing a monaural output – it served as an upper bound on both directivity and RMS ITD error.

   Structure: Optimal Lowpass/Highpass (Figure 4-16) with the lowpass and highpass filters having a zero cutoff frequency[8], $f_c = 0$ Hz.

[6]For single-array systems, 'perfect' ITDs mean that the system maintains the $ITD_{desired}$ defined in Equation 3.8. These ITDs do *not* necessarily equal the naturally occurring ITDs at the wearer's ears, which are shown for the dual cardioid binaural hearing aid in Figure 4-4 (b).

[7]An infinite cutoff frequency means that the lowpass filter is simply a short circuit and the highpass filter is an open circuit.

[8]A zero cutoff frequency means that the lowpass filter an open circuit and the highpass filter is a short circuit.

3. Uniform Weighting: The inputs were averaged to form the output signal, which resulted in moderate levels of directivity from an extremely simple structure and a monaural output – it served as an upper bound on directivity and RMS ITD error for the case of simple processing.

   Structure: Sub-optimal Lowpass/Highpass (Figure 4-17) with the lowpass and highpass filters having a zero cutoff frequency.

4. Combined, $\tau(\omega) = 40$ μsec: The weights satisfied Equation 3.12 for the desired level of $\tau(\omega)$, and, therefore, this system was an intermediate between the extreme cases above – it achieved some directivity gains at each frequency by allowing a small amount of RMS ITD error.

   Structure: General Single-Array (Figure 4-15).

5. Lowpass/Highpass ($f_c = 1000$ Hz): The low-frequency portion of the output signals was formed using the Pass Through system while the common high-frequency component came from the Optimal Directivity system.

   Structure: Optimal Lowpass/Highpass (Figure 4-16).

For all systems above, the filters $W_i(\omega)$ were implemented using 127-tap, FIR equiripple approximations and the lowpass and highpass filters (in cases where they had neither infinite nor zero cutoffs) had 300-Hz transition regions, centered at the cutoff, and were implemented using 63-tap, FIR equiripple approximations.

4.4.2 Array Mountings

The single-array systems were tested for three different mounting conditions: (1) free-field, (2) head-mounted across the front of eyeglasses, and (3) head-mounted on a headband. Figure 4-18 shows the two head mountings. Note that for both of these mountings, the array had the same 14-cm linear span, but that the headband mounting required a slight bending of the array along the top of the head.

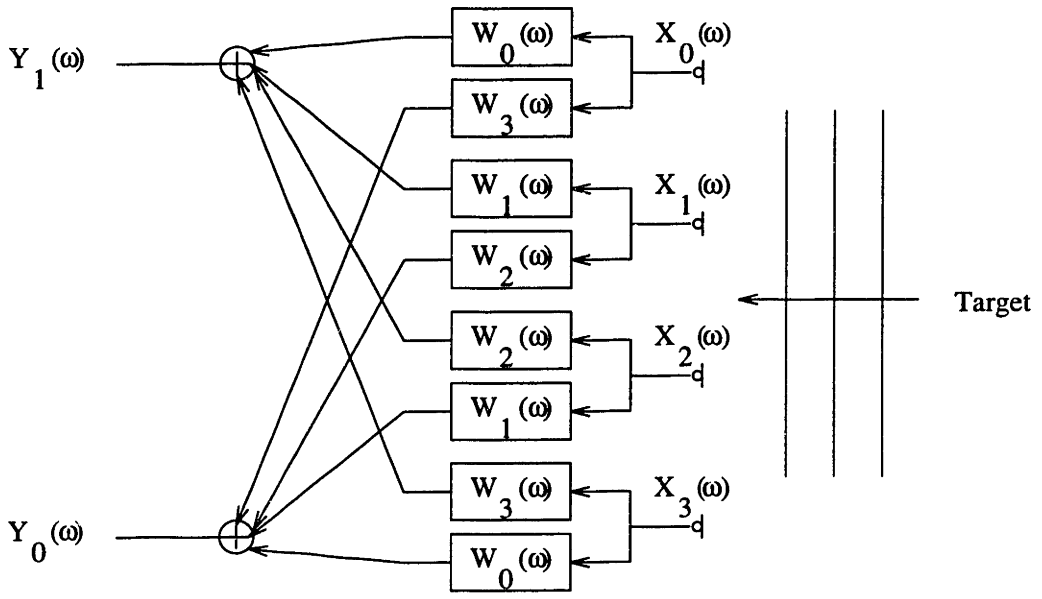

Figure 4-15: General Single-Array Structure.

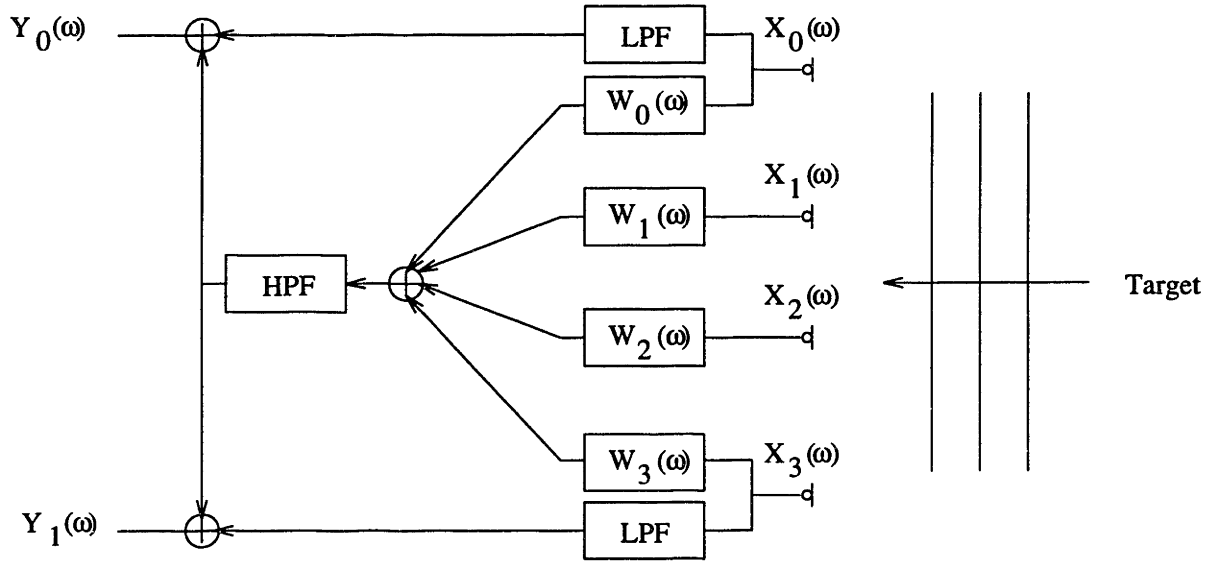

Figure 4-16: Optimal Lowpass/Highpass Structure.

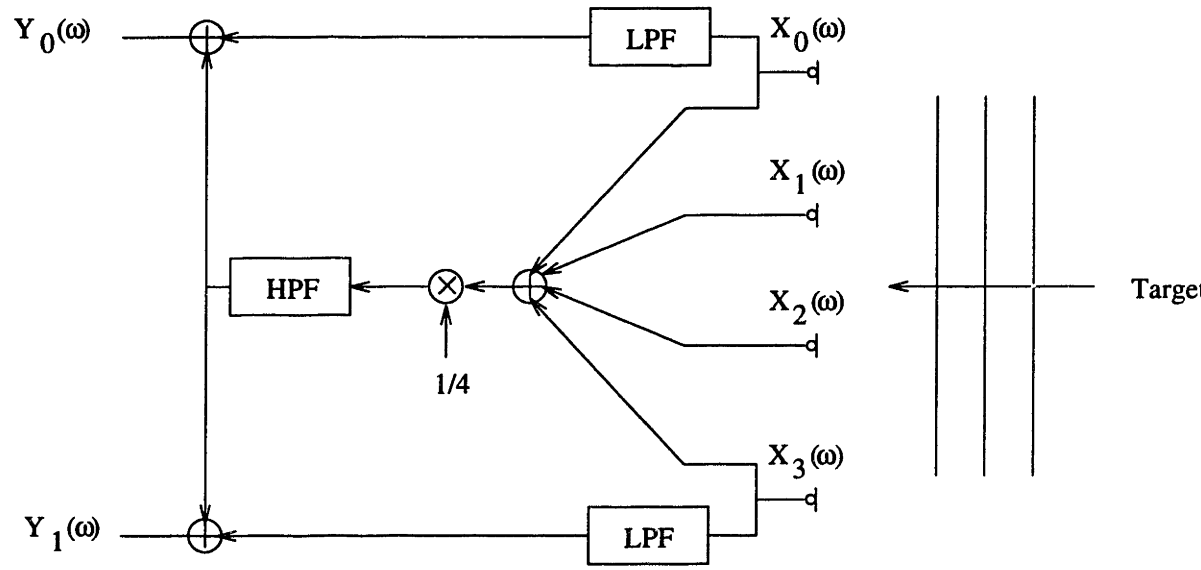

Figure 4-17: Sub-optimal Lowpass/Highpass Structure.

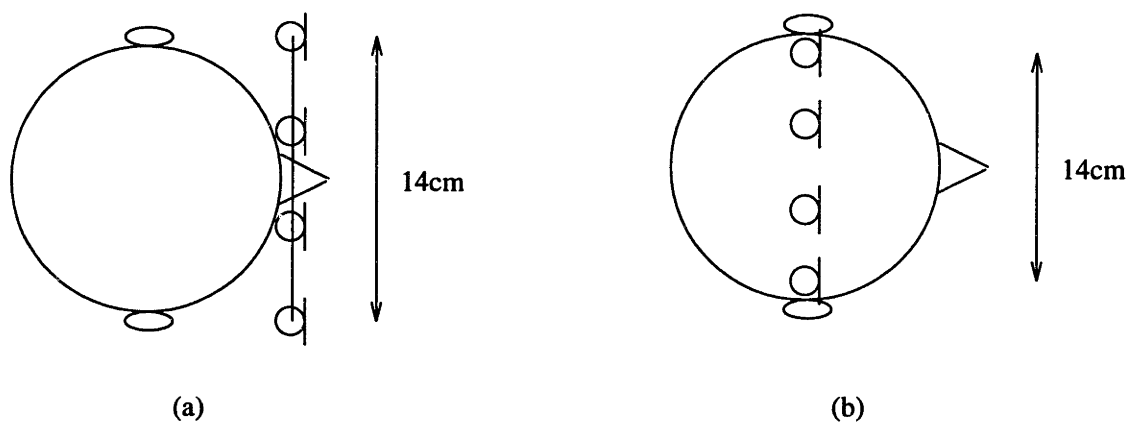

Figure 4-18: Single-array system head-mountings: (a) eyeglasses and (b) headband.

4.4.3 Directionality Measurements

Table 4.4 shows the theoretically predicted values of D_{IW}, $D_{IW,az}$ and Ψ_{IW} for the five test systems. These provide a means for comparing the expected system directionality and reveal three interesting properties:

1. The easily implemented Uniform Weighting system achieves almost the same levels of D_{IW} as the Optimal Directivity system and has a lower noise sensitivity.

2. The values of D_{IW} for the Combined and Lowpass/Highpass systems indicate that some degree of ITDs can be maintained without sacrificing too much directionality.

3. The values of $D_{IW,az}$ are close to the values of D_{IW}, a fact that arises because the directional patterns of broadside arrays are 'narrow' only horizontally and not vertically. Since most of the conventional directivity gains are due to the horizontal narrowness, the azimuthal directivity is close to, if not greater than, the three-dimensional directivity.

Table 4.4: Theoretical values of D_{IW}, $D_{IW,az}$ and Ψ_{IW} for the five test systems

Single-Array System	D_{IW} (dB)	$D_{IW,az}$ (dB)	Ψ_{IW} (dB)
Pass Through	4.67	4.22	7.94
Optimal Directivity	8.03	8.26	7.50
Uniform Weighting	7.18	7.47	1.91
Combined ($\tau(\omega) = 40\mu sec$)	7.06	7.08	8.44
LP/HP (f_c=1000 Hz)	7.66	7.61	6.03

Table 4.5 lists the theoretical free-field D_{IW}, the theoretical free-field $D_{IW,az}$ and the measured free-field and head-mounted $D_{IW,az}$ for all five systems and all array mountings.

Table 4.5: Theoretical and measured directional performance for the five sample systems with the three different mountings. For binaural systems, (R) indicates right ear and (L) indicates left ear.

Single-Array System	Theoretical D_{IW} (dB) Free-Field	Theoretical $D_{IW,az}$ (dB) Free-Field	Measured $D_{IW,az}$ (dB)		
			Free-Field	Eyeglass	Headband
Pass Through	4.67	4.22	4.02 (R) 4.19 (L)	4.26 (R) 4.20 (L)	3.85 (R) 3.90 (L)
Optimal Directivity	8.03	8.26	7.88	8.22	7.51
Uniform Weighting	7.18	7.47	7.06	7.60	7.24
Combined ($\tau = 40\mu sec$)	7.06	7.08	6.73 (R) 6.90 (L)	7.37 (R) 7.26 (L)	6.30 (R) 6.78 (L)
LP/HP ($f_c = 1000\ Hz$)	7.66	7.61	7.47 (R) 7.55 (L)	7.58 (R) 7.78 (L)	7.01 (R) 7.10 (L)

To discuss these directional results, first consider Table 4.5 *within each column.* For each of the three mounting cases, the relative performance levels of the five test systems behave as predicted by theory: the Optimal Directivity system always possesses the highest $D_{IW,az}$ and the Pass Through system possesses the lowest. The only case where the theoretical ordering of the $D_{IW,az}$ values are *not* preserved is for the headband mounting, with which the Uniform Weighting system achieves a higher $D_{IW,az}$ than the Lowpass/Highpass system. A possible reason for this is that headband mounting involves a slight bending of the linear array. As discussed below,

this bending does not degrade the Uniform Weighting system to the same extent as the other systems. In general, the columns of Table 4.5 are consistent, and the relative performance between the systems is hardly affected by head mounting.

Now, consider Table 4.5 *within each row.* This shows that head mounting has very little effect upon the performance of any given system. In fact, the eyeglass-mounted systems exhibit better performance than the free-field systems! This arises due to the head shadow effects in the azimuth-plane – in particular, the head shadows sources arriving from behind the wearer, increasing overall sensitivity in the forward target direction. The headband mounting, on the other hand, tends to degrade performance slightly, partly because the headband mounting does not enjoy the same azimuth-plane head-shadow benefits of the eyeglass mounting, but more importantly because the headband mounting introduces a slight curvature into the array structure. To determine the effects of curvature upon array performance, consider the four array systems tested (Pass Through is excluded here, because it is not technically an array system in that each output is formed by using only one microphone). Of these four systems, the Optimal Directivity, Combined and Lowpass/Highpass were all designed for *linear* arrays with a precisely known structure while the Uniform Weighting system is independent of the array structure. As shown in Table 4.5, when compared to free-field mounting, headband mounting degrades the performance of all three structure-dependent systems while it actually improves the performance of the structure-independent system, which suggests that the slight change in array structure is, in fact, the primary degrading factor in the performance of the headband-mounted systems. For all of the measured cases of Table 4.5, however, the variations of $D_{IW,az}$ across any given row are small (less than 1 dB), and so these results show that head mounting has relatively little effect on performance.

To illustrate the effects of head mounting on the azimuth plane directional characteristic, Figure 4-19 shows the theoretical and measured $|G_{IW}(\theta, \phi = 0)|$ for the

Optimal Directivity system[9]. Overall, the measured characteristics follow the theoretically predicted ones very closely, except for the small lobe toward the rear of the system (180°). Since the theoretical null at 180° arises from the cardioid microphones, the small rear lobe most likely arises from the failure of the actual microphones to exhibit perfectly cardioid behavior. This lobe probably accounts for the fact that all free-field measured values of $D_{IW,az}$ in Table 4.5 are lower than the theoretical values. Also, as indicated in Table 4.5, the eyeglass mounting performs slightly better than the free-field system and the headband-mounted system performs slightly worse. The intelligibility-weighted polar plots of the remaining four systems exhibit behavior similar to that predicted in Table 4.5.

4.4.4 Output ITD Measurements

The Pass Through system theoretically maintains the ITDs produced by two microphones located 14 cm apart, with the output ITDs given by Equation 3.8:

$$\mathrm{ITD}_{output}(\omega, \theta, \phi) = \frac{14\ cm}{c} sin\theta\ cos\phi.$$

This is the ITD that the Combined system is designed to maintain (within its specified constraints) and that the Lowpass/Highpass system does maintain at low frequencies. To see the variations in the output ITDs produced by these three systems, Figures 4-20 through 4-22 show the theoretical free-field output ITDs for the three single-array binaural output systems for azimuth-plane sources arriving from 0°, 30°, 60°, and 90°. The Pass Through system (Figure 4-20) produces exactly the $\mathrm{ITD}_{desired}$ as defined by Equation 3.8, and so the output ITDs are constant over frequency for any given arrival angle. The Combined system (Figure 4-21) allows some degree of RMS ITD error at all frequencies and, consequently, exhibits deviations from the

[9]The remaining four systems exhibit similar relationships between the measured curves and the theoretical curves as the Optimal Directivity system. In the binaural output cases, the left and right outputs behave almost identically, except for a left-right 'flip' in all of the curves.

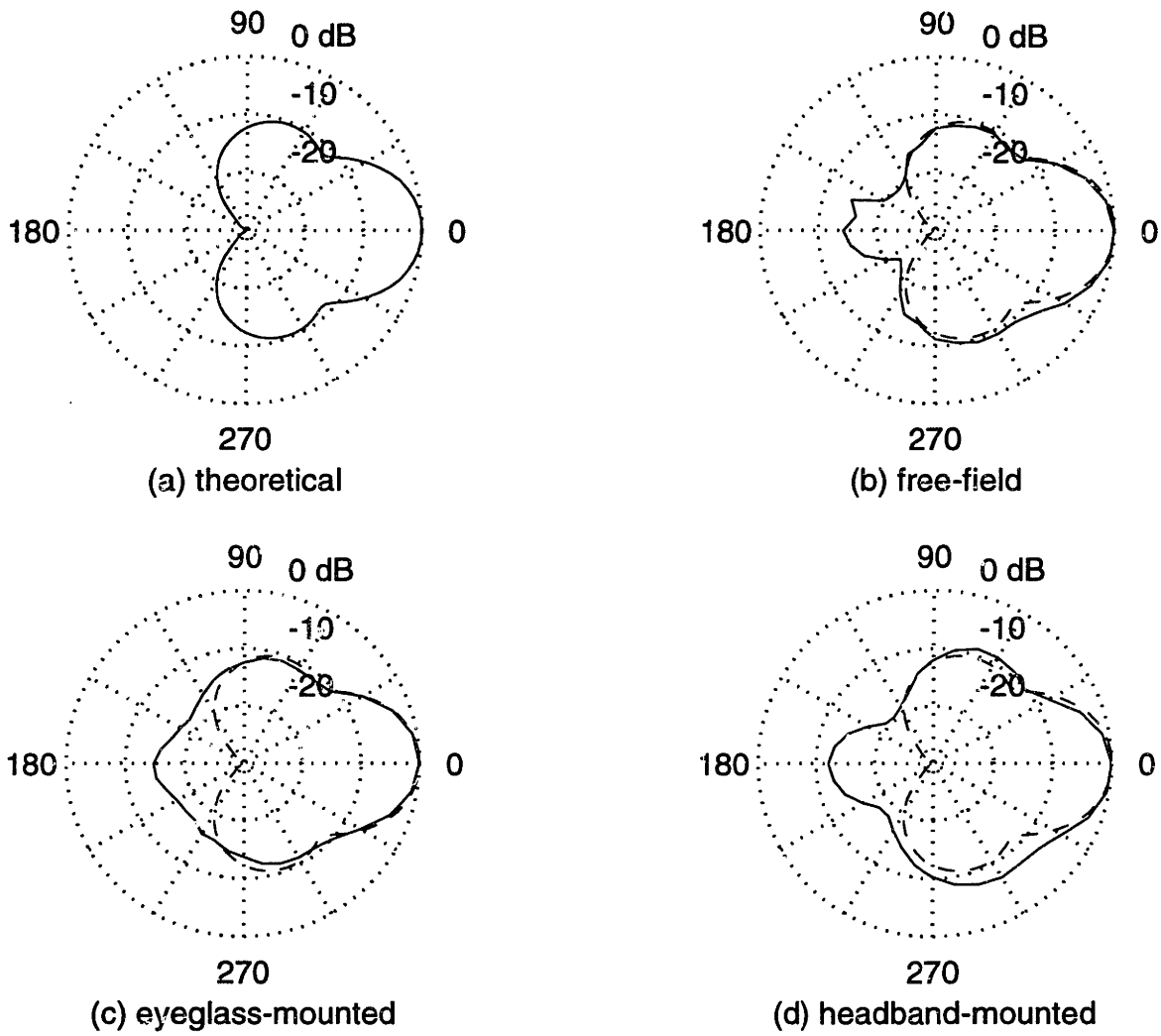

Figure 4-19: Polar plot of intelligibility-weighted azimuth-plane directional characteristic for the optimal directivity system: (a) theoretical, (b) measured free-field, (c) measured eyeglass-mounted, and (d) measured headband-mounted.

desired ITDs. Note that the basic trends of the $ITD_{desired}$ are maintained in that the ITDs produced by sources closer to 90° are greater than ITDs produced by sources closer to 0°. The Lowpass/Highpass system (Figure 4-22) maintains the ITDs at low frequencies and has zero ITDs (monaural output) at high frequencies. Note that all three systems perfectly maintain ITDs for sounds arriving from 0° = the target direction, a property caused by the imposed symmetry of the weights in the single-array structures, shown in Figure 4-15. Figures 4-23 through 4-25 depict the measured output ITDs produced by the three binaural systems for the free-field and the eyeglass-mounted cases. (Appendix C shows the measured ITDs produced by the headband-mounted systems – these ITDs resemble those of the eyeglass-mounted systems.)

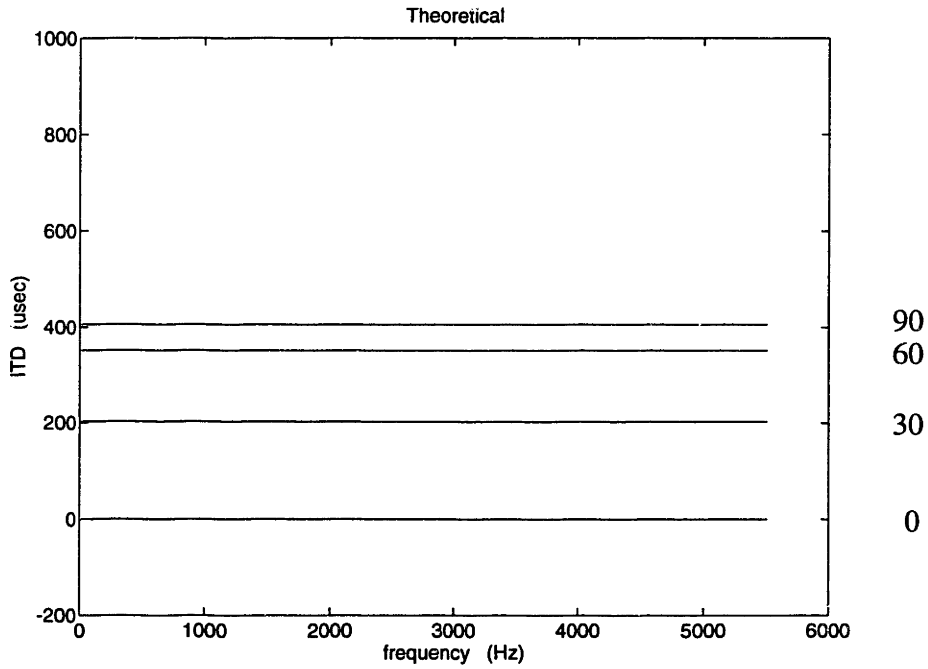

Figure 4-20: Theoretical free-field ITDs for the Pass Through system. Perfectly matches desired ITDs.

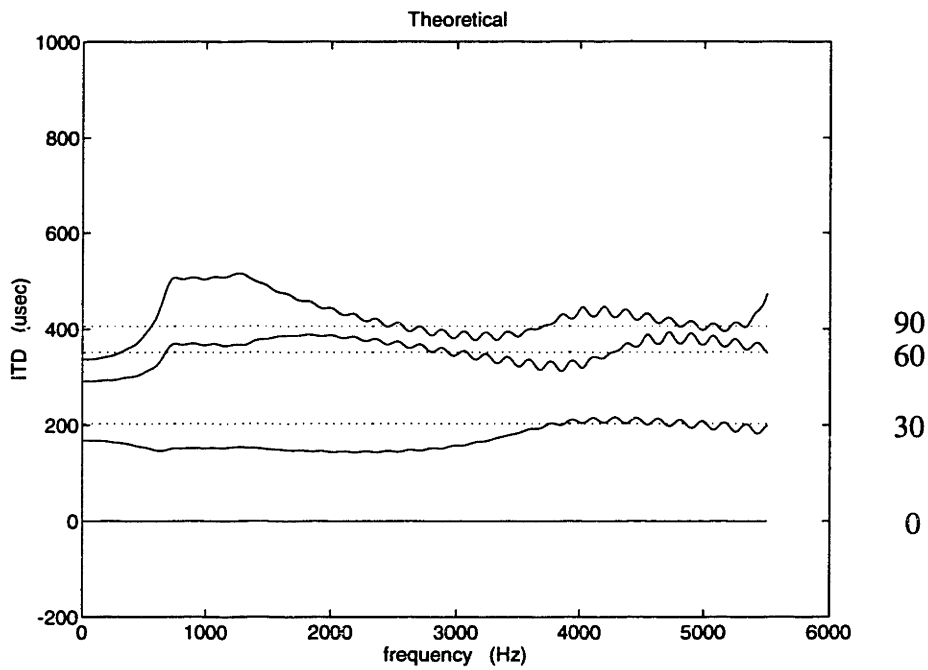

Figure 4-21: Theoretical free-field ITDs for the Combined system, $\tau(\omega) = 40\mu sec$ (solid line) and for the Pass Through system (dotted lines).

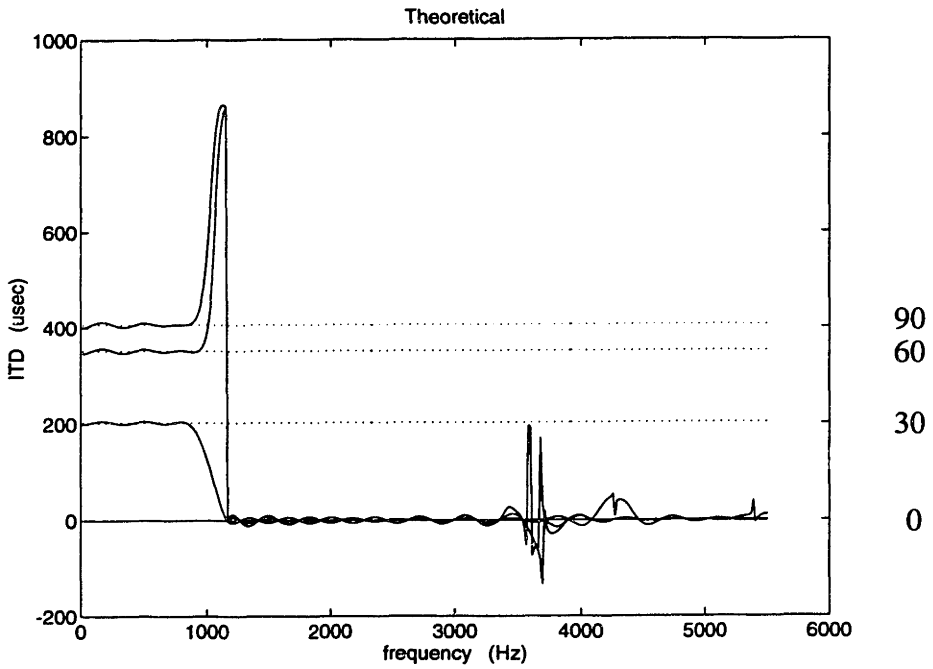

Figure 4-22: Theoretical free-field ITDs for the Lowpass/Highpass system, $f_c = 1000$ Hz (solid lines) and for the Pass Through system (dotted lines).

Figure 4-23 shows measurements for the Pass Through system, which theoretically maintains 'perfect' ITDs. In both cases, the output ITDs resemble the theoretical ITDs. The free-field results follow the theoretical predictions extremely closely, while the eyeglass-mounted results show some deviation, that increase at low frequencies. These low-frequency ITDs (which are the ones of interest in sound localization) are *greater* in the eyeglass-mounted cases than in the free-field case, behavior that arises due to sound diffraction about the head. This increase in low-frequency ITDs is actually desirable, because it causes the system to produce output ITDs that are closer to the natural ones, as shown in Figure 4-4 (b) for the conventional binaural hearing aid.

Figure 4-24 shows the output ITDs for the Combined system. As with the Pass-Through system, the free-field results follow the theoretical predictions closely, while the eyeglass-mounted results show deviations that increase at low frequencies. Actually, the eyeglass-mounted low-frequency ITDs are as large as those measured near the ears with the conventional binaural hearing aid, Figure 4-4 (b), and so head-mounting again has the desirable effect of rendering the low-frequency ITDs more realistic. Chapter 5 will explore whether the variations of these ITDs as functions of frequency has any degrading effect upon the wearer's localization abilities.

Figures 4-25 shows the output ITDs for the Lowpass/Highpass system. These results behave as expected, with the lowpass portion of the output ITDs being similar to the Pass Through system ITDs for the two different mountings. The free-field ITDs follow theory quite closely while the eyeglass mounted ITDs are larger. The high-frequency ITDs are always zero for this system, which is expected due to the monaural high frequency component.

Note that all head-mounted single-array ITDs are *lower* than those of the head-mounted Dual-Cardioid system. This indicates that single-array systems produce ITDs that are smaller than the naturally occurring ones, which should affect the wearer's ability to localize sound. These ITDs could be made more realistic by increas-

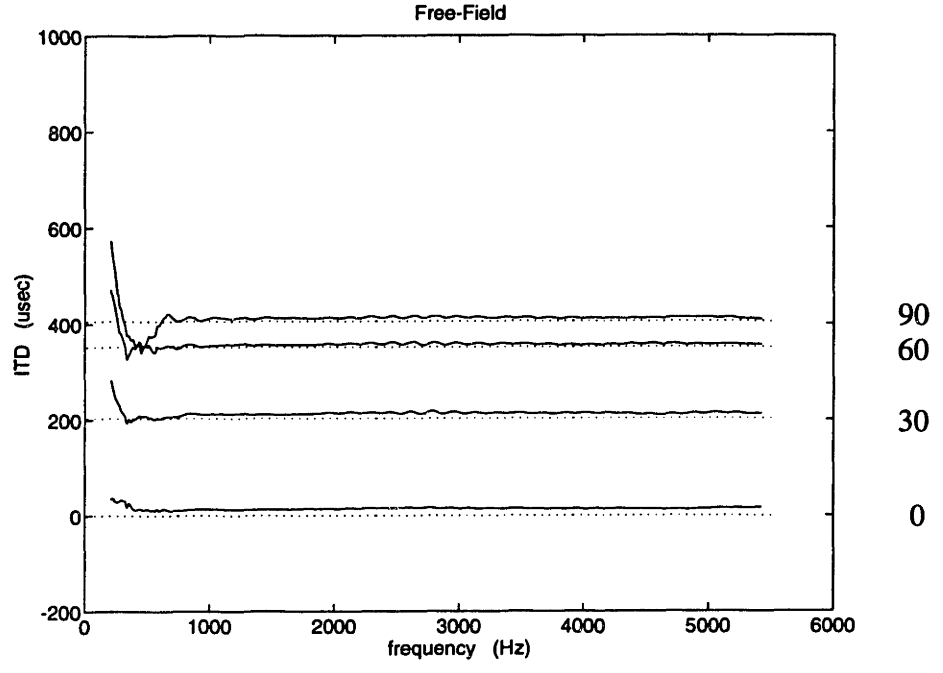

(a)

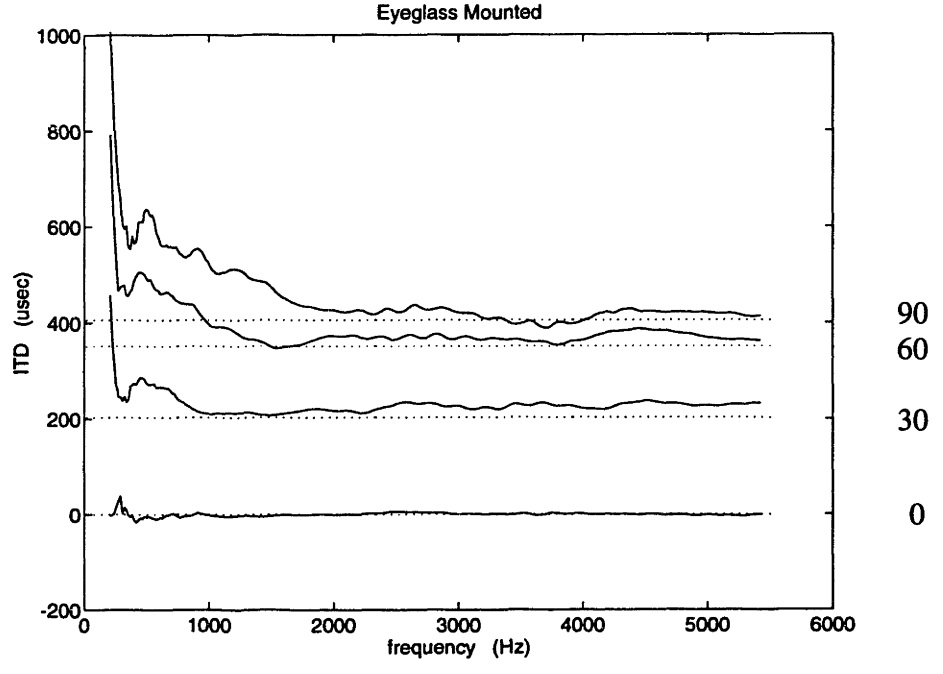

(b)

Figure 4-23: Measures ITDs for the Pass Through system with (a) free-field mounting and (b) eyeglass mounting. Dotted lines indicate theoretical free-field behavior.

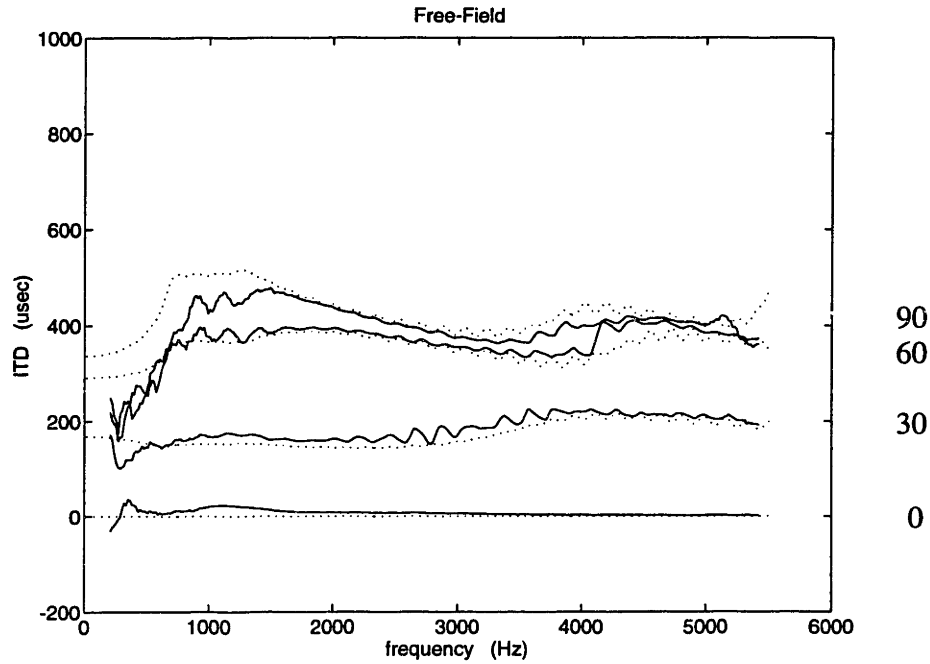

(a)

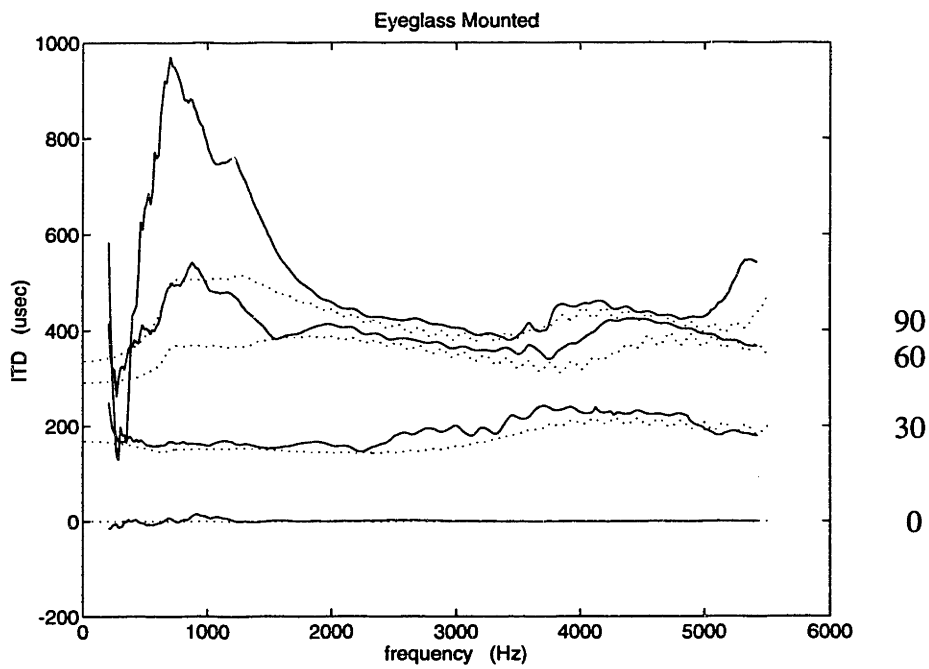

(b)

Figure 4-24: Measured ITDs for the Combined ($\tau(\omega) = 40\mu sec$) system with (a) free-field mounting and (b) eyeglass mounting. Dotted lines indicate theoretical free-field behavior.

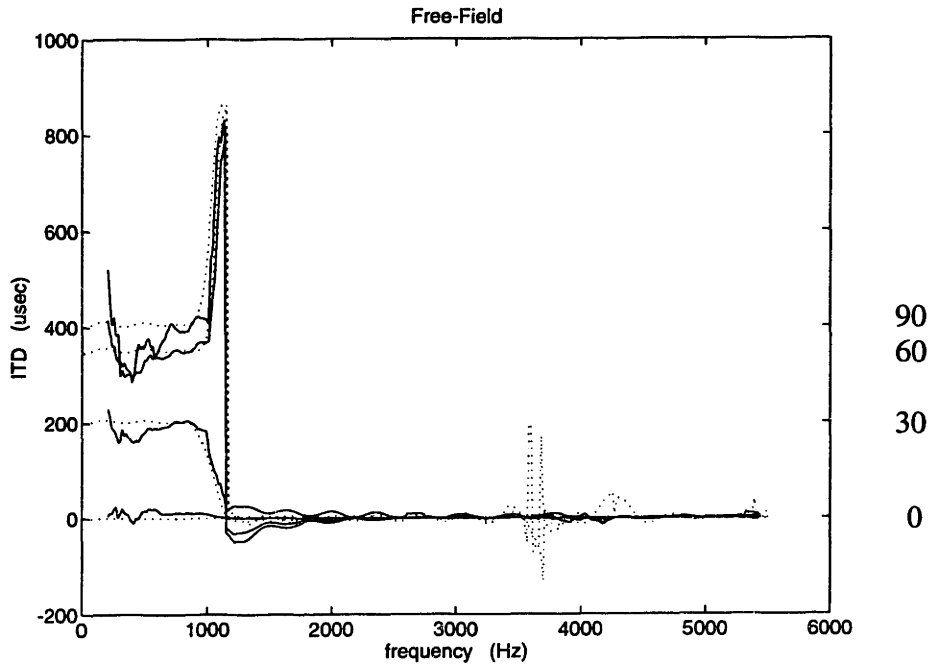

(a)

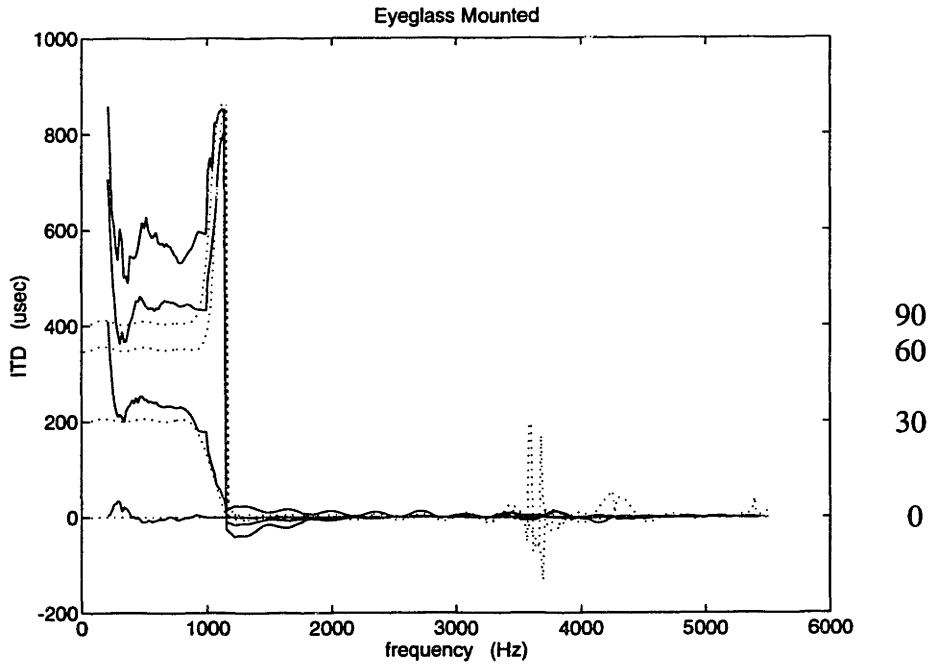

(b)

Figure 4-25: Measured ITDs for the Lowpass/HighPass ($f_c = 1000\ Hz$) system with (a) free-field mounting and (b) eyeglass mounting. Dotted lines indicate theoretical free-field behavior.

ing the broadside array span so that spacing between the outermost array elements more accurately reflected the natural inter-ear spacing.

4.5 Interpretation of Results

4.5.1 Directionality

The directionality results for both the dual-array (Table 4.3) and single-array (Table 4.5) systems suggest that the multimicrophone, binaural output hearing aid structures developed in Chapter 3 are capable of increasing overall directionality, relative to a conventional, Dual-Cardioid binaural hearing aid, while still producing a realistic binaural output. All multimicrophone test systems (excluding the Pass Through single-array system, which served as a lower bound on directionality) exhibited theoretical free-field levels of D_{IW} that were 3-4 dB greater than the corresponding levels for the Dual-Cardioid aid. Moreover, the measured results, $D_{IW,az}$, indicate that these systems retain their increased directionality when mounted upon the head.

Comparing the two classes of binaural multimicrophone system to each other, the dual-array systems (Table 4.3) consistently exhibited higher levels of theoretical D_{IW} than the single-array systems (Table 4.5). The measured values of $D_{IW,az}$, as well as the actual intelligibility-weighted polar plots, $|G_{IW}(\theta, \phi = 0)|$, indicate, however, that head mounting degrades the dual-array systems to a greater degree than single-array systems. One cause of this discrepancy in head-mounting effects lies in the fact that all measurements were made in the azimuth-plane, in which head-shadow effects degrade dual-array endfire performance to a greater degree than they affect single-array broadside performance. To see why this is so, consider the head-mounted dual- and single-array systems. The only single-array mounting in which head shadow had a serious effect on azimuth-plane performance was the eyeglass mounting – the head did not block azimuth sources with the headband mounting. In the eyeglass-mounted case, the head shadowed sources arrive from behind the listener, thus reinforcing the

system null at 180° and improving performance relative to the measured free-field performance. For the head-mounted dual-array systems, however, head shadow affected sources to one side of the listener. The resulting diffraction effects degraded the nulls that these arrays have to the sides and, consequently, degraded the directional performance.

Overall, head shadowing caused a greater degradation of azimuth-plane performance in dual-array endfire systems versus single-array broadside systems. The overall levels of degradation due to head mounting were reasonably similar for *all* systems tested, dual- or single-array, and no one system exhibited strikingly different behavior upon head mounting.

4.5.2 Output ITDs

Comparing the output ITDs of the binaural multimicrophone systems with the output ITDs of the conventional binaural hearing aid reveals that the multimicrophone systems can produce output ITDs that reflect the naturally occurring ITDs near the ears. In all cases, head mounting has the desirable effect of increasing the 'naturalness' of the output ITDs – the output ITDs become closer to their values at the ears, shown in Figure 4-4 (b).

Comparing the two classes of multimicrophone systems, the single and dual-array systems perform comparably, with the dual-array systems producing slightly more realistic ITDs. This arises due to the more natural location of the arrays in the dual-array systems – one array on either side of the head. This array placement results in the dual-array systems experiencing greater azimuth-plane head shadowing effects, and so their output ITDs are more natural. The only exception to this conclusion is the Dual +/- Gradient array, for which the locations of the nulls in the directional pattern together with the high noise sensitivity result in inaccurate output ITDs.

In summary, this chapter has demonstrated that the systems presented in Chapter 3 do indeed meet both goals of this thesis. They exhibit both directionality and

binaural fidelity to varying degrees. Moreover, these results have shown that the systems can be designed for free-field operation and subsequently head-mounted without substantial performance loss. In fact, head mounting results in *more* realistic output ITDs for all systems.

Chapter 5

Behavioral Evaluation

This chapter presents the results of a behavioral evaluation performed on normal-hearing subjects and consisting of two parts:

1. Speech Intelligibility in Noise: Directionality was explored by measuring system intelligibility weighted gain, G_I, and by testing the wearer's ability to comprehend target-direction speech in a diffuse noise field.

2. Sound Localization: Binaural cue fidelity was measured by testing the wearer's ability to localize sound sources in the azimuth plane.

5.1 Test Systems

Evaluations were conducted on thirteen head-mounted system designs, all of which were also tested in Chapter 4 (with the exception of the Lowpass/Highpass single-array system that was tested with a cutoff frequency of 1000 Hz in Chapter 4 and 800 Hz in this chapter). The systems are:

- System 1. Naked Ear (i.e. no hearing aid): This served as the primary reference system. This 'system' provided no enhancement of directional sensitivity, but it retained perfectly natural binaural cues.

- System 2. Dual-Cardioid: This served as the secondary reference system. It is the simplest case of a directional, binaural hearing aid, consisting of two cardioid microphones (Knowles EL-3085, port-spacing = 14 mm) located at the ears and providing some enhancement in the wearer's directional sensitivity with near perfect preservation of the natural binaural cues.

- Systems 3-4. Dual-Array Systems: These form the first subclass of binaural output, multimicrophone hearing aids (Section 3.2). These test systems consisted of two endfire arrays, each implemented with two cardioid microphones (Knowles EL-3085, port-spacing = 14 mm). These systems were:

  - 3. Dual-Optimal Endfire: Each endfire array was designed to maximize free-field directivity, $D(\omega)$. The center-to-center microphone spacing was 9.2 cm (total array span of 10.6 cm, including the 14 mm microphone port-spacing) and the arrays were mounted along the temples of a pair of eyeglasses, as shown in Figure 4-8. (See Figure 4-5 for the interior structure of this system.)

  - 4a,4b. Dual +/- Gradient: Each array output was formed by subtracting the output of the rear microphone from that of the front microphone. In this case the center-to-center microphone spacing was 2.6 cm (total array span of 4 cm, including the 14 mm microphone port spacing) and the arrays were head-mounted in two different ways: (a) along eyeglass temples near the front of the eyeglasses and (b) along the temples near the ears, as shown in Figure 4-9. (See Figure 4-7 for the interior structure of this system.)

- Systems 5-8. Single-Array Systems: These form the second subclass of multimicrophone, binaural output systems (Section 3.3). All single-array systems consisted of a broadside array with four equispaced cardioid microphones (Knowles EB-1979, port-spacing = 8.5 mm). Two separate head mountings, shown in Figure 4-18, were investigated for each system: (a) mounted along the front of

a pair of eyeglasses, and (b) mounted on a headband.

- 5a,5b. Optimal Directivity: Each output signal was formed to maximize free-field directivity. As discussed in Chapter 3, this led to a monaural output, and so this system preserved no binaural cues. Figure 4-16, with zero cutoff frequency, $f_c = 0$ Hz, gives the detailed system structure.
- 6a,6b. Uniform Weighting: Each output signal is simply the average of the array inputs. Note that, like the Optimal Directivity system, this system produces a monaural output, and, consequently, these two systems should exhibit similar results for sound localization. For this reason, localization measurements were made only for the Optimal Directivity system. Figure 4-17 with zero cutoff frequency, $f_c = 0$ Hz, gives the system structure.
- 7a,7b. Combined ($\tau(\omega) = 40\mu sec$): System filters were chosen according to Equation 3.12 in order to maximize directivity, $D(\omega)$, while keeping RMS ITD error, $E(\omega)$, below $40\mu sec$. Figure 4-15 shows the detailed structure of this system.
- 8a,8b. Lowpass/Highpass ($f_c = 800$ Hz): The outermost array inputs were sent directly to the corresponding ears as the low-frequency ($f < f_c$) component of the outputs and the maximum directivity signal was sent to both output signals as the common high-frequency ($f > f_c$) component of the outputs. This system maintained RMS ITD error at 0 for low frequencies and maximized directivity for high frequencies. Figure 4-16 shows the basic structure of this system, with the lowpass and highpass filters both having cutoff frequencies at $f_c = 800$ Hz[1].

Table 5.1 summarizes the thirteen test systems along with their associated numerical labels.

[1]This system differs slightly from the Lowpass/Highpass system tested in Chapter 4 in that the cutoff frequency has been changed from 1000 Hz to 800 Hz.

Table 5.1: The thirteen test systems and their numerical labels.

Number	Reference Systems
1	Naked Ear
2	Dual Cardioid at ear
Number	**Dual Array Systems**
3	Dual Optimal Endfire along eyeglass temple mounting
4a	Dual +/- Gradient - front of eyeglass temple mounting
4b	Dual +/- Gradient - near ear mounting
Number	**Single Array Systems**
5a	Optimal Directivity - eyeglasses mounting
5b	Optimal Directivity - headband mounting
6a	Uniform Weighting - eyeglasses mounting
6b	Uniform Weighting - headband mounting
7a	Combined ($\tau(\omega) = 40\mu sec$) - eyeglass mounting
7b	Combined ($\tau(\omega) = 40\mu sec$) - headband mounting
8a	Lowpass/Highpass (f_c = 800 Hz) - eyeglass mounting
8b	Lowpass/Highpass (f_c = 800 Hz) - headband mounting

All hearing aid systems, Systems 2-8b, were implemented using two Ariel DSP96000 boards, each of which contained a Motorola 96000 signal processor and dual-channel I/O. The filters $W_i(\omega)$, as specified by Equation 2.11, were implemented using 127-tap, equiripple FIR approximations to the ideal filters, and the lowpass and highpass filters were implemented using 63-tap, equiripple FIR approximations, with transition regions 300 Hz wide centered at the cutoff frequency. The array outputs were amplified using a Crown D-75 amplifier and presented to the wearer via a set of Etymotic Research ER-3A insert earphones. Insert earphones were employed avoid the effects of the headset.

5.2 Testing Procedures and Results

The 13 systems were evaluated on five (paid) normal-hearing subjects, who ranged in age from 18-22 years. The following two sections present the detailed descriptions of the speech intelligibility in noise and the sound localization test procedures.

5.2.1 Speech Intelligibility in Noise

This test consisted of two parts:

1. Measurement of the intelligibility-weighted gain G_I [10] of each test system was performed within the specific speech-intelligibility test environment. G_I, mathematically defined in the following section, is a measure of the expected intelligibility gain provided by a given system and will serve as a reference against which to compare the actual speech intelligibility improvements attained by the subjects.

2. Subjects' speech reception thresholds (SRTs) were determined using the Hearing In Noise Test (HINT) [19] for the thirteen test systems with target sentences presented from 1 m directly ahead of the subject and noise presented in a quasi-diffuse field.

Figure 5-1 shows the experimental setup for both of these tests. Four Optimus Pro-7 loudspeakers were positioned in the corners of a non-treated room (6.1x4.0x2.7 m) and driven to create a quasi-diffuse[2] noise field about the subject. Each loudspeaker played a separate track of HINT Noise[3], amplified by an Optimus SA-155 amplifier, and together they generated a free-field noise level of 65 dBA at the location of the subject. Target sentences, also amplified by an Optimus SA-155, were played from an Optimus Pro-7 loudspeaker located 1 m directly in front of the subject. Target level was adjusted so that HINT Noise played through the target loudspeaker produced a reference level of 65 dBA at the subject.

Intelligibility-weighted Gain, G_I

Method: As mentioned above, G_I predicts the intelligibility gain provided by a given system. Theoretically, in a perfectly diffuse noise field, the free-field G_I should equal the intelligibility-weighted free-field directivity, D_{IW} (presented in Chapter 2). By definition, G_I [10] is given by:

$$G_I = \sum_{i=1}^{14} \gamma_i (\mathrm{TJR}_{output}(\omega_i) - \mathrm{TJR}_{input}(\omega_i)), \tag{5.1}$$

where the γ_i are the intelligibility weights for the 14 third-octave bands from 200-4000 Hz (defined in Chapter 2), $\mathrm{TJR}_{output}(\omega_i)$ is the output target-to-jammer ratio at the frequency ω_i, $\mathrm{TJR}_{input}(\omega_i)$ is the input target-to-jammer at the frequency ω_i, and the ω_i are the fourteen center frequencies of the third-octave bands mentioned above. More specifically, the $\mathrm{TJR}_{input}(\omega_i)$ is the ratio (expressed in dB) of the power due to the target signal (with no noise) at ω_i to the power due to noise (with no target) at ω_i, as measured by an omnidirectional microphone. The $\mathrm{TJR}_{output}(\omega_i)$ is a similar ratio measured for the output signals of the hearing aid in question.

[2]Measurements in Appendix D indicate that the noise field was *weaker*, by about 2 dB, from the up-down direction relative to the horizontal directions.

[3]HINT Noise is colored noise that is spectrally matched to the speaker of the HINT sentences used to determine the SRTs.

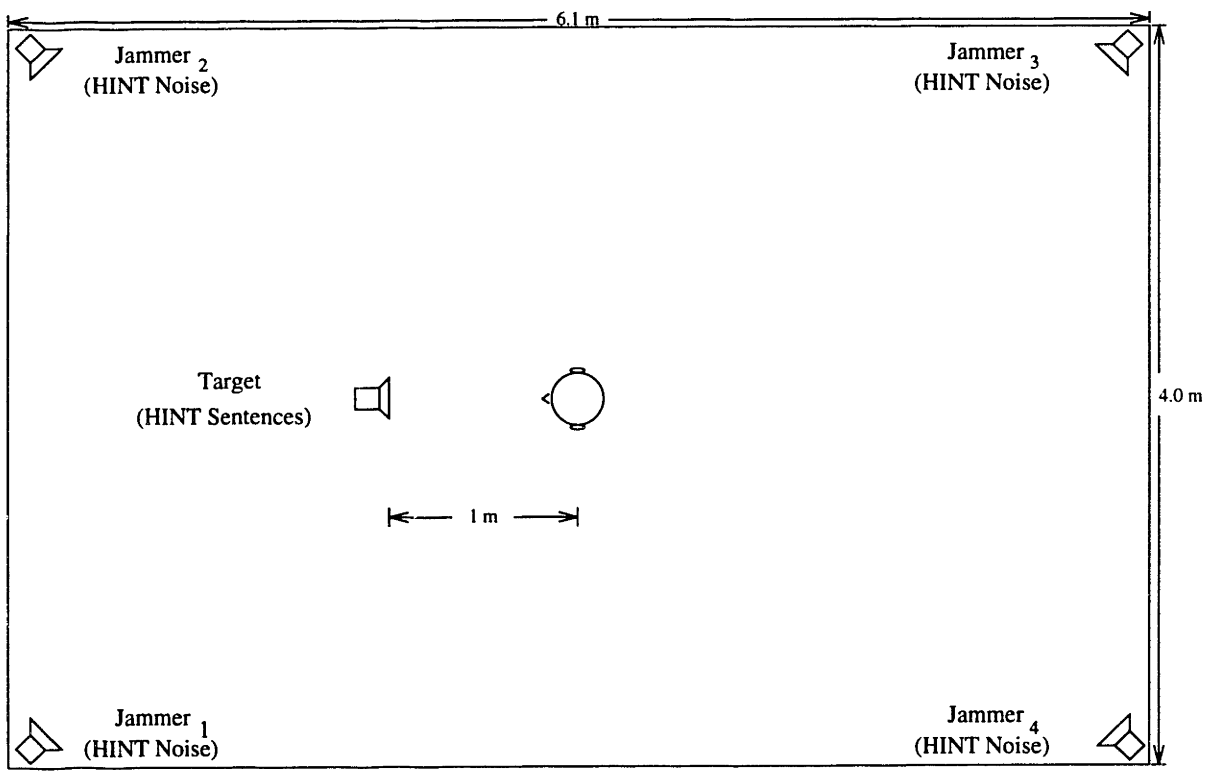

Figure 5-1: Experimental setup for the speech intelligibility evaluation (room dimensions 6.1x4.0x2.7m).

The TJR_{input} was determined by measuring the power spectrum produced by the target loudspeaker playing HINT noise, and the power spectrum produced by the quasi-diffuse noise field produced by the four jammer loudspeakers. These measurements employed an omnidirectional microphone (Knowles BT-1759) located in the free-field at the position of the subject's head, with the subject absent, and an HP35660A spectrum analyzer. The measured power spectra were then processed to determine the target and noise powers within each of the fourteen third-octave bands. The ratios of the fourteen target-output powers to their respective noise-field powers were then interpreted as $TJR_{input}(\omega_i)$ at the fourteen ω_i.

The $TJR_{output}(\omega_i)$ were measured with the KEMAR manikin as the 'subject' and were obtained as above, except that the output power spectra were obtained from the system under measurement and not from an omnidirectional microphone. For the Naked Ear case, the power spectra were measured directly by microphones (Etymotic Research ER-11) placed in the ears of KEMAR. For the aided cases, the hearing aid outputs were presented to KEMAR via the Etymotic ER-3A insert earphones and the power spectra were obtained from the microphones in KEMAR's ears.

The TJR_{output} values were obtained for both the right and left outputs of the thirteen test systems, and, therefore, G_Is were obtained for both ears. These values were averaged to form a single G_I for each system.

Results: Table 5.2 shows the right, left, and averaged G_I values, as well as the theoretical D_{IW} values, for each of the thirteen test systems. Although the measured G_I clearly demonstrate that all aided systems provide some intelligibility gain over the unaided case, the gains are all significantly *lower* than the theoretical D_{IW} values (which they should match). Within each class of systems, however, the ordering of G_I does reflect the ordering of D_{IW} (systems with higher relative D_{IW}s have higher relative G_Is). This correspondence suggests that the discrepancies between G_I and D_{IW} are due to overall common factors that affect all systems within a given class. Four possible causes of the performance degradation evident in the measured G_Is are:

Table 5.2: G_I measurements (in dB) for the test systems, along with the corresponding theoretical, three-dimensional D_{IW} values.

System	System Number	Right Ear	Left Ear	Average G_I	Theoretical Free-field D_{IW}
Reference Systems					
Naked Ear	1	0.64	0.19	0.40	N/A
Dual-Cardioid	2	2.30	1.72	2.01	4.59
Dual-array Systems					
Dual-Optimal Endfire	3	3.21	3.79	3.50	8.12
Dual +/- Gradient	4a	3.82	4.45	4.13	8.53
	4b	4.14	3.96	4.05	
Single-array Systems					
Optimal Directivity	5a	6.39	6.31	6.35	8.03
	5b	6.01	5.09	5.55	
Uniform Weighting	6a	5.27	5.65	5.46	7.18
	6b	5.58	4.45	5.02	
Combined	7a	5.28	4.52	4.90	7.06
	7b	4.87	4.75	4.81	
Lowpass/Highpass	8a	6.68	5.74	6.21	7.66
	8b	5.44	5.51	5.48	

1. Head-mounting: Theoretical D_{IW}s were determined for the free-field case whereas G_Is were measured for the head-mounted cases. Chapter 4 demonstrated that head-mounting tends to degrade the directional performance of a given system, thus resulting in measured G_I lower than theoretical D_{IW}.

2. Non-direct target: Equality of G_I with D_{IW} assumes that the received target power is purely direct. In that the received target contains both direct and reverberant power, the measured G_I will be lower.

3. Non-diffuse noise: Equality of G_I and D_{IW} requires a diffuse noise field within the test environment. If the noise is not diffuse, the G_I measurements will not equal the theoretical D_{IW} values.

4. Non-omnidirectional reference microphone: The TJR_{input} measurements used to form G_I assume that the reference microphone is omnidirectional. This omnidirectional reference is required for measured G_I to equal theoretical D_{IW}. If the reference microphone were more sensitive in the target direction, this would lower measured G_I values.

In order to explore the contributions of these four factors in lowering the measured G_I in Table 5.2, Table 5.3 shows the difference between measured G_I and theoretical D_{IW} for the reference Dual-Cardioid system, the dual-array systems and the single-array systems. Note that the values for the dual- and single-array systems are the *average* values over all systems within that class. Observe that the degradation in G_I for single-array systems (2.0 dB) is smaller than that of the dual-array systems (4.5 dB). This difference arises, in part, because the endfire-arrays in the dual-array systems are more sensitive to head-mounting than the broadside-arrays in the single-array systems. To support this, Table 5.3 also shows the measured drop in G_I that arises due to head-mounting for three-example systems: the Dual-Cardioid, the Dual +/- Gradient (as an example of dual-array systems), and the Uniform Weighting (as

an example of single-array systems)[4]. These results show that head-mounting does degrade single-array systems less than the Dual-Cardioid or dual-array systems.

Table 5.3: Average degradation between G_I and D_{IW}. The table also shows the drop in G_I that arises upon head-mounting the system.

System	Average Loss in G_I	Loss due to Head-Mounting
Dual-Cardioid	2.6	1.2
Dual-Array Systems	4.5	1.2
Single-Array Systems	2.0	0.3

Regarding the rightmost column of Table 5.3 as the G_I degradation due to head-mounting and subtracting these values from the overall G_I degradation, the remaining degradations (1.4 dB for the Dual-Cardioid system, 3.3 dB for the Dual-Array systems, and 1.7 dB for the Single-Array systems) must arise from the other three factors listed above. Of these, the non-omnidirectional response of the reference microphone is probably least significant. Non-direct target is likely to be substantial with an expected direct-to-reverberant power ratio estimated to be near 0 dB. Non-diffuse noise is also significant, as shown by additional measurements in Appendix D that indicate less power (about 2.5 dB) from the up-down direction (due to acoustic ceiling tile) than from horizontal directions.

Determination of Speech Reception Thresholds (SRTs)

Method: The SRTs of the various test systems were determined using the Hearing In Noise Test (HINT) [19] with the following procedure:

1. For each system and with the diffuse noise field in place, one list of HINT sentences was played from the target loudspeaker located at 1 m directly in

[4]These values were obtained by measuring G_I for both the free-field and head-mounted cases.

front of the subject.

2. Under the HINT procedure, the levels of successive target sentences were adjusted based upon the correctness[5] of the subjects responses.

3. The final six presentation levels were averaged to form the subject's Speech Reception Threshold (SRT) for the system under evaluation, where the SRT is an estimate of the presentation level of the target signal required for a subject to recognize speech materials 50% of the time.

Each subject was tested twice with each system, and the two SRTs were averaged (in dB) to form an overall system SRT[6]. All SRTs for a given subject were normalized by the SRT of the Naked Ear system, and so the results presented are *relative to* the Naked Ear case.

Results: Table 5.4 shows the SRTs obtained for each of the five subjects, DB, ME, CK, JP, and JS, as well as the average (in dB) across subject and the corresponding standard deviations. These SRTs indicate how much gain needs to be applied to the target source so that the subjects' speech comprehension is the same as with the Naked Ear[7] and should roughly equal the negatives of the measured G_I values (Table 5.2). Figure 5-2 shows the SRT results. Note: as a measure of the total variability of these measurements, the overall average standard deviation[8] is equal to 1.30 dB. Observations arising from these data are:

1. The dual- and single-array systems exhibit similar SRTs, 3-4 dB, which indicates that neither class of system provides superior speech intelligibility performance.

[5]To be considered 'correct', a subject's response had to identify correctly all words in the sentence, with the exception of articles (e.g. 'a' ve 'the') and tenses of 'to be' (e.g. 'is' vs 'was').

[6]Subject ME was unable to undergo the second set of tests, and so her results were based on a single SRT measurement for each system.

[7]The actual Naked Ear SRTs for subjects DB, ME, CK, JP, and JS are 2.86, 2.28, 2.28, 2.28, and 2.14 dB, respectively, with an average SRT = 2.39 dB.

[8]Given by $\sigma_{avg} = \frac{1}{n}\sum_i \sigma_i$, where σ_i are the standard deviations of the test systems.

Table 5.4: Average differences in SRT (in dB), relative to the Naked Ear, for each of the five subjects and averaged over subject. The rightmost column is the standard deviation across subject.

System	System Number	DB SRT	ME SRT	CK SRT	JP SRT	JS SRT	Average SRT	σ
Reference Systems								
Naked Ear	1	0	0	0	0	0	0	N/A
Dual-Cardioid	2	-1.14	0	-0.86	-0.43	-0.44	-0.57	0.44
Dual-Array Systems								
Dual-Optimal Endfire	3	-5.29	-2.86	-3.43	-3.72	-2.72	-3.60	1.03
Dual +/- Gradient	4a	-4.57	-1.15	-4.14	-4.86	-3.86	-3.72	1.49
	4b	-2.56	-4.00	-3.43	-5.43	-3.29	-3.74	1.07
Average		-4.14	-2.67	-3.67	-4.67	-3.29	-3.69	0.77
Single-Array Systems								
Optimal Directivity	5a	-5.72	-7.43	-3.00	-3.15	-0.15	-3.89	2.79
	5b	-2.14	-4.01	-4.00	-4.57	-2.15	-3.37	1.40
Uniform Weighting	6a	-3.71	-1.15	-4.00	-2.29	-1.00	-2.43	1.40
	6b	-3.43	-6.29	-3.71	-5.15	-2.14	-4.14	1.61
Combined	7a	-4.57	-3.43	-2.00	-3.71	-3.00	-3.34	0.94
	7b	-3.00	-4.57	-4.57	-6.56	-1.57	-4.05	1.88
Lowpass/Highpass	8a	-3.43	-4.57	-2.85	-2.86	-3.00	-3.34	0.73
	8b	-4.14	-6.86	-5.06	-4.57	-4.71	-5.07	1.05
Average		-3.77	-4.79	-3.65	-4.11	-2.22	-3.71	0.94

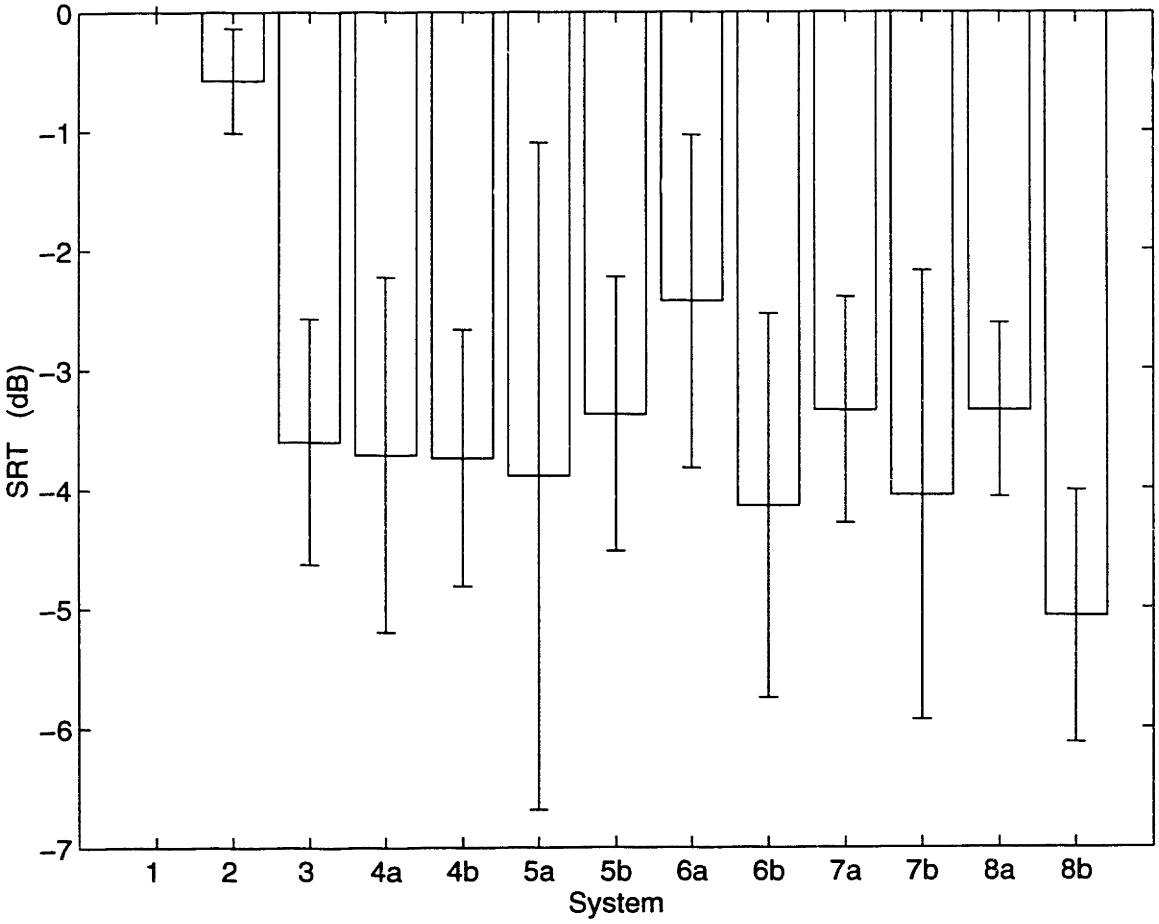

Figure 5-2: Average SRTs and corresponding standard deviations.

2. The simplified, sub-optimal systems yield similar SRTs to their more complex, optimal counterparts. This is an important result – substantial speech intelligibility improvements can be obtained with simple, easy-to-construct systems.

3. The SRTs are all lower than the measured G_Is. In part, these differences result from the fact that the SRTs are intelligibility gains measured relative to the Naked Ear, whereas the G_Is are intelligibility gains measured relative to an omnidirectional microphone. To compare the SRTs with the G_Is, all G_I measurements should be normalized to the 0.4 dB Naked Ear gain in G_I (Table 5.2).

4. Great correspondence between SRT and G_I is achieved when the results are normalized to the Dual-Cardioid system, rather than the Naked Ear. These re-normalized values (see Table 5.5) demonstrate a better correspondence between SRT and G_I, especially for the single-array systems.

5. Within the dual- and single-array classes, the relative ordering of the SRTs does *not* reflect the ordering of the corresponding G_Is. However, variability in the SRT results limits their precision. Had more test runs been made on each subject for each of the test systems, a better correspondence might be found. As an indication of the intra-test variability of the SRTs, Table 5.6 shows the standard deviation between the first and second test runs, averaged (in dB) over the thirteen test systems[9]. The overall average intra-test variability was $\sigma_{\text{intra-test}} = 1.28$ dB.

Overall, these results demonstrate that the binaural output, multimicrophone hearing aids provide the wearer with significant speech intelligibility benefits over the Naked Ear case. No one class of systems exhibits superior performance, however, and, more importantly, equivalent performance levels are achieved with both optimal systems and their simplified, sub-optimal counterparts.

[9]Appendix E gives the individual subject test results.

Table 5.5: SRT and G_I measurements presented relative to the Dual-Cardioid system.

System	System Number	SRT (dB)	G_I
Reference Systems			
Dual-Cardioid	2	0	0
Dual-Array Systems			
Dual-Optimal Endfire	3	-3.03	1.49
Dual +/- Gradient	4a	-3.15	2.12
	4b	-3.17	2.04
Average		-3.12	1.88
Single-Array Systems			
Optimal Directivity	5a	-3.29	4.34
	5b	-2.80	3.54
Uniform Weighting	6a	-1.86	3.45
	6b	-3.57	3.01
Combined	7a	-2.77	2.89
	7b	-3.48	2.80
Lowpass/Highpass	8a	-2.77	4.20
	8b	-4.50	3.47
Average		-3.13	3.46

Table 5.6: Subject and average inter-test variability, in dB.

Subject	$\sigma_{subject}$
DB	1.92
CK	0.62
JP	1.43
JS	1.15
$\sigma_{\text{intra-test}} =$	1.28

5.2.2 Sound Localization

Method: The subject was seated at the center of a seven-loudspeaker (Optimus Pro-7) semi-circle, with the loudspeakers located in the subject's azimuthal plane from $-90°$ to $90°$ at $30°$ intervals at a distance of 1 m (see Figure 5-3). A speech fragment of about 2-3 seconds duration was played from a loudspeaker chosen at random and the subject was asked to identify the speaker. The speech fragments, taken from an analog cassette that continuously repeated a single male speaker reading a 1.5 minute passage, were presented at a level of 60 dBA, and the system gain was adjusted to the loudest comfortable level for the subject[10]. A test run included 70 speech fragments (10 per speaker). For each of the eleven test systems[11], two runs were performed.

Results: The results are presented in the form of confusion matrices, totaled over all five subjects[12], as well as the percent-correct responses and the RMS angle-identification error for each of the eleven systems tested (see Figure 5-4). The systems are referred to by *numerical label* (see Table 5.1 for the corresponding systems), and for each matrix, the rows correspond to the stimulus speaker (S) actually presented and the columns correspond to the response speaker (R) given by the subjects. Several results follow from these confusion matrices:

1. Figure 5-4(a) shows that the subjects achieved near perfect sound localization with the Naked Ear. In fact, four of the six total errors involved a left/right reversal; they were all due to the same subject and may have resulted from a sign error made in reporting rather than an actual sound localization error. If the signs of these responses were reversed, the percentage correct would be 99.6% and the RMS localization error would be 1.96°.

[10]One subject, ME, experienced difficulties in obtaining a good seal with the ear insert earphones. Consequently, the presentation level was reduced to 57 dBA and the system gain increased by about 3 dB.

[11]Recall that the Uniform weighting systems, 6a and 6b, were *not* tested for sound localization.

[12]Appendix F contains the individual subject results.

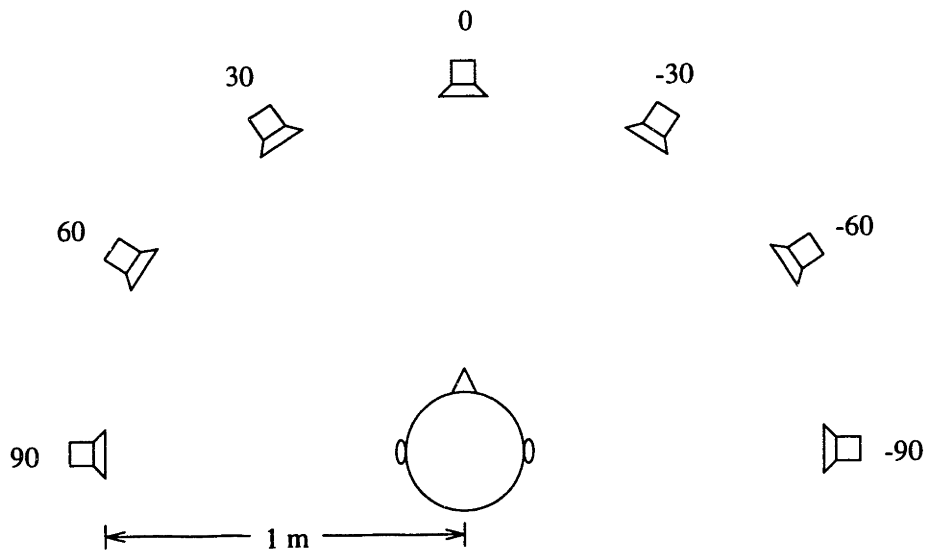

Figure 5-3: Physical setup of the sound localization experiment, in which the subject was asked to determine the source loudspeaker from a semi-circle of seven loudspeakers located in the subject's azimuth plane.

2. Figure 5-4(b) demonstrates that the Dual-Cardioid binaural aid leads to very good localization. The majority of the errors occur when the source is at $\pm 90°$, which indicates that a binaural aid located at the ears maintains binaural cues for sources located centrally ahead of the listener but not (perfectly) for lateral sources. These results serve as an upper bound on the localization performance for the aided systems, 2 through 8b.

3. Figure 5-4(c) demonstrates that the localization performance with the Dual-Optimal Endfire system is slightly worse than that with the Dual-Cardioid system – there were greater difficulties localizing lateral sounds, with the range of difficulty expanding from $\pm 90°$ (as occurred for the dual-cardioid aid) to also include sources arriving from $\pm 60°$.

4. Figures 5-4(d) and (e) demonstrate that the performance with the Dual +/- Gradient systems is slightly worse than the Dual-Optimal Endfire system – subjects have some difficulty localizing central as well as lateral sources. One phenomenon evident with these systems is the left-right reversal that occurs with sources at $\pm 90°$. Recall from Figure 4-14 that the output ITDs produced by the Dual +/- Gradient are unreliable for sources arriving from $\pm 90°$. Therefore, although the subjects had a rough idea that lateral sources were different from central sources, they had difficulty discerning the correct side.

5. Figures 5-4(f) and (g) indicate that both head mountings of the Optimal Directivity system, which has a monaural output, provide few localization cues. Performance was not random, however, indicating that some cues were available. Cues may have arisen due to leakage through the insert earphones and due to the system's directional response itself. This system is most sensitive to sources from $0°$, and given that the speech fragments were presented at the same level from all seven loudspeakers, the $0°$ source always sounded louder and fuller than off-axis sources. Thus, subjects were able to identify $0°$ cor-

rectly three-quarters of the time. Similarly, the more central sources tended to be less attenuated, and some subjects could identify whether a source was closer to 0° or more towards ±90°. While these cues did assist the subjects in judging a sources arrival angle, they provided for no left-right discrimination. Any remaining localization cues evident in these 'monaural' results are probably due to leakage through the headphones. Based on the approximate symmetry of the confusion matrices, leakage cues appear to have been small.

6. Figures 5-4(h) through (k) demonstrate that the Combined and Lowpass/Highpass systems both provided similar localization cues for both types of head mountings. As with all of the binaural systems, the localization errors increase for sources located further away from the center target direction. A particular property of these systems, however, was that subjects tended to compress the source arrival directions towards 0° – identifying sources as arriving from angles closer to 0° than they actually were. This behavior arose, presumably, from the short span of these 14-cm broadside arrays relative to the natural inter-ear spacing. Recall that all single array systems were designed to preserve the ITDs experienced by the two outermost array elements, and, consequently, for these arrays, the ITDs being preserved were smaller than the ITDs actually experienced at the ears (as evident in the physical measurements shown in Figures 4-4, 4-24, and 4-25). Smaller ITDs resulted in the compression of perceived source arrival angle. Another conclusion from these confusion matrices is that the more complex processing of the Combined system, which partially preserves ITDs over the entire frequency spectrum, yields sound localization performance equivalent to that of the much simpler Lowpass/Highpass system, which preserves ITDs only up to 800 Hz. Thus, preserving only low-frequency ITDs appears adequate for sound localization.

Considering all of these results, the test systems behaved as expected, and the deviations from the Naked Ear case and from each other can be qualitatively accounted

for by considering the geometry and directional behavior of the different systems.

The primary conclusions that can be drawn from the evaluations in this chapter are:

- All dual- and single-array systems (3-8b) exhibit similar speech intelligibility gains relative to the reference systems (1,2) – no system exhibits discernibly better performance. Furthermore, the SRTs indicate that the simpler test systems, i.e. the Dual +/- Gradient systems (4a,4b), the Uniform Weighting systems (6a,6b), and the Lowpass/Highpass systems (8a,8b), yield speech intelligibility gains similar to those of their more complex counterparts.

- All binaural output dual- and single-array systems provide sufficient binaural cues that allow for reasonably accurate localization for sources located close to the target direction but that are less accurate for lateral sources. Of these, the dual-array systems generally provide more realistic binaural cues than the single-array systems, except in the case of the Dual +/- Gradient systems, which exhibit left-right confusions for extreme lateral sources. Single-array binaural cues would be more accurate if the span of these systems were adjusted to better reflect true interaural spacing.

Overall, neither dual- nor single-array systems exhibit decisively superior speech intelligibility or sound localization performance. Therefore, the choice of the 'best' system depends on the aesthetics of system mounting and on the complexity of system implementation.

S \ R	-90	-60	-30	0	30	60	90
-90	98	1	-	-	-	1	-
-60	1	98	-	-	-	1	-
-30	-	-	98	-	2	-	-
0	-	-	-	100	-	-	-
30	-	-	-	-	100	-	-
60	-	-	-	-	-	100	-
90	-	-	-	-	-	-	100

(a) Syst. 1: 99.1% correct, 2.31° RMS error

S \ R	-90	-60	-30	0	30	60	90
-90	77	22	-	1	-	-	-
2	1	99	-	-	-	-	-
-30	-	-	100	-	-	-	-
0	-	-	-	100	-	-	-
30	-	-	-	-	100	-	-
60	-	-	-	-	-	100	-
90	-	-	-	-	-	23	77

(b) Syst. 2: 93.3% correct, 6.22° RMS error

S \ R	-90	-60	-30	0	30	60	90
-90	73	27	-	-	-	-	-
-60	20	79	1	-	-	-	-
-30	1	-	99	-	-	-	-
0	-	-	-	99	1	-	-
30	-	-	-	-	100	-	-
60	-	-	1	-	-	94	5
90	-	-	-	-	-	14	96

(c) Syst. 3: 90.0% correct, 7.03° RMS error

S \ R	-90	-60	-30	0	30	60	90
-90	17	2	-	-	1	16	64
-60	6	72	19	1	-	1	1
-30	-	10	89	1	-	-	-
0	-	1	4	94	1	-	-
30	-	-	-	2	96	2	-
60	-	-	-	1	16	83	-
90	26	7	2	2	1	13	49

(d) Syst. 4a: 71.4% correct, 51.6° RMS error

S \ R	-90	-60	-30	0	30	60	90
-90	48	2	1	-	1	10	39
-60	15	69	15	1	-	-	-
-30	-	10	89	-	1	-	-
0	-	-	3	97	-	-	-
30	-	-	-	1	96	3	-
60	-	-	1	-	5	90	4
90	22	1	2	1	-	12	62

(e) Syst. 4b: 78.7% correct, 32.9° RMS error

Figure 5-4: Sound localization confusion matrices.

S \ R	-90	-60	-30	0	30	60	90
-90	31	27	12	2	3	10	15
-60	1	44	20	9	21	4	1
-30	2	18	22	20	27	9	2
0	-	3	7	75	15	-	-
30	1	4	15	52	23	4	1
60	2	12	13	11	30	21	11
90	32	14	5	1	13	15	20

(f) Syst. 5a: 33.7% correct, 47.7° RMS error

S \ R	-90	-60	-30	0	30	60	90
-90	42	26	2	3	1	6	20
-60	3	27	44	10	11	4	1
-30	2	14	28	22	28	6	-
0	1	2	8	77	11	1	-
30	-	5	27	44	23	1	-
60	5	12	6	4	37	30	6
90	10	13	2	2	25	25	23

(g) Syst. 5b: 35.7% correct, 44.9° RMS error

S \ R	-90	-60	-30	0	30	60	90
-90	52	47	1	-	-	-	-
-60	1	39	60	-	-	-	-
-30	-	3	90	7	-	-	-
0	-	-	-	99	1	-	-
30	-	-	-	18	77	2	3
60	-	-	-	1	54	39	6
90	-	-	-	-	-	59	44

(h) Syst. 7a: 62.9% correct, 11.8° RMS error

S \ R	-90	-60	-30	0	30	60	90
-90	45	49	6	-	-	-	-
-60	2	30	68	-	-	-	-
-30	2	1	87	9	1	-	-
0	-	-	-	100	-	-	-
30	-	-	-	24	71	5	-
60	-	-	-	-	65	31	4
90	-	-	-	-	11	62	27

(i) Syst. 7b: 55.9% correct, 13.5° RMS error

S \ R	-90	-60	-30	0	30	60	90
-90	38	55	11	-	-	-	-
-60	3	44	51	2	-	-	-
-30	-	2	80	17	1	-	-
0	-	-	1	99	-	-	-
30	-	-	-	14	81	4	1
60	-	-	-	-	52	34	14
90	-	-	-	-	-	72	28

(j) Syst. 8a: 57.7% correct, 13.7° RMS error

S \ R	-90	-60	-30	0	30	60	90
-90	45	49	6	-	-	-	-
-60	-	38	62	-	-	-	-
-30	-	-	98	2	-	-	-
0	-	-	-	100	-	-	-
30	-	-	1	24	73	2	-
60	-	-	-	1	61	31	7
90	-	-	-	-	10	59	31

(k) Syst. 8b: 58.6% correct, 13.4° RMS error

Figure 5-4 (*cont*): Sound localization confusion matrices.

Chapter 6

Summary and Discussion

This thesis has developed and evaluated several methods for creating multimicrophone hearing aids that are both directional and binaural. Aids have been designed to exhibit enhanced sensitivity in the desired target direction (directly in front of the wearer) and to generate a binaural output whose inter-output time differences reflect naturally occurring interaural time differences (ITDs). These systems increase the wearer's ability to comprehend target speech in a noisy background while providing the wearer with a realistic sense of space.

Chapter 3 presented the two main classes of binaural, multimicrophone aids, including dual-array and single-array structures, together with the free-field design methods for these systems. These two classes use fundamentally different approaches to solving the design problem. Dual-array systems use two arrays to independently produce the two output signals, where each array is designed only for increased directionality and the physical spacing between the arrays generates the desired output ITDs. Single-array systems, on the other hand, use one array to produce both output signals, with the array designed for *both* increased directionality and ITD maintenance. These different system classes lead to different structures and design procedures, which, in turn, cause these systems to behave differently. First, dual-array systems use *endfire* arrays and single-array systems use *broadside* arrays, which re-

sults in different directional symmetry and behavior for these two types of systems, especially when head-mounted. Second, ITD maintenance is an actual design parameter for single-array systems, whereas it is a byproduct of the array structure for dual-array systems. This results in different binaural cues being maintained by the two classes of systems. Chapters 4 and 5 explored these differences in directional behavior and ITD maintenance and examined how these differences affected a subject's performance. Chapter 3 also introduced sub-optimal, simplified versions of the dual- and single-array systems. These systems are much simpler to design and implement than the optimal systems.

Chapter 4 presented the results of a physical evaluation made upon several example binaural, multimicrophone systems as well as several reference systems (all designed for free-field operation). The primary reference was the Dual-Cardioid system, which is the simplest form of binaural, directional hearing aid, consisting of two cardioid microphones located near the ears with their outputs sent directly to their respective ears. This evaluation compared the theoretical free-field system performance with the actual measured free-field and head-mounted (upon the KEMAR manikin) performance – it explored whether the system behaved as predicted and investigated the degrading effects of head-mounting upon these free-field designed systems. These results demonstrated that:

- In the free-field, all test systems behaved approximately as predicted.
- Head-mounting minimally degraded the directional performance of the test system relative to the free-field, although it degraded dual-array systems (consisting of two endfire arrays) to a greater extent than it degraded single-array systems (consisting of one broadside array).
- In all test systems, head-mounting resulted in more realistic output ITDs than the free-field case. The dual-array systems generally produced more realistic ITDs than the single-array systems – single-array systems tended to produce

smaller than natural ITDs, because the span of the broadside array used for the single array system was *smaller* than the effective inter-ear spacing.

Chapter 5 presented the results of a behavioral evaluation conducted on several test and reference systems. This evaluation was conducted using normal-hearing subjects and consisted of two parts: speech-intelligibility in noise and sound localization. For speech intelligibility, the system intelligibility-weighted gains, G_Is, were measured and compared to both the predicted intelligibility gains, as measured by directivity, D_{IW}, and with the actual SRT changes (re the Naked Ear) produced by the subjects wearing the test systems. For sound localization, the subjects identified arrival angle for azimuth-plane sources. Throughout this evaluation, the relative performances of the different system classes (dual-array vs. single-array) and of the different systems within each class (optimal vs. sub-optimal) were considered. Overall, the dual- and single-array systems provided roughly 3 dB of gain relative to the Dual-Cardioid reference system while providing the wearer with sufficient binaural cues to maintain a reasonably realistic sense of space. Specific speech intelligibility and binaural output results indicated that:

- The measured G_Is, for all test systems, were consistently *lower* than the theoretical D_{IW}, although the relative G_I ordering within each system class did reflect the relative D_{IW} ordering. This could be qualitatively accounted for, however, by considering the effects of head-mounting, the direct-to-reverberant ratio of the target signal in the room, and a non-diffuse noise field.

- The measured SRTs were lower than the G_Is, and the relative differences between them did not reflect the relative differences between the G_Is. It was noted, however, that SRTs and G_Is were rendered more consistent when the Dual-Cardioid system was used as a reference, as opposed to the Naked Ear. Still, the relative differences in G_I were not observed in SRT measurements due to the intra-test variability.

- In general, dual- and single-array systems both provided similar speech intelligibility in noise benefits.

- Dual-array systems generally provided more realistic ITDs and better localization performance than single-array systems, although the sub-optimal dual-array system (i.e. the Dual +/- Gradient system) exhibited left-right confusions for peripheral sources (located at either side, $\pm 90°$, of the subject). Single-array ITDs could be improved, however, if the array span were increased to more accurately reflect the natural inter-ear spacing.

- Within the dual- and single-array classes, very little performance, in either speech intelligibility or sound localization, was lost when sub-optimal systems were used.

This thesis has presented several binaural output, multimicrophone hearing aid designs. It has shown that these designs behave as theoretically expected and that they all provide similar benefits to normal-hearing wearers. The most practical finding with regard to the future development of actual body-worn aids is that simple, sub-optimal systems provide similar benefits as more complex, optimal systems. This indicates that simple, body-worn units can be constructed and that they can enhance the wearer's speech intelligibility while allowing them to retain a realistic sense of space.

Appendix A

Inter-Microphone Phase Increments

This appendix derives the inter-element phase differences, $\alpha(\omega, \theta, \phi)$, for standard broadside and endfire linear arrays with equally spaced elements, located d apart. These phase differences are necessary to form the source to array transfer functions, $H_i(\omega, \theta, \phi)$, defined in Chapter 2.

Figure A-1 shows a detailed view of a source signal incident upon the array from the (θ, ϕ) direction. In particular, it shows the extra distance that the signal must travel when traveling from microphone 0 to microphone 1, shown by the bold line, which is equal to $d\ sin\theta\ cos\phi$. The time required to travel this extra distance is simply the distance divided by c = the speed of sound: $\tau = \frac{d}{c} sin\theta cos\phi$. Hence, the increase in phase between the signal arriving at microphone 1 and microphone 0 is simply $\omega\tau$, and so $\alpha_{broadside}(\omega, \theta, \phi)$ is given by:

$$\alpha_{broadside}(\omega, \theta, \phi) = \frac{\omega d}{c} sin\theta cos\phi. \tag{A.1}$$

In an exactly analogous manner, Figure A-2 shows the same situation for an endfire

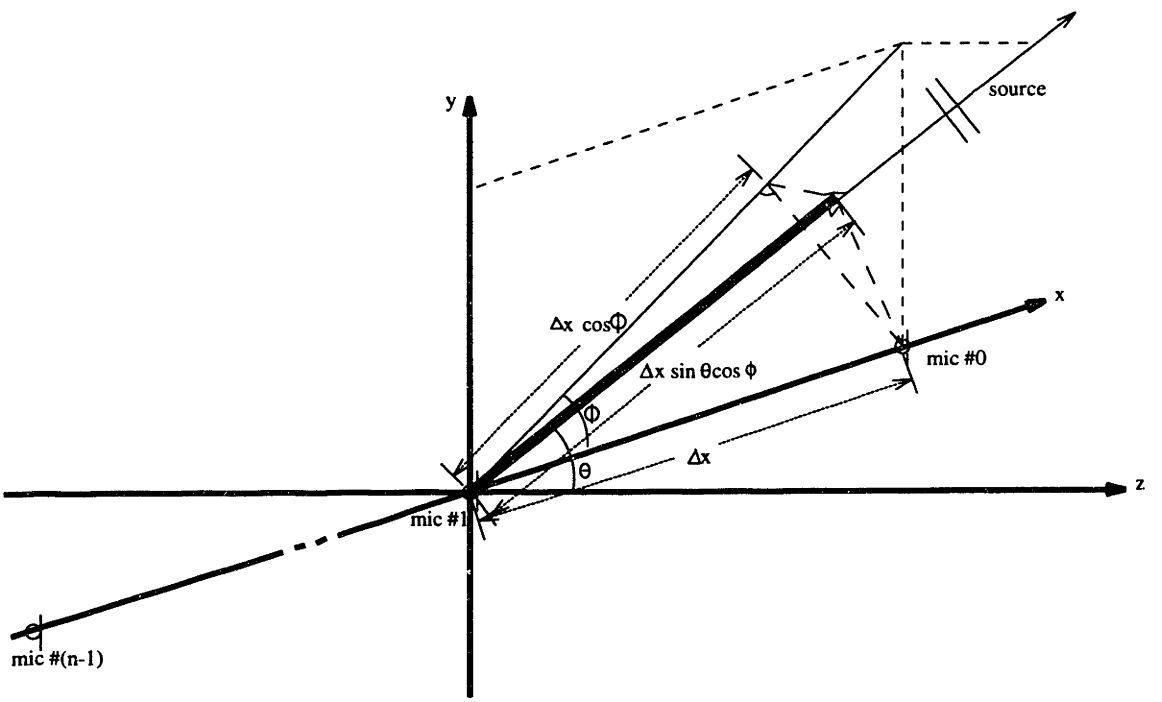

Figure A-1: Figure showing extra distance traveled by source signal in going from microphone 0 to microphone 1 of a broadside array.

array. In this case, the extra distance traveled from microphone 0 to microphone 1 is $d\ cos\theta$. Thus, $\tau = \frac{d}{c}cos\theta$ and the increase in phase between microphones 1 and 0 is:

$$\alpha_{broadside}(\omega, \theta, \phi) = \frac{\omega d}{c}cos\theta. \tag{A.2}$$

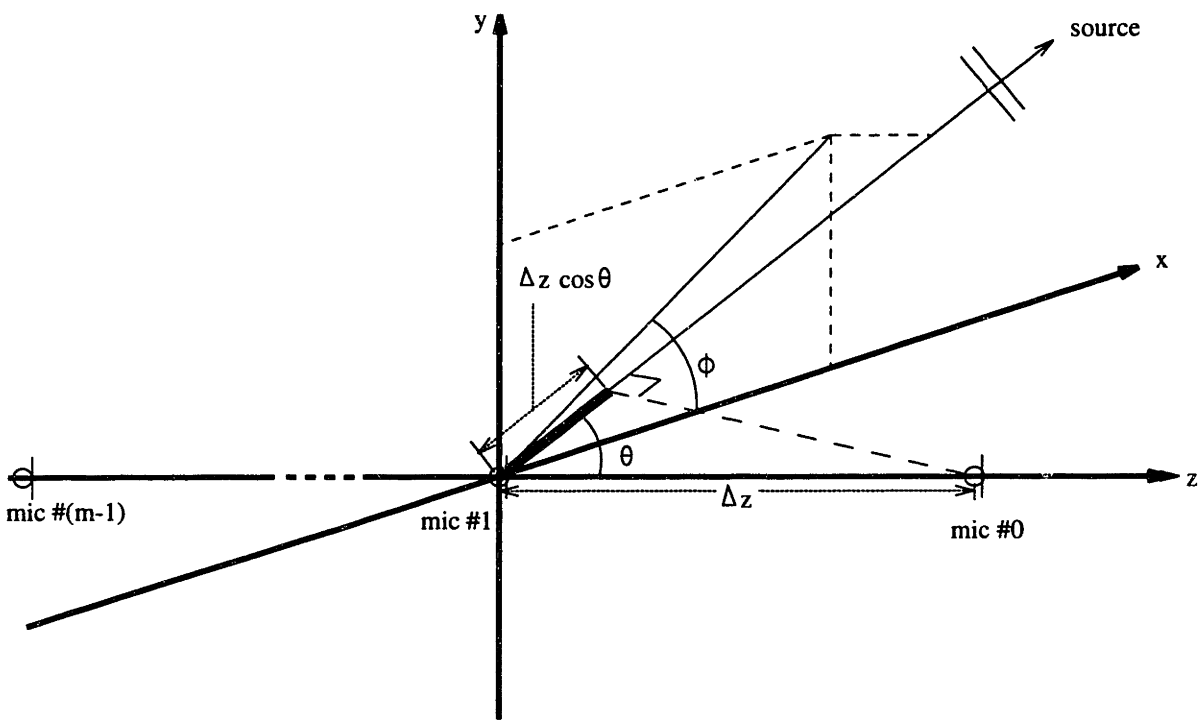

Figure A-2: Figure showing extra distance traveled by source signal in going from microphone 0 to microphone 1 of an endfire array.

Since the arrays in both cases consist of *equally spaced* elements, the additional phases given in Equations A-1 and A-2 are the phase differences between microphones i and $i-1$ in general.

Appendix B

Derivation of Directivity and ITD Expressions

This appendix derives the expressions, in terms of the $n-1$ ratios $R_i(\omega)$, for directivity, $D(\omega)$, and for RMS ITD error, $E(\omega)$ for the single array, multimicrophone hearing aid, as discussed in Chapter 3. Figure B-1 repeats the basic configuration of this system, which consists of a single broadside array, whose microphone output signals, $X_0(\omega)$ through $X_{n-1}(\omega)$, serve to generate the two system output signals, $Y_0(\omega)$ and $Y_1(\omega)$. Note that the filters are arranged in such a way that the system exhibits symmetric behavior about the mid-sagittal plane, and so:

$$\begin{aligned} Y_0(\omega) &= \underline{W}^T(\omega)\underline{X}(\omega), \\ Y_1(\omega) &= \underline{W}_{rev}^T(\omega)\underline{X}(\omega), \end{aligned}$$

where, as shown in Chapters 2 and 3:

$$\underline{X}(\omega) = \begin{pmatrix} X_0(\omega) \\ X_1(\omega) \\ \vdots \\ X_{n-1}(\omega) \end{pmatrix}, \quad \underline{W}(\omega) = \begin{pmatrix} W_0(\omega) \\ W_1(\omega) \\ \vdots \\ W_{n-1}(\omega) \end{pmatrix}, \quad \underline{W}_{rev}(\omega) = \begin{pmatrix} W_{n-1}(\omega) \\ W_{n-2}(\omega) \\ \vdots \\ W_0(\omega) \end{pmatrix}.$$

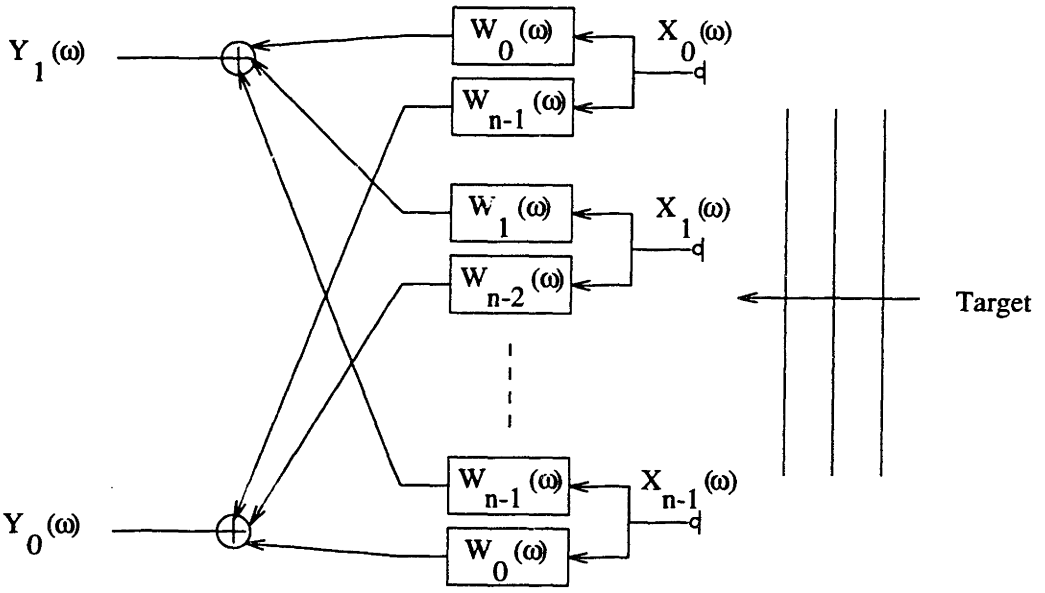

Figure B-1: Standard configuration of combined system approach. Note, this array is assumed to contain *n identical* directional elements, each with response $P(\omega, \theta, \phi)$.

B.0.3 Determination of the System Directivity, $D(\omega)$

According to Equation 2.5 from Chapter 2, the directivity for the output $Y_0(\omega)$, $D_0(\omega)$, can be expressed as:

$$D_0(\omega) = \frac{\underline{W}^T(\omega)\underline{H}_d(\omega, 0, 0)\underline{H}_d^H(\omega, 0, 0)\underline{W}^*(\omega)}{\underline{W}^T(\omega)S_{zz}(\omega)\underline{W}^*(\omega)}, \tag{B.1}$$

where * represents complex conjugate and ^{H} represents hermitian or complex conjugate transpose. Here, $\underline{W}(\omega)$ is as defined above, $\underline{H}_d(\omega,0,0)$ is the directional vector of target-source-to-array transfer functions, presented in Section 2.1.3, and $S_{zz}(\omega)$ is the system correlation matrix, defined as:

$$S_{zz}(\omega) = \frac{1}{4\pi}\int_{\theta=0}^{\pi}\int_{\phi=0}^{2\pi} P(\omega,\theta,\phi)\underline{H}(\omega,\theta,\phi)\underline{H}^H(\omega,\theta,\phi)P^*(\omega,\theta,\phi)sin\theta\, d\phi d\theta.$$

Factoring out $|W_0(\omega)|^2$ from both the numerator and denominator of Equation B.1 leads to an expression for $D(\omega)$ that depends only upon the $n-1$ ratios $R_1(\omega) = \frac{W_1(\omega)}{W_0(\omega)}$, $R_2(\omega) = \frac{W_2(\omega)}{W_0(\omega)}$, ..., $R_{n-1}(\omega) = \frac{W_{n-1}(\omega)}{W_0(\omega)}$, rather than upon the n weights themselves:

$$D_1(\omega) = \frac{\underline{R}^T(\omega)P(\omega,0,0)\underline{H}(\omega,0,0)\underline{H}^H(\omega,0,0)P^*(\omega,0,0)\underline{R}^*(\omega)}{\underline{R}^T(\omega)S_{zz}(\omega)\underline{R}^*(\omega)}. \qquad \text{(B.2)}$$

In this case, $\underline{R}(\omega)$ is defined as:

$$\underline{R}(\omega) = \begin{pmatrix} 1 \\ R_1(\omega) \\ R_2(\omega) \\ \vdots \\ R_{n-1}(\omega) \end{pmatrix} = \begin{pmatrix} 1 \\ \frac{W_1(\omega)}{W_0(\omega)} \\ \frac{W_2(\omega)}{W_0(\omega)} \\ \vdots \\ \frac{W_{n-1}(\omega)}{W_0(\omega)} \end{pmatrix}.$$

It should be noted that these ratios, together with a constraint of unit array gain in the target direction, completely specify the system filters, $W_i(\omega)$.

Due to the symmetric relationship between $\underline{W}(\omega)$ and $\underline{W}_{rev}(\omega)$ (and the analogous relationship between $\underline{R}(\omega)$ and $\underline{R}_{rev}(\omega)$), together with the fact that the matrices $[\underline{H}_d(\omega,0,0)\underline{H}_d^H(\omega,0,0)]$ and $S_{zz}(\omega)$ are *hermitian*,[1] it can be easily shown that the directivity for the output signal $Y_1(\omega)$ is exactly equal to $D_0(\omega)$. Hence, this system has only *one* directivity to consider, $D(\omega) = D_0(\omega) = D_1(\omega)$.

[1] A hermitian matrix in one whose complex conjugate transpose equals the matrix itself, $A = A^H$.

B.0.4 Determination of the RMS ITD Error, $E(\omega)$

Recall from Chapter 3 that the RMS ITD is defined as:

$$E(\omega) = \sqrt{\frac{1}{4\pi}\int_0^{2*\pi}\int_0^{\pi}(\mathrm{ITD}_{desired}(\omega,\theta,\phi) - \mathrm{ITD}_{output}(\omega,\theta,\phi))^2 sin\theta\, d\theta d\phi}, \quad \text{(B.3)}$$

where $\mathrm{ITD}_{desired}$ is the ITD that the system is trying to preserve and ITD_{output} is the ITD actually generated by the system. This section will derive the expressions for $\mathrm{ITD}_{desired}$ and ITD_{output} in terms of the ratios $R_i(\omega)$.

The $\mathrm{ITD}_{desired}$ is assumed to be the ITD experienced by the two outermost array inputs, $X_0(\omega)$ and $X_{n-1}(\omega)$. For this thesis, this ITD is defined as the *phase delay*[2] between these two signals for a source ariving from (θ,ϕ):

$$\begin{aligned}
\mathrm{ITD}_{desired}(\omega,\theta,\phi) &= \frac{1}{\omega}[\angle X_{n-1}(\omega,\theta,\phi) - \angle X_0(\omega,\theta,\phi)] \\
&= \frac{1}{\omega}[\angle H_{d,n-1}(\omega,\theta,\phi)S(\omega) - \angle H_{d,0}(\omega,\theta,\phi)S(\omega)] \\
&= \frac{1}{\omega}[\angle H_{d,n-1}(\omega,\theta,\phi)P(\omega,\theta,\phi)S(\omega) - \angle H_{d,0}(\omega,\theta,\phi)P(\omega,\theta,\phi)S(\omega)] \\
&= \frac{1}{\omega}[(\angle H_{d,n-1}(\omega,\theta,\phi) + \angle P(\omega,\theta,\phi)S(\omega)) \\
&\quad -(\angle H_{d,0}(\omega,\theta,\phi) + \angle P(\omega,\theta,\phi)S(\omega))] \\
&= \frac{1}{\omega}[\angle H_{d,n-1}(\omega,\theta,\phi) - \angle H_{d,0}(\omega,\theta,\phi)] \\
&= \frac{1}{\omega}[\angle e^{-j(n-1)\alpha_{broadside}(\omega,\theta,\phi)} - \angle 1] \\
&= \frac{1}{\omega}(n-1)\alpha_{broadside}(\omega,\theta,\phi)
\end{aligned}$$

$$\mathrm{ITD}_{desired}(\omega,\theta,\phi) = \frac{(n-1)d}{c} sin\theta cos\phi, \quad \text{(B.4)}$$

where $H_{d,i}(\omega,\theta,\phi)$ is the i^{th} element of the directional source to array transfer function

[2]Recall that if the Fourier Transform of $x(t)$ is $X(\omega)$, then $x(t-\tau) \longleftrightarrow X(\omega)e^{-j\omega\tau} = X_{delayed}(\omega)$, and so the delay at any frequency is simply $\tau = \frac{\angle X_{delayed}(\omega)}{\omega}$.

vector, $\underline{H}_d(\omega,\theta,\phi)$, the definitions of $\underline{H}_d(\omega,\theta,\phi)$, $P(\omega,\theta,\phi)$, and $H_i(\omega,\theta,\phi)$ from Chapter 2 are used and the definition of $\alpha_{broadside}(\omega,\theta,\phi)$ from Appendix A is used.

ITD_{output} is obtained in a similar fashion as the phase delay experienced between the two output signals for a source arriving from (θ,ϕ). In this case, however, the system filters, $W_i(\omega)$, play an integral part in the determination of the output phases.

$$\begin{aligned}
\text{ITD}_{output}(\omega,\theta,\phi) &= \frac{1}{\omega}[\angle Y_1(\omega) - \angle Y_0(\omega)] \\
&= \frac{1}{\omega}[\angle \underline{W}(\omega)^T \underline{X}(\omega,\theta,\phi) - \angle \underline{W}_{rev}^T \underline{X}(\omega,\theta,\phi)] \\
&= \frac{1}{\omega}[\angle \underline{W}(\omega)^T \underline{H}_d(\omega,\theta,\phi)S(\omega) \\
&\quad -\angle \underline{W}_{rev}^T \underline{H}_d(\omega,\theta,\phi)S(\omega)] \\
&= \frac{1}{\omega}[\angle \underline{W}(\omega)^T \underline{H}(\omega,\theta,\phi)P(\omega,\theta,\phi)S(\omega) \\
&\quad -\angle \underline{W}_{rev}^T \underline{H}(\omega,\theta,\phi)P(\omega,\theta,\phi)S(\omega)] \\
&= \frac{1}{\omega}[(\angle \underline{W}(\omega)^T \underline{H}(\omega,\theta,\phi) + \angle P(\omega,\theta,\phi)S(\omega)) \\
&\quad -(\angle \underline{W}_{rev}^T \underline{H}(\omega,\theta,\phi) + \angle P(\omega,\theta,\phi)S(\omega))] \\
&= \frac{1}{\omega}[\angle \underline{W}(\omega)^T \underline{H}(\omega,\theta,\phi) - \angle \underline{W}_{rev}^T \underline{H}(\omega,\theta,\phi)],
\end{aligned}$$

where $\underline{W}(\omega)$ and $\underline{W}_{rev}(\omega)$ are as defined above and $\underline{H}_d(\omega,\theta,\phi)$, $P(\omega,\theta,\phi)$, and $\underline{H}(\omega,\theta,\phi)$ are as defined in Chapter 2. Recall from Chapter 2 that[3] $H_i(\omega,\theta,\phi) = e^{-ji\alpha(\omega,\theta,\phi)}$, and so:

$$\underline{W}^T(\omega)\underline{H}(\omega,\theta,\phi) = \sum_{i=0}^{n-1} W_i(\omega)e^{-ji\alpha(\omega,\theta,\phi)}$$

and

$$\underline{W}_{rev}^T(\omega)\underline{H}(\omega,\theta,\phi) = \sum_{i=0}^{n-1} W_{n-i-1}(\omega)e^{-ji\alpha(\omega,\theta,\phi)}.$$

Substituting these expressions into the equation above,

$$\text{ITD}_{output}(\omega,\theta,\phi) = \angle\sum_{i=0}^{n-1} W_i(\omega)e^{-ji\alpha(\omega,\theta,\phi)} - \angle\sum_{i=0}^{n-1} W_{n-i-1}(\omega)e^{-ji\alpha(\omega,\theta,\phi)}$$

[3]For this system, $\alpha(\omega,\theta,\phi)=\alpha(\omega,\theta,\phi)= \frac{\omega d}{c} sin\theta cos\phi$.

$$
\begin{aligned}
&= \angle W_0(\omega)[1 + \sum_{i=1}^{n-1} \frac{W_i(\omega)}{W_0(\omega)} e^{-ji\alpha(\omega,\theta,\phi)}] \\
&\quad -\angle W_0(\omega) e^{-j(n-1)\alpha(\omega,\theta,\phi)}[(\sum_{i=1}^{n-1} \frac{W_i(\omega)}{W_0(\omega)} e^{ji\alpha(\omega,\theta,\phi)}) + 1] \\
&= \angle W_0(\omega) + \angle[1 + \sum_{i=1}^{n-1} R_i(\omega) e^{-ji\alpha(\omega,\theta,\phi)}] \\
&\quad -\angle W_0(\omega) + (n-1)\alpha(\omega,\theta,\phi) - \angle[(\sum_{i=1}^{n-1} R_i(\omega) e^{ji\alpha(\omega,\theta,\phi)}) + 1]
\end{aligned}
$$

$$
\begin{aligned}
\mathrm{ITD}_{output}(\omega,\theta,\phi) &= (n-1)\alpha(\omega,\theta,\phi) \\
&\quad + tan^{-1}\left(\frac{\sum_{i=1}^{n-1} |R_i(\omega)| sin[\angle R_i(\omega) - i\alpha(\omega,\theta,\phi)]}{1 + \sum_{i=1}^{n-1} |R_i(\omega)| cos[\angle R_i(\omega) - i\alpha(\omega,\theta,\phi)]}\right) \\
&\quad - tan^{-1}\left(\frac{\sum_{i=1}^{n-1} |R_i(\omega)| sin[\angle R_i(\omega) + i\alpha(\omega,\theta,\phi)]}{1 + \sum_{i=1}^{n-1} |R_i(\omega)| cos[\angle R_i(\omega) + i\alpha(\omega,\theta,\phi)]}\right). \quad \text{(B.5)}
\end{aligned}
$$

As discussed in Chapter 3, all systems in this thesis that were designed using $E(\omega)$ resulted in filters with *identical* phase responses (i.e. all $\angle W_i(\omega)$ were the same). In this case, the $R_i(\omega)$ are *real* and the expression for $\mathrm{ITD}_{output}(\omega,\theta,\phi)$ can be further simplified, as $\angle R_i(\omega) = 0$.

$$
\begin{aligned}
\mathrm{ITD}_{output}(\omega,\theta,\phi) &= (n-1)\alpha(\omega,\theta,\phi) \\
&\quad + tan^{-1}\left(\frac{\sum_{i=1}^{n-1} R_i(\omega) sin[-i\alpha(\omega,\theta,\phi)]}{1 + \sum_{i=1}^{n-1} R_i(\omega) cos[i\alpha(\omega,\theta,\phi)]}\right) \\
&\quad - tan^{-1}\left(\frac{\sum_{i=1}^{n-1} R_i(\omega) sin[i\alpha(\omega,\theta,\phi)]}{1 + \sum_{i=1}^{n-1} R_i(\omega) cos[i\alpha(\omega,\theta,\phi)]}\right)
\end{aligned}
$$

$$
\begin{aligned}
&= (n-1)\alpha(\omega,\theta,\phi) \\
&\quad + tan^{-1}\left(-\frac{\sum_{i=1}^{n-1} R_i(\omega) sin[i\alpha(\omega,\theta,\phi)]}{1 + \sum_{i=1}^{n-1} R_i(\omega) cos[i\alpha(\omega,\theta,\phi)]}\right) \\
&\quad - tan^{-1}\left(\frac{\sum_{i=1}^{n-1} R_i(\omega) sin[i\alpha(\omega,\theta,\phi)]}{1 + \sum_{i=1}^{n-1} R_i(\omega) cos[i\alpha(\omega,\theta,\phi)]}\right)
\end{aligned}
$$

$$
= (n-1)\alpha(\omega,\theta,\phi)
$$

$$-tan^{-1}\left(\frac{\sum_{i=1}^{n-1} R_i(\omega)sin[i\alpha(\omega,\theta,\phi)]}{1+\sum_{i=1}^{n-1} R_i(\omega)cos[i\alpha(\omega,\theta,\phi)]}\right)$$
$$-tan^{-1}\left(\frac{\sum_{i=1}^{n-1} R_i(\omega)sin[i\alpha(\omega,\theta,\phi)]}{1+\sum_{i=1}^{n-1} R_i(\omega)cos[i\alpha(\omega,\theta,\phi)]}\right)$$

$$\begin{aligned}\mathrm{ITD}_{output}(\omega,\theta,\phi) &= (n-1)\alpha(\omega,\theta,\phi) \\ &\quad -2tan^{-1}\left(\frac{\sum_{i=1}^{n-1} R_i(\omega)sin[i\alpha(\omega,\theta,\phi)]}{1+\sum_{i=1}^{n-1} R_i(\omega)cos[i\alpha(\omega,\theta,\phi)]}\right). \qquad \text{(B.6)}\end{aligned}$$

Together, Equations B.4 and B.5, or in the case of real ratios Equations B.4 and B.6, define the RMS ITD Error in terms of the $n-1$ system ratios $R_i(\omega)$.

The expressions for $D(\omega)$ and $E(\omega)$ derived in this appendix serve as measures of the performance of single and, to a certain degree, of dual array approaches to multimicrophone hearing aids with binaural output. Expressing these measures in terms of the $n-1$ system ratios help to simplify the overall design process, especially for the Combined system of Section 3.3.2, which involves intense numerical optimization.

Appendix C

Single-Array Headband-Mounted ITDs

This appendix contains the anechoic chamber ITD measurements for 'the headband mounted cases of the binaural output, single-array test systems. These results show the measured (solid lines) and theoretical (dotted line) output ITDs produced for sources arriving from 0°, 30°, 60°, and 90° in the azimuth plane. Specifically, Figures C-1 through C-3 show the results for the Pass Through, Combined, and Lowpass/Highpass test systems, respectively. These figures resemble the eyeglass-mounted ITDs shown in Figures 4-23 through 4-25.

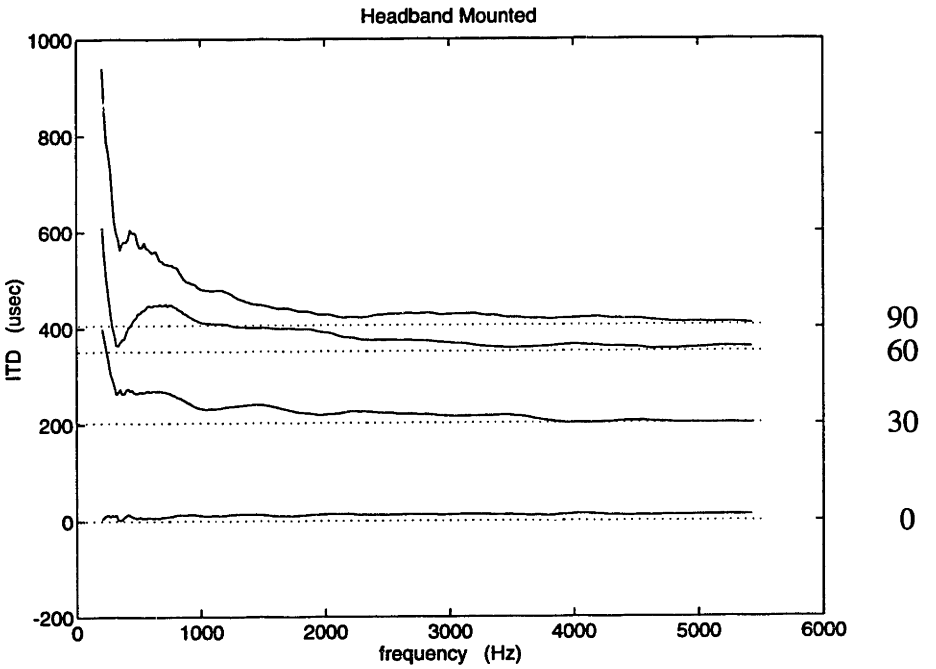

Figure C-1: Measured output ITDs for headband-mounted Pass Through system.

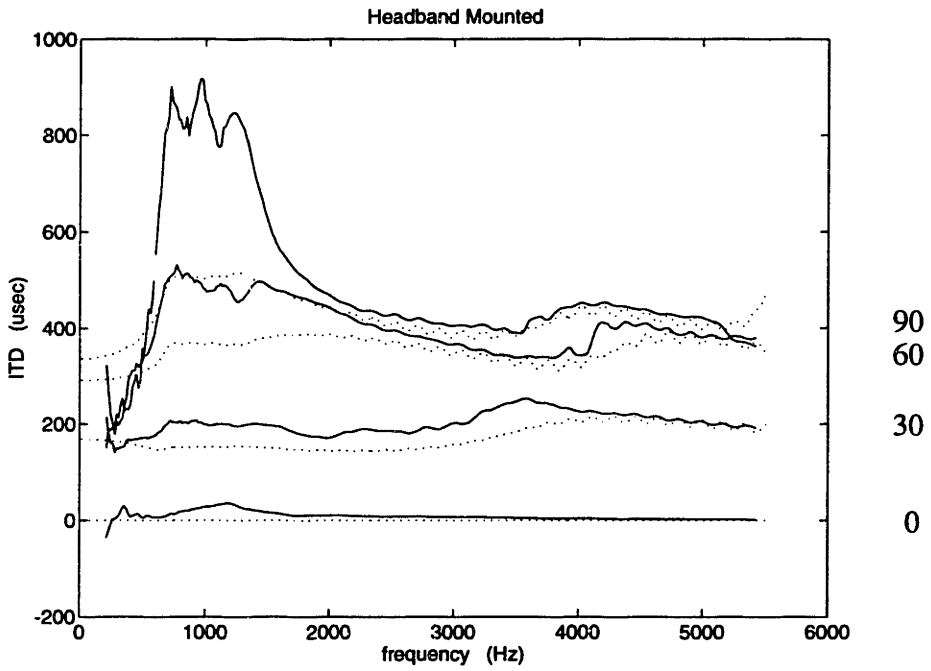

Figure C-2: Measured output ITDs for headband-mounted Combined system.

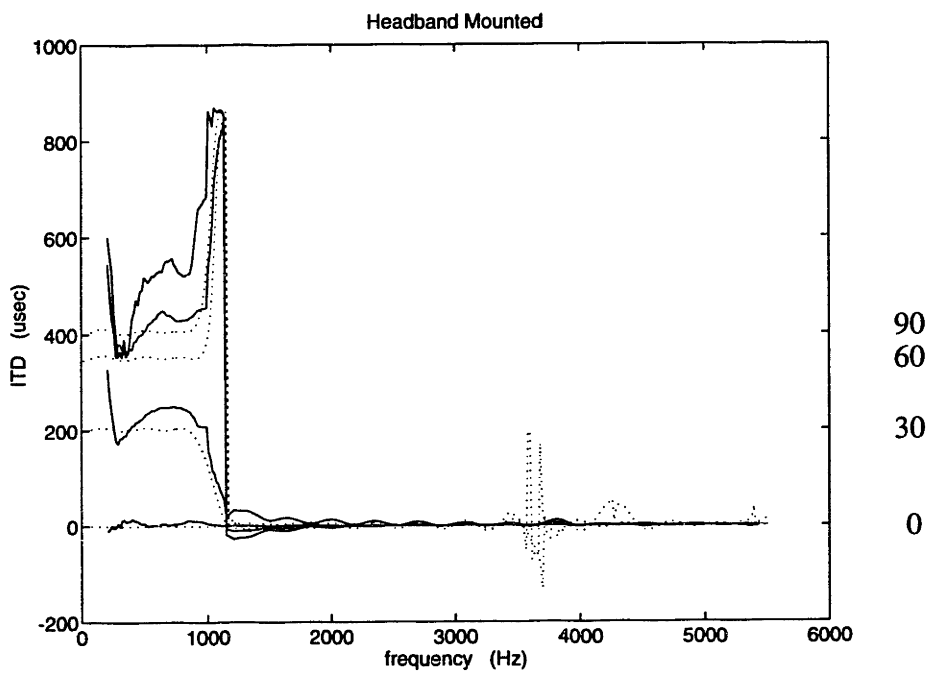

Figure C-3: Measured output ITDs for headband-mounted Low-pass/Highpass system.

Appendix D

Diffuseness Measurements

This appendix presents measurements made to determine the diffuseness of the noise field used in the speech-intelligibility measurements of Chapter 5. These measurements were made by pointing a dipole microphone (Knowles BW-1789) in several different directions with the noise field in place. The resulting average powers (expressed in dB) in the fourteen third octave bands from 200 to 4000 Hz were then generated and compared to see if the noise field was stronger in any given direction. Table D.1 gives these measurements, as well as the maximum and minimum reading in each band and the difference between them. Interesting measurements to note in this table are:

- Measurement 1: the dipole microphone points in the front/back directions (recall, front = target direction).
- Measurements 2 and 3: the dipole microphone points (roughly) at the left-front/right-rear and right-front/left-rear jammer loudspeaker pairs, respectively.
- Measurement 5: the dipole microphone points in the up/down directions.

These measurements indicate a quasi-diffuse field, with the widest variation in measurements (5-6 dB) occurring for the 400 Hz and 1000 Hz bands. It should be noted that the bands from 400 Hz to 4000 Hz all exhibit *minimum* power for

measurement 5, in which the microphone points in the up/down directions. This indicates that the noise field is not perfectly diffuse and is, in fact, weaker (about 2.5 dB) in the up/down directions than in the azimuth plane.

Table D.1: Measurements to determine diffuseness of noise field used in Chapter 5.

Meas.	Angle		Average Power in Band						
No.	θ	ϕ	200	250	315	400	500	630	800
1	0	0	-60.10	-62.67	-63.88	-63.76	-67.77	-65.78	-64.07
2	$\frac{\pi}{4}$	0	-58.56	-62.25	-64.22	-61.44	-67.88	-64.80	-63.60
3	$\frac{\pi}{4}$	π	-58.40	-61.06	-63.87	-64.40	-68.98	-66.40	-64.68
4	$\frac{\pi}{2}$	0	-59.44	-62.37	-67.00	-65.53	-69.90	-66.72	-64.53
5	$\frac{\pi}{2}$	$\frac{\pi}{2}$	-58.03	-60.52	-64.86	-66.97	-70.33	-67.26	-66.40
6	$\frac{\pi}{4}$	$\frac{\pi}{4}$	-59.06	-62.57	-64.61	-64.47	-67.83	-66.51	-64.54
7	$\frac{\pi}{4}$	$\frac{3\pi}{4}$	-58.65	-62.47	-64.09	-62.29	-67.77	-65.71	-63.63
8	$\frac{\pi}{4}$	$\frac{5\pi}{4}$	-58.37	-61.83	-65.23	-65.93	-69.34	-66.91	-64.90
9	$\frac{\pi}{4}$	$\frac{7\pi}{4}$	-59.48	-61.95	-65.22	-64.71	-68.11	-65.89	-64.82
max			-58.03	-60.52	-63.87	-61.44	-67.77	-64.80	-63.60
min			-60.10	-62.67	-67.00	-66.97	-70.33	-67.26	-66.40
|max−min|			2.07	2.15	3.12	5.53	2.56	2.46	2.80

Meas.	Angle		Average Power in Band						
No.	θ	ϕ	1000	1250	1600	2000	2500	3150	4000
1	0	0	-69.27	-77.16	-78.12	-76.94	-74.29	-80.25	-85.63
2	$\frac{\pi}{4}$	0	-68.65	-77.13	-79.28	-77.13	-74.97	-81.07	-84.72
3	$\frac{\pi}{4}$	π	-70.13	-77.89	-79.41	-77.48	-74.73	-79.92	-84.62
4	$\frac{\pi}{2}$	0	-70.36	-77.85	-79.93	-78.29	-75.89	-81.23	-86.08
5	$\frac{\pi}{2}$	$\frac{\pi}{2}$	-74.04	-80.61	-80.84	-78.86	-76.12	-81.84	-87.85
6	$\frac{\pi}{4}$	$\frac{\pi}{4}$	-69.58	-77.61	-79.35	-77.17	-75.39	-81.29	-85.80
7	$\frac{\pi}{4}$	$\frac{3\pi}{4}$	-67.94	-76.99	-79.70	-76.61	-73.98	-80.09	-84.47
8	$\frac{\pi}{4}$	$\frac{5\pi}{4}$	-70.95	-77.88	-79.11	-77.65	-75.57	-81.39	-85.66
9	$\frac{\pi}{4}$	$\frac{7\pi}{4}$	-71.16	-77.90	-79.30	-77.15	-75.74	-81.65	-85.10
max			-67.94	-76.99	-78.12	-76.61	-73.98	-79.92	-84.47
min			-74.04	-80.61	-80.84	-78.86	-76.12	-81.84	-87.85
|max−min|			6.10	3.61	2.71	2.25	2.13	1.92	3.37

Appendix E

Subject SRT Measurements

This appendix presents the measured SRTs for each test run of the five subjects. Subjects DB (Table E.1), CK (Table E.2), JP (Table E.3), and JS (Table E.4) were each run twice, and, therefore, the statistical standard deviations are listed in the left-most column, with an 'subject' standard deviation, σ_{subj}, which equals the standard deviations averaged over system, given at the bottom of the column. The average (in dB) of the four subject standard deviations gives an idea of the overall inter-test variability of this SRT experiment: $\sigma_{\text{intra-test}} = 1.28$ dB. Note that subject ME (Table E.5) was run only one time, and so no standard deviations are given.

Table E.1: SRTs for subject DB.

System Number	First Run SRT (dB)	Second Run SRT (dB)	Average SRT (dB)	Standard Deviation (dB)
1	0	0	0	N/A
2	2.29	-4.57	-1.14	4.85
3	-3.14	-7.43	-5.29	3.03
4a	-4.57	-4.57	-4.57	0
4b	-2.84	-2.28	-2.56	0.37
5a	-4.00	-7.43	-5.72	2.43
5b	-2.86	-1.43	-2.15	1.41
6a	-3.42	-4.00	-3.71	0.41
6b	-1.14	-5.71	-3.43	3.23
7a	-6.85	-2.28	-4.57	3.23
7b	-4.85	-1.14	-3.00	2.62
8a	-4.00	-2.85	-3.43	0.81
8b	-4.57	-3.71	-4.14	0.60
σ_{DB} = standard deviation for DB =				1.92

Table E.2: SRTs for subject CK.

System Number	First Run SRT (dB)	Second Run SRT (dB)	Average SRT (dB)	Standard Deviation (dB)
1	0	0	0	N/A
2	-1.14	-0.57	-0.86	0.40
3	-5.14	-1.71	-3.43	2.42
4a	-4.00	-4.28	-4.14	0.20
4b	-3.43	-3.42	-3.43	0.01
5a	-2.57	-3.42	-3.00	0.60
5b	-2.85	-5.14	-4.00	1.62
6a	-4.00	-4.00	-4.00	0
6b	-2.85	-4.57	-3.71	1.22
7a	-1.71	-2.28	-2.00	0.40
7b	-4.57	-4.57	-4.57	0
8a	-2.85	-2.85	-2.85	0
8b	-4.57	-5.42	-5.06	0.60
σ_{CK} = standard deviation for CK =				0.62

Table E.3: SRTs for subject JP.

System Number	First Run SRT (dB)	Second Run SRT (dB)	Average SRT (dB)	Standard Deviation (dB)
1	0	0	0	N/A
2	-0.29	-0.57	-0.43	0.20
3	-5.72	-1.71	-3.72	2.84
4a	-6.29	-3.43	-4.86	2.02
4b	-5.15	-5.71	-5.43	0.40
5a	-2.29	-4.00	-3.15	1.21
5b	-3.43	-5.71	-4.57	1.61
6a	-2.29	-2.29	-2.29	0
6b	-6.86	-3.43	-5.15	2.43
7a	-6.29	-1.14	-3.71	3.64
7b	-6.86	-6.29	-6.56	0.40
8a	-4.58	-1.14	-2.86	2.43
8b	-4.57	-4.57	-4.57	0
σ_{JP} = standard deviation for JP =				1.43

Table E.4: SRTs for subject JS.

System Number	First Run SRT (dB)	Second Run SRT (dB)	Average SRT (dB)	Standard Deviation (dB)
1	0	0	0	N/A
2	-1.72	0.85	-0.44	1.82
3	-3.43	-2.00	-2.72	1.01
4a	-3.43	-4.28	-3.86	0.60
4b	-1.71	-4.86	-3.29	2.23
5a	0	0.29	-0.15	0.20
5b	-2.86	-1.43	-2.15	1.01
6a	-1.72	-0.28	-1.00	1.02
6b	-2.28	-2.00	-2.14	0.20
7a	-2.28	-3.72	-3.00	1.02
7b	-2.28	-0.85	-1.57	1.01
8a	-5.14	-0.85	-3.00	3.03
8b	-5.14	-4.28	-4.71	0.61
σ_{JS} = standard deviation for JS =				1.15

Table E.5: SRTs for subject ME.

System Number	First Run SRT (dB)
1	0
2	0
3	-2.86
4a	-1.15
4b	-4.00
5a	-7.43
5b	-4.01
6a	-1.15
6b	-6.29
7a	-3.43
7b	-4.57
8a	-4.57
8b	-6.86

Appendix F

Subject Sound Localization Results

This appendix contains the confusion matrices of the sound localization test results for the five subjects DB (Figure F-1), ME (Figure F-2), CK (Figure F-3), JP (Figure F-4), and JS (Figure F-5). In all figures, the systems are referred to by *number*, as defined in Table 5.1.

S \ R	-90	-60	-30	0	30	60	90
-90	19	-	-	-	-	1	-
-60	-	19	-	-	-	1	-
-30	-	-	18	-	2	-	-
0	-	-	-	20	-	-	-
30	-	-	-	-	20	-	-
60	-	-	-	-	-	20	-
90	-	-	-	-	-	-	20

(a) Syst. 1: 97.1% correct, 12.5° RMS error

S \ R	-90	-60	-30	0	30	60	90
-90	11	9	-	-	-	-	-
-60	1	19	-	-	-	-	-
-30	-	-	20	-	-	-	-
0	-	-	-	20	-	-	-
30	-	-	-	-	20	-	-
60	-	-	-	-	-	20	-
90	-	-	-	-	-	8	12

(b) Syst. 2: 87.1% correct, 10.6° RMS error

S \ R	-90	-60	-30	0	30	60	90
-90	16	4	-	-	-	-	-
-60	1	18	1	-	-	-	-
-30	-	-	20	-	-	-	-
0	-	-	-	19	1	-	-
30	-	-	-	-	20	-	-
60	-	-	-	-	-	17	3
90	-	-	-	-	-	10	10

(c) Syst. 3: 85.7% correct, 11.1° RMS error

S \ R	-90	-60	-30	0	30	60	90
-90	-	-	-	-	-	3	17
-60	1	8	9	-	-	1	1
-30	-	1	19	-	-	-	-
0	-	-	-	20	-	-	-
30	-	-	-	-	19	1	-
60	-	-	-	-	5	15	-
90	7	-	2	1	1	2	7

(d) Syst. 4a: 62.8% correct, 81.8° RMS error

S \ R	-90	-60	-30	0	30	60	90
-90	16	2	-	-	-	1	1
-60	5	11	3	1	-	-	-
-30	-	-	20	-	-	-	-
0	-	-	-	20	-	-	-
30	-	-	-	-	20	-	-
60	-	-	-	-	1	18	1
90	9	-	-	1	-	1	9

(e) Syst. 4b: 81.4% correct, 49.6° RMS error

Figure F-1: Sound localization confusion matrices for subject DB.

S \ R	-90	-60	-30	0	30	60	90
-90	10	2	3	-	-	1	4
-60	-	10	3	1	4	2	-
-30	-	5	4	4	3	3	1
0	-	-	-	20	-	-	-
30	1	2	3	7	5	1	1
60	-	4	6	2	2	3	3
90	13	-	-	-	-	1	6

(f) Syst. 5a: 49.4% correct, 79.3° RMS error

S \ R	-90	-60	-30	0	30	60	90
-90	12	8	-	-	-	-	-
-60	1	5	12	1	1	-	-
-30	1	3	8	2	5	1	-
0	-	-	-	19	1	-	-
30	-	-	4	13	3	-	-
60	2	1	2	2	8	4	1
90	5	2	1	-	-	4	8

(g) Syst. 5b: 42.1% correct, 54.0° RMS error

S \ R	-90	-60	-30	0	30	60	90
-90	8	12	-	-	-	-	-
-60	1	15	4	-	-	-	-
-30	-	2	18	-	-	-	-
0	-	-	-	20	-	-	-
30	-	-	-	-	15	2	3
60	-	-	-	1	1	12	6
90	-	-	-	-	-	3	17

(h) Syst. 7a: 75.0% correct, 16.9° RMS error

S \ R	-90	-60	-30	0	30	60	90
-90	6	9	5	-	-	-	-
-60	2	7	11	-	-	-	-
-30	2	1	17	-	-	-	-
0	-	-	-	20	-	-	-
30	-	-	-	1	16	3	-
60	-	-	-	-	6	10	4
90	-	-	-	-	-	3	17

(i) Syst. 7b: 66.4% correct, 20.9° RMS error

S \ R	-90	-60	-30	0	30	60	90
-90	8	12	-	-	-	-	-
-60	1	16	3	-	-	-	-
-30	-	1	19	-	-	-	-
0	-	-	-	20	-	-	-
30	-	-	-	-	16	4	-
60	-	-	-	-	-	6	14
90	-	-	-	-	-	2	18

(j) Syst. 8a: 73.6% correct, 15.4° RMS error

S \ R	-90	-60	-30	0	30	60	90
-90	6	13	1	-	-	-	-
-60	-	9	11	-	-	-	-
-30	-	-	20	-	-	-	-
0	-	-	-	20	-	-	-
30	-	-	-	1	18	1	-
60	-	-	-	-	-	9	7
90	-	-	-	-	-	1	19

(k) Syst. 8b: 72.1% correct, 16.4° RMS error

Figure F-1 (*cont*).

S \ R	-90	-60	-30	0	30	60	90
-90	20	-	-	-	-	-	-
-60	1	19	-	-	-	-	-
-30	-	-	20	-	-	-	-
0	-	-	-	20	-	-	-
30	-	-	-	-	20	-	-
60	-	-	-	-	-	20	-
90	-	-	-	-	-	-	20

(a) Syst. 1: 99.3% correct, 1.79° RMS error

S \ R	-90	-60	-30	0	30	60	90
-90	17	3	-	-	-	-	-
-60	-	20	-	-	-	-	-
-30	-	-	20	-	-	-	-
0	-	-	-	20	-	-	-
30	-	-	-	-	20	-	-
60	-	-	-	-	-	20	-
90	-	-	-	-	-	1	19

(b) Syst. 2: 97.1% correct, 5.07° RMS error

S \ R	-90	-60	-30	0	30	60	90
-90	19	1	-	-	-	-	-
-60	3	17	-	-	-	-	-
-30	-	-	20	-	-	-	-
0	-	-	-	20	-	-	-
30	-	-	-	-	20	-	-
60	-	-	1	-	-	19	-
90	-	-	-	-	-	-	20

(c) Syst. 3: 96.4% correct, 8.77° RMS error

S \ R	-90	-60	-30	0	30	60	90
-90	10	-	-	-	-	-	10
-60	3	16	1	-	-	-	-
-30	-	-	20	-	-	-	-
0	-	-	-	19	1	-	-
30	-	-	-	1	19	-	-
60	-	-	-	-	-	20	-
90	2	-	-	-	-	-	18

(d) Syst. 4a: 87.1% correct, 40.9° RMS error

S \ R	-90	-60	-30	0	30	60	90
-90	8	-	-	-	-	1	11
-60	3	17	-	-	-	-	-
-30	-	4	16	-	-	-	-
0	-	-	-	20	-	-	-
30	-	-	-	-	20	-	-
60	-	-	-	-	-	19	1
90	2	-	-	-	-	-	18

(e) Syst. 4b: 84.3% correct, 56.6° RMS error

Figure F-2: Sound localization confusion matrices for subject ME.

S \ R	-90	-60	-30	0	30	60	90
-90	5	9	2	1	1	1	-
-60	1	11	3	0	4	1	-
-30	2	8	5	1	3	1	-
0	-	-	5	7	8	-	-
30	-	1	5	10	2	2	-
60	1	7	2	3	1	4	2
90	7	6	-	-	3	3	1

(f) Syst. 5a: 25.0% correct, 72.4° RMS error

S \ R	-90	-60	-30	0	30	60	90
-90	14	3	-	-	-	1	2
-60	-	2	10	8	-	-	-
-30	-	7	6	4	2	1	-
0	-	1	2	13	4	-	-
30	-	4	12	4	-	-	-
60	3	7	1	-	5	4	-
90	1	3	-	-	8	5	3

(g) Syst. 5b: 35.7% correct, 61.0° RMS error

S \ R	-90	-60	-30	0	30	60	90
-90	9	11	-	-	-	-	-
-60	-	4	16	-	-	-	-
-30	-	-	17	3	-	-	-
0	-	-	-	19	1	-	-
30	-	-	-	1	19	-	-
60	-	-	-	-	10	10	-
90	-	-	-	-	-	11	9

(h) Syst. 7a: 62.1% correct, 18.4° RMS error

S \ R	-90	-60	-30	0	30	60	90
-90	12	8	-	-	-	-	-
-60	-	3	17	-	-	-	-
-30	-	-	13	6	1	-	-
0	-	-	-	20	-	-	-
30	-	-	-	2	18	-	-
60	-	-	-	-	17	3	-
90	-	-	-	-	-	19	1

(i) Syst. 7b: 50.0% correct, 21.6° RMS error

S \ R	-90	-60	-30	0	30	60	90
-90	8	10	2	-	-	-	-
-60	-	5	15	-	-	-	-
-30	-	-	16	4	1	-	-
0	-	-	-	20	-	-	-
30	-	-	-	1	19	-	-
60	-	-	-	-	10	10	-
90	-	-	-	-	-	18	2

(j) Syst. 8a: 57.1% correct, 20.6° RMS error

S \ R	-90	-60	-30	0	30	60	90
-90	13	7	-	-	-	-	-
-60	-	8	12	-	-	-	-
-30	-	-	16	4	-	-	-
0	-	-	-	20	-	-	-
30	-	-	-	10	10	-	-
60	-	-	-	-	16	4	-
90	-	-	-	-	-	18	2

(k) Syst. 8b: 52.1% correct, 20.7° RMS error

Figure F-2 (*cont*).

S \ R	-90	-60	-30	0	30	60	90
-90	19	1	-	-	-	-	-
-60	-	20	-	-	-	-	-
-30	-	-	20	-	-	-	-
0	-	-	-	20	-	-	-
30	-	-	-	-	20	-	-
60	-	-	-	-	-	20	-
90	-	-	-	-	-	-	20

(a) Syst. 1: 99.3% correct, 1.79° RMS error

S \ R	-90	-60	-30	0	30	60	90
-90	13	7	-	-	-	-	-
-60	-	20	-	-	-	-	-
-30	-	-	20	-	-	-	-
0	-	-	-	20	-	-	-
30	-	-	-	-	20	-	-
60	-	-	-	-	-	20	-
90	-	-	-	-	-	8	12

(b) Syst. 2: 89.3% correct, 9.77° RMS error

S \ R	-90	-60	-30	0	30	60	90
-90	8	12	-	-	-	-	-
-60	3	17	-	-	-	-	-
-30	-	-	20	-	-	-	-
0	-	-	-	20	-	-	-
30	-	-	-	-	20	-	-
60	-	-	-	-	-	20	-
90	-	-	-	-	-	-	20

(c) Syst. 3: 89.3% correct, 9.67° RMS error

S \ R	-90	-60	-30	0	30	60	90
-90	2	2	-	-	1	6	9
-60	-	17	2	1	-	-	-
-30	-	9	11	-	-	-	-
0	-	1	4	15	-	-	-
30	-	-	-	1	18	1	-
60	-	-	-	1	9	10	-
90	4	1	-	-	-	9	6

(d) Syst. 4a: 56.4% correct, 66.3° RMS error

S \ R	-90	-60	-30	0	30	60	90
-90	3	-	-	-	1	7	9
-60	4	5	11	-	-	-	-
-30	-	6	14	-	-	-	-
0	-	-	3	17	-	-	-
30	-	-	-	1	18	1	-
60	-	-	-	-	3	15	2
90	7	1	2	-	-	5	5

(e) Syst. 4b: 55.0% correct, 73.5° RMS error

Figure F-3: Sound localization confusion matrices for subject CK.

S \ R	-90	-60	-30	0	30	60	90
-90	10	5	5	-	-	-	-
-60	-	16	4	-	-	-	-
-30	-	3	5	3	8	1	-
0	-	1	2	17	-	-	-
30	-	-	4	16	-	-	-
60	-	-	2	4	12	1	1
90	6	2	-	-	6	4	2

(f) Syst. 5a: 36.4% correct, 53.9° RMS error

S \ R	-90	-60	-30	0	30	60	90
-90	3	9	2	3	1	-	2
-60	-	6	8	5	1	-	-
-30	-	3	1	7	9	-	-
0	1	1	4	11	2	1	-
30	-	-	4	13	3	-	-
60	-	3	2	1	8	5	1
90	3	2	-	2	9	3	1

(g) Syst. 5b: 19.3% correct, 60.9° RMS error

S \ R	-90	-60	-30	0	30	60	90
-90	3	17	-	-	-	-	-
-60	-	2	18	-	-	-	-
-30	-	1	17	2	-	-	-
0	-	-	-	20	-	-	-
30	-	-	-	11	9	-	-
60	-	-	-	-	20	-	-
90	-	-	-	-	-	16	4

(h) Syst. 7a: 39.3% correct, 23.4° RMS error

S \ R	-90	-60	-30	0	30	60	90
-90	-	20	-	-	-	-	-
-60	-	1	19	-	-	-	-
-30	-	-	17	3	-	-	-
0	-	-	-	20	-	-	-
30	-	-	-	16	3	1	-
60	-	-	-	-	20	-	-
90	-	-	-	-	7	13	-

(i) Syst. 7b: 29.3% correct, 27.8° RMS error

S \ R	-90	-60	-30	0	30	60	90
-90	1	11	8	-	-	-	-
-60	2	5	11	2	-	-	-
-30	-	-	9	11	-	-	-
0	-	-	1	19	-	-	-
30	-	-	-	11	8	-	1
60	-	-	-	-	19	1	-
90	-	-	-	-	-	19	1

(j) Syst. 8a: 31.4% correct, 28.8° RMS error

S \ R	-90	-60	-30	0	30	60	90
-90	-	15	5	-	-	-	-
-60	-	2	18	-	-	-	-
-30	-	-	17	3	-	-	-
0	-	-	-	20	-	-	-
30	-	-	-	12	7	1	-
60	-	-	-	-	20	-	-
90	-	-	-	-	10	10	-

(k) Syst. 8b: 32.6% correct, 29.9° RMS error

Figure F-3 (*cont*).

S \ R	-90	-60	-30	0	30	60	90
-90	20	-	-	-	-	-	-
-60	-	20	-	-	-	-	-
-30	-	-	20	-	-	-	-
0	-	-	-	20	-	-	-
30	-	-	-	-	20	-	-
60	-	-	-	-	-	20	-
90	-	-	-	-	-	-	20

(a) Syst. 1: 100% correct, 0° RMS error

S \ R	-90	-60	-30	0	30	60	90
-90	20	-	-	-	-	-	-
-60	-	20	-	-	-	-	-
-30	-	-	20	-	-	-	-
0	-	-	-	20	-	-	-
30	-	-	-	-	20	-	-
60	-	-	-	-	-	20	-
90	-	-	-	-	-	4	16

(b) Syst. 2: 97.1% correct, 3.59° RMS error

S \ R	-90	-60	-30	0	30	60	90
-90	18	2	-	-	-	-	-
-60	8	12	-	-	-	-	-
-30	1	-	19	-	-	-	-
0	-	-	-	20	-	-	-
30	-	-	-	-	20	-	-
60	-	-	-	-	-	19	1
90	-	-	-	-	-	3	17

(c) Syst. 3: 89.3% correct, 10.7° RMS error

S \ R	-90	-60	-30	0	30	60	90
-90	5	-	-	-	-	4	11
-60	1	19	-	-	-	-	-
-30	-	-	19	1	-	-	-
0	-	-	-	20	-	-	-
30	-	-	-	-	20	-	-
60	-	-	-	-	-	20	-
90	2	4	-	-	-	1	13

(d) Syst. 4a: 82.9% correct, 63.5° RMS error

S \ R	-90	-60	-30	0	30	60	90
-90	6	-	-	-	-	-	14
-60	1	19	-	-	-	-	-
-30	-	-	19	-	1	-	-
0	-	-	-	20	-	-	-
30	-	-	-	-	18	2	-
60	-	-	1	-	1	18	-
90	4	-	-	-	-	4	12

(e) Syst. 4b: 80.0% correct, 65.5° RMS error

Figure F-4: Sound localization confusion matrices for subject JP.

S \ R	-90	-60	-30	0	30	60	90
-90	2	2	-	1	1	6	8
-60	-	2	5	8	4	-	1
-30	-	2	4	7	7	-	-
0	-	2	-	16	2	-	-
30	-	-	3	13	3	1	-
60	1	1	3	2	10	2	1
90	1	4	4	1	2	4	4

(f) Syst. 5a: 23.6% correct, 77.8° RMS error

S \ R	-90	-60	-30	0	30	60	90
-90	7	4	-	-	-	3	6
-60	-	1	9	4	5	1	-
-30	-	-	6	7	7	-	-
0	-	-	2	17	1	-	-
30	-	-	2	15	3	-	-
60	-	1	1	1	14	2	1
90	-	2	1	-	7	6	4

(g) Syst. 5b: 28.6% correct, 61.0° RMS error

S \ R	-90	-60	-30	0	30	60	90
-90	15	4	1	-	-	-	-
-60	-	3	17	-	-	-	-
-30	-	-	19	1	-	-	-
0	-	-	-	20	-	-	-
30	-	-	-	6	14	-	-
60	-	-	-	-	18	2	-
90	-	-	-	-	-	17	3

(h) Syst. 7a: 54.3% correct, 20.7° RMS error

S \ R	-90	-60	-30	0	30	60	90
-90	13	6	1	-	-	-	-
-60	-	3	17	-	-	-	-
-30	-	-	20	-	-	-	-
0	-	-	-	20	-	-	-
30	-	-	-	5	14	1	-
60	-	-	-	-	20	-	-
90	-	-	-	-	4	16	-

(i) Syst. 7b: 50.0% correct, 23.4° RMS error

S \ R	-90	-60	-30	0	30	60	90
-90	6	13	1	-	-	-	-
-60	-	5	15	-	-	-	-
-30	-	1	18	-	1	-	-
0	-	-	-	20	-	-	-
30	-	-	-	2	18	-	-
60	-	-	-	-	14	6	-
90	-	-	-	-	-	18	2

(j) Syst. 8a: 53.6% correct, 21.4° RMS error

S \ R	-90	-60	-30	0	30	60	90
-90	13	7	-	-	-	-	-
-60	-	6	14	-	-	-	-
-30	-	-	19	1	-	-	-
0	-	-	-	20	-	-	-
30	-	-	1	1	18	-	-
60	-	-	-	1	17	2	-
90	-	-	-	-	-	20	-

(k) Syst. 8b: 55.7% correct, 20.9° RMS error

Figure F-4 (*cont*).

S \ R	-90	-60	-30	0	30	60	90
-90	20	-	-	-	-	-	-
-60	-	20	-	-	-	-	-
-30	-	-	20	-	-	-	-
0	-	-	-	20	-	-	-
30	-	-	-	-	20	-	-
60	-	-	-	-	-	20	-
90	-	-	-	-	-	-	20

(a) Syst. 1: 100% correct, 0° RMS error

S \ R	-90	-60	-30	0	30	60	90
-90	16	3	-	1	-	-	-
-60	-	20	-	-	-	-	-
-30	-	-	20	-	-	-	-
0	-	-	-	20	-	-	-
30	-	-	-	-	20	-	-
60	-	-	-	-	-	20	-
90	-	-	-	-	-	2	18

(b) Syst. 2: 95.7% correct, 9.05° RMS error

S \ R	-90	-60	-30	0	30	60	90
-90	12	8	-	-	-	-	-
-60	5	15	-	-	-	-	-
-30	-	-	20	-	-	-	-
0	-	-	-	20	-	-	-
30	-	-	-	-	20	-	-
60	-	-	-	-	-	19	1
90	-	-	-	-	-	1	19

(c) Syst. 3: 89.3% correct, 9.81° RMS error

S \ R	-90	-60	-30	0	30	60	90
-90	-	-	-	-	-	3	17
-60	1	12	7	-	-	-	-
-30	-	-	20	-	-	-	-
0	-	-	-	20	-	-	-
30	-	-	-	-	20	-	-
60	-	-	-	-	2	18	-
90	11	2	-	1	-	1	5

(d) Syst. 4a: 67.9% correct, 23.0° RMS error

S \ R	-90	-60	-30	0	30	60	90
-90	15	-	-	-	-	1	4
-60	2	17	1	-	-	-	-
-30	-	-	20	-	-	-	-
0	-	-	-	20	-	-	-
30	-	-	-	-	20	-	-
60	-	-	-	-	-	20	-
90	-	-	-	-	-	2	18

(e) Syst. 4b: 92.3% correct, 25.4° RMS error

Figure F-5: Sound localization confusion matrices for subject JS.

S \ R	-90	-60	-30	0	30	60	90
-90	4	9	2	-	-	2	3
-60	-	5	5	-	9	1	-
-30	-	-	4	5	6	4	1
0	-	-	-	15	5	-	-
30	-	1	-	6	13	-	-
60	-	-	-	-	5	11	4
90	5	2	1	-	2	3	7

(f) Syst. 5a: 42.1% correct, 63.9° RMS error

S \ R	-90	-60	-30	0	30	60	90
-90	6	2	-	-	-	2	10
-60	-	5	7	-	4	3	1
-30	1	1	7	2	5	4	-
0	-	-	-	17	3	-	-
30	-	-	-	2	17	1	-
60	-	-	-	-	2	15	3
90	1	4	-	-	1	7	7

(g) Syst. 5b: 52.9% correct, 63.4° RMS error

S \ R	-90	-60	-30	0	30	60	90
-90	17	3	-	-	-	-	-
-60	-	15	5	-	-	-	-
-30	-	-	19	1	-	-	-
0	-	-	-	20	-	-	-
30	-	-	-	-	20	-	-
60	-	-	-	-	5	15	-
90	-	-	-	-	-	9	11

(h) Syst. 7a: 83.6% correct, 12.1° RMS error

S \ R	-90	-60	-30	0	30	60	90
-90	14	6	-	-	-	-	-
-60	-	16	4	-	-	-	-
-30	-	-	20	-	-	-	-
0	-	-	-	20	-	-	-
30	-	-	-	-	20	-	-
60	-	-	-	-	2	18	-
90	-	-	-	-	-	11	9

(i) Syst. 7b: 83.6% correct, 12.1° RMS error

S \ R	-90	-60	-30	0	30	60	90
-90	15	5	-	-	-	-	-
-60	-	13	7	-	-	-	-
-30	-	-	18	2	-	-	-
0	-	-	-	20	-	-	-
30	-	-	-	-	20	-	-
60	-	-	-	-	9	11	-
90	-	-	-	-	-	15	5

(j) Syst. 8a: 72.9% correct, 15.6° RMS error

S \ R	-90	-60	-30	0	30	60	90
-90	13	7	-	-	-	-	-
-60	-	13	7	-	-	-	-
-30	-	-	20	-	-	-	-
0	-	-	-	20	-	-	-
30	-	-	-	-	20	-	-
60	-	-	-	4	16	-	-
90	-	-	-	-	-	10	10

(k) Syst. 8b: 80.0% correct, 13.4° RMS error

Figure F-5 (*cont*).

Bibliography

[1] ANSI (**1969**). *American National Standard Methods for the Calculation of the Articulation Index*, Technical Report ANSI S3.5-1969, American National Standard Institute, Inc., 1430 Broadway, New York, NY 10018.

[2] Bilsen, F. A. and Raatgever, J. (**1973**). "Spectral dominance in binaural lateralization," Acustica **23**, 131-132.

[3] Bronkhorst, A. W., and Plomp, R. (**1988**). "The effect of head-induced interaural time and level differences on speech intelligibility in noise," J. Acoust. Soc. Am. **83**, 1508-1516.

[4] Bronkhorst, A. W., and Plomp, R. (**1989**). "Binaural speech intelligibility in noise for hearing-impaired listeners," J. Acoust. Soc. Am. **86**, 1374-1383.

[5] Cox, H., Zeskind, R. M., and Kooij, T. (**1986**). "Practical supergain," IEEE Transactions on Acoustics, Speech, and Signal Processing, **ASSP**-34(3), 393-398.

[6] Durlach, N. I., Corbett, C. R., McConnell, M. V., Peterson, P. M., Rabinowitz, W. M., and Zurek, P. M. (**1987**). "Multimicrophone monaural hearing aids," Proc. 10th Conf. Rehab. Eng. (RESNA), 395-397.

[7] French, N. R. and Steinberg, J. C. (**1947**). "Factors governing the intelligibility of speech sounds," J. Acoust. Soc. Am. **19**(1), 90-119.

[8] Gorike, R. (**1990**). "Eyeglass frame with electroacoustic device tor the enhancement of sound," United States Patent, number 4,904,078.

[9] Greenberg, J. E. and Zurek, P. M. (**1992**). "Evaluation of an adaptive beamforming method for hearing aids," J. Acoust. Soc. Am. **91**, 1662-1676.

[10] Greenberg, J. E., Peterson, P. M., and Zurek, P. M. (**1993**). "Intelligibility-weighted measures of speech-to-interference ratio and speech system performance," J. Acoust. Soc. Am. **94** 3009-3010.

[11] Henning, G. B. (**1973**). "Detectability of interaural delay in high frequency complex waveforms," J. Acoust. Soc. Am. **55**, 84-90.

[12] Kryter, K. D. (**1962a**). "Methods for the calculation and use of the articulation indes," J. Acoust. Soc. Am. **34**(11), 1689-1697.

[13] Kryter, K. D. (**1962b**). "Validation of the articulation index," J. Acoust Soc. Am. **34**(11), 1698-1702.

[14] Kuhn, G. F. (**1977**). "Model for interaural time differences in the azimuthal plane," J. Acoust. Soc. Am. **62**, 157-167.

[15] McFadden, P. and Pasanen, E. G. (**1975**). "Lateralization at high frequencies based on interaural time differences," J. Acoust. Soc. Am. **59**, 634-639.

[16] Middlebrooks, J. C. and Green, D. M. (**1990**). "Directional dependence of interaural envelope delays," J. Acoust. Soc. Am. **87**, 2149-2162.

[17] Middlebrooks, J. C., Markous, J. C. and Green, D. M. (**1989**). "Directional sensitivity of sound-pressure levels in the human ear canal," J. Acoust. Soc. Am. **86**, 89-108.

[18] Mills A. W. (**1972**). "Auditory Localization," *Foundations of Modern Auditory Theory, vol. II*, ed. Tobias, J. V., pp. 303-348.

[19] Nilsson, M., Soli, S. D., Sullivan, J. A. (**1994**). "Development of the Hearing in Noise Test for the measurement of speech reception thresholds in quiet and in noise," J. Acoust. Soc. Am. **95**, 1085-1099.

[20] Peterson, P. M. "Adaptive Array Processing for multiple microphone hearing aids," MIT PhD Dissertation, RLE Technical Report No. 541, Feb. 1989.

[21] Soede, W., Berkhout, A. J., Bilsen, F. A. (**1993**). "Development of a directional hearing instrument based on array technology," J. Acoust. Soc. Am. **94**, 785-798.

[22] Soede, W., Bilsen, F. A., Berkhout, A. J. (**1993**). "Assessment of a directional microphone array for hearing impaired listeners," J. Acoust. Soc. Am. **64**, 799-808.

[23] Stadler, R. W. and Rabinowitz, W. M., (**1993**). "On the potential of fixed arrays for hearing aids," J. Acoust. Soc. Am. **94**, 1332-1342.

[24] Stadler, R.W. "Optimally Directive Microphones for Hearing Aids," MIT S.M. Thesis, Sept., 1992.

[25] Welker, D. P., "A Real-Time Binaural Adaptive Hearing Aid," MIT S.M. Thesis, May., 1994.

[26] Wightman, F. L. and Kistler, D. J. (**1991**). "The dominant role of low-frequency interaural time differences in sound localization," J. Acoust. Soc. Am. **91**, 1648-1661.

[27] Zurek, P. M. (**1992**), "Binaural Advantages and Directional Effects in Speech Intelligibility," *Acoustical Factors Affecting Hearing Aid Performance, Second Edition*," ed. Srudebaker, G. A. and Hochberg, I., Boston: Allyn and Bacon, pp 255-276.

[28] Zwicker, E. and Beckenbauer, T. (**1988**). "Hearing aid with locating microphones," United States Patent, number 4,773,095.